Master of Science Thesis

Ultrasonic Plastic Welding of Carbon Fiber Reinforced Polyamide 6 to Aluminium and Steel

An Experimental Study

S. Bolt

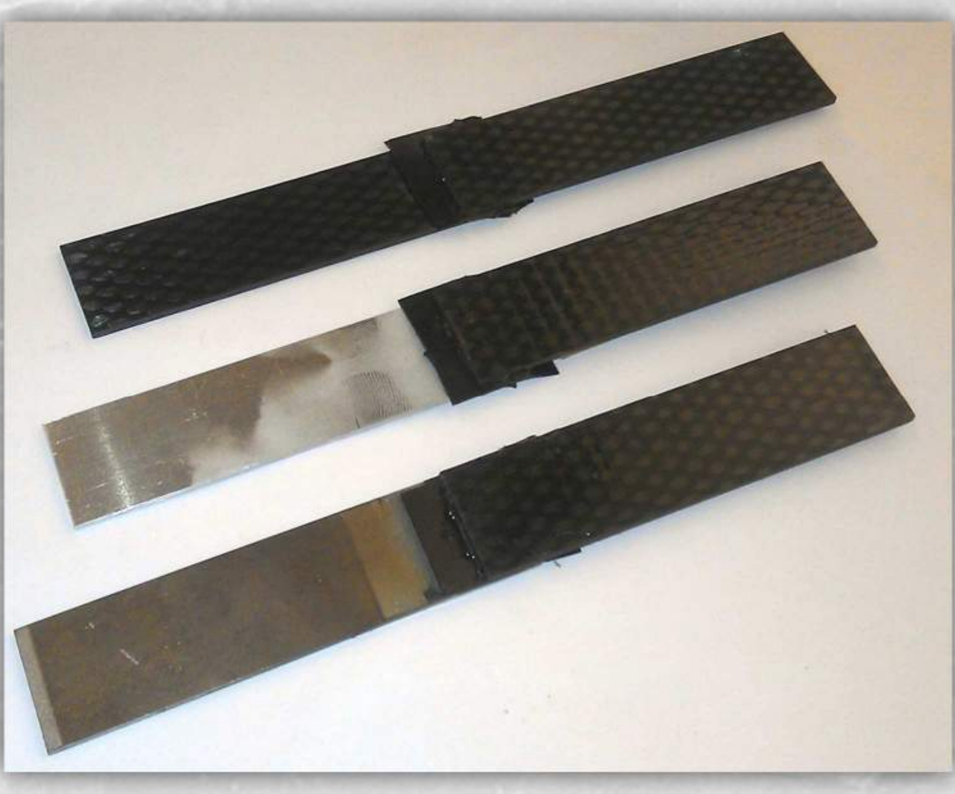

Faculty of Aerospace Engineering · Delft University of Technology

TU Delft Delft University of Technology

Ultrasonic Plastic Welding of Carbon Fiber Reinforced Polyamide 6 to Aluminium and Steel

An Experimental Study

Master of Science Thesis

For obtaining the degree of Master of Science in Aerospace Engineering
at Delft University of Technology

S. Bolt

18th of December, 2014

Faculty of Aerospace Engineering · Delft University of Technology

Delft University of Technology
Faculty of Aerospace Engineering
Department of Aerospace Structures and Materials

GRADUATION COMMITTEE

Dated: 18$^{\text{th}}$ of December, 2014

Chair holder: ______________________
Prof.dr.ir. R. Benedictus

Committee members: ______________________
Dr. I. Fernandez Villegas

____
Dr.ir. S. Wijskamp

____
Dr. M.M. Abdalla

Abstract

In order to reduce energy consumption of modern automotive vehicles, ways to effectively implement carbon fiber reinforced thermoplastics in these vehicles are being sought. Major identified challenges in the application of carbon fiber reinforced thermoplastics are the lack in knowledge about hybridization and bonding technology, together with industrialization and integration of composite manufacturing.

An experimental study has been performed to examine the application of displacement controlled Ultrasonic Plastic Welding (UPW) in the creation of joints between aluminium or steel and carbon fiber reinforced polyamide 6 (CFR-PA6). This bonding technique is known as a fast welding technique in which in the order of seconds an effective joint can be created by means of fusion bonding of thermoplastics. This is a result of viscoelastic heating and interfacial friction induced by perpendicular ultrasonic vibrations of a sonotrode which is pressed on the welding overlap. The potential of the application of this welding technique lies in a reduction of joining times in the assembly line, while maintaining high joint strengths with low variation.

This study has been focused on an assessment of the power and displacement feedback obtained during welding, the electro-insulating behavior of the created joints and their single lap shear strength & fracture. Both non-hybrid and hybrid joints have been welded. For hybrid welds, both steel and aluminium were used as metallic substrate. For aluminium substrates, the effect of not applying a coating has been assessed as well.

The absence of a coating was found to result in no bond between the applied thermoplastic and pretreated metallic surface. Application of a coating on the pretreated metallic surface enables the successful creation of joints. With the applied welding settings, hybrid welds showed to dissipate the same amount of energy as non-hybrid welds, in the order of 700 Joules on average, at an average welding time in the order of 0.5 seconds. Villegas identified stages in the feedback of dissipated power of the welding process which complied with the start of vibration (1), the onset of melting (2), complete melting in the overlap enabling onset of flow (3), onset of melting and flow of thermoplastic between the carbon fibers (4), and diminished adhesive layer thickness (5). In case of welding hybrid joints with the CFR-PA6 adherend in contact with the sonotrode, these stages could not be clearly identified in the dissipated power feedback. These were however identified when the aluminium substrate was in contact with the sonotrode. Welding resulted in an electro-insulating thermoplastic adhesive layer of about 200 µm thick between both adherends for hybrid welds. With grit blasted and coated aluminium samples, an average single lap shear strength (SLSS) of 11 MPa could be reached. Single lap shear testing of welded samples with a grit blasted, nitric acid etched and coated aluminium surface resulted in a bond with an average SLSS of 16.5 MPa with a coefficient of variation of 2.2 %. This strength is up to 80% of a tested adhesive reference. It was found, that fiber bundle deformation was limited at 100 % displacement. The fracture of hybrid welded samples resulted in adhesive peel fracture on the metallic surface. Hybrid welds with coated grit blasted steel and the used welding settings proved to result in an average SLSS of 8 MPa. In that case, further research is needed in which a lower amplitude is applied.

The findings support the application of displacement controlled ultrasonic plastic welding in the creation of hybrid joints between CFR-PA6 and thermoplastic coated metals like aluminium or steel. This could be implemted in further development of efficient and effective hybridization. For following studies, it is recommended to assess the processing boundaries, the controllability of the adhesive layer thickness, the influence of sonotrode displacement on the mechanical strength, and the long term durability of the created joints.

Summary

The purpose of the thesis is to analyze the applicability of ultrasonic plastic welding in the creation of joints between metals such as aluminium and steel and carbon fiber reinforced thermoplastics. In order to reduce energy consumption of modern automotive vehicles, ways to effectively implement carbon fiber reinforced thermoplastics in these vehicles are being sought. Major identified challenges in the application of carbon fiber reinforced thermoplastics in the automotive industry are the lack in knowledge about hybridization and bonding technology, together with industrialization and integration of composite manufacturing in the production process. The thesis is composed of six chapters, each of them dealing with different aspects of the performed research in ultrasonic plastic welding.

Introduction

Chapter 1 is an introduction to the thesis which deals with the current state of the art in the performed technology. Welding is favored to other techniques, according to Stavrov [1], as mechanical fastening results in stress concentrations, delamination during drilling and extensive labor & time requirements, and adhesive bonding requires extensive surface preparation of the thermoplastic and often possess long curing cycles. Welding techniques have already been researched and applied, like ultrasonic metal welding, induction welding and laser welding. Ultrasonic plastic welding has been applied as well in the past to create joints between metal and thermoplastic. Wise et al. [2] and Ramarathnam et al. [3] used welding between thermoplastic and metal, welding either based on time or energy, respectively. Both applied a thermoplastic coating on the metallic pretreated surface before welding to preserve the metallic surface and ensure a bond between the thermoplastic and metal. In the work of Krüger et al. [4] welding was applied between aluminium and GFR-PA66, in which the metallic adherend was in contact with the sonotrode during welding. Here, no coating was applied and a coefficient of variation of 40 % was obtained during single lap shear testing.

Literature

Ultrasonic plastic welding (UPW) is known as a welding technique in which an ultrasonic vibration perpendicular to the joining interface induces surface frictional- and viscoelastic

heating of the thermoplastic. The thermoplastic starts to melt as a result, flows and diffuses, by which a joint is created. Once this vibration is stopped, the consolidation phase begins, by which the thermoplastic is cooled down and solidifies under pressure. This process takes up to ten seconds per weld. During welding, the ultrasonic vibration is transferred from the piezo converter to a booster which amplifies the vibration. Through the booster, the vibration reach the following sonotrode, which again amplifies and transfers the vibration to the welding interface. A pneumatic pressure actuator presses this welding stack onto an anvil during welding. UPW can be controlled by the time of vibration, the dissipated welding energy and the vertical displacement of the sonotrode which is a result of squeezing out the thermoplastic in the bond line. Next to this, the amplitude of vibration and the applied pressure can be selected. The heating process during welding can be focused to less stiff thermoplastic in the welding area, as this experiences the largest strains, due to which it melts preferentially. The experienced stress is dependent on the total thickness of the welding overlap, the stiffness of each layer and the applied amplitude through Equation 1:

$$\left(\frac{E}{h}\right)_{eq.} = \left(\sum_{i=1}^{n} \frac{h_i}{E_i}\right)^{-1} \tag{1}$$

During welding, the created heat is distributed by conduction through the material. In case metals are used, this results in fast cooling of the thermoplastic in contact with the metallic adherend. From the work of Villegas [5], 5 stages were identified during the vibration phase. Welding is ideally stopped in the stage in which the thermoplastic is squeezed out, but melting and flow of the thermoplastic in the composite stays limited.

In the creation of a joint between metal and CFRTP structures by welding, several types of adhesion are applied. Firstly, there is diffusion within the thermoplastic to bond when it melts. Secondly, between the metal and thermoplastic two types of adhesion can occur. Mechanical interlocking can be caused in the pits created in the metallic structure. Next to that, adsorption occurs of thermoplastic on the metallic surface by chemically pre-treating the surface structure. For hot melt adhesion, adhering to a warm aluminium is preferred, as this prevents consolidations of the thermoplastic upon contact with the aluminium. In bonding to metallic surfaces, the creation of a clean surface is essential. Often acetone cleaning is used to degrease the surface before bonding. The surface area can be improved by abrasion techniques. Subsequent etching and anodizing treatments increase the chemical adsorption. In comparable studies, most often a treatment of acetone degreasing, grit blasting and nitric acid etching have been applied [6, 7]. For steel samples, acetone degreasing and grit blasting are applicable surface treatment techniques. The usage of acidic fluids is generally not applied on steel surfaces, as this results in corrosion on the non-passivating surface.

When carbon fibers are in contact with aluminium or steel in a corrosive environment, galvanic corrosion is greatly enhanced as a result of the difference in corrosion potential. A number of ways are found to reduce such effects. The most effective way is found to be the creation of an electro-insulating joint through the thermoplastic between the metallic surface and the carbon fibers.

Objective

The objective of the current study is to evaluate the application of displacement controlled ultrasonic plastic welding in the creation of joints between carbon fiber reinforced thermoplastic and metals such as aluminium and steel. An electro-insulating joint should be created within a few seconds, which shows a highly repeatable strength and is controllable by selecting the right welding settings. The main questions in this research are the following. Firstly, how does the obtained welding feedback compare for different welding set-ups? Secondly, can the method as proposed by Villegas for controlling the UPW process for non-hybrid welded joints be applied in the creation of joints between carbon fiber reinforced thermoplastic and aluminium or steel as well? Thirdly, can the application of a coating be avoided? Fourthly, what processing times can be achieved with the application of UPW for the applied welding series? Fifthly, can an electro-insulating joint be achieved between aluminium or steel and carbon fiber reinforced thermoplastics by means of UPW? And lastly, what is the single lap shear strength of the created displacement controlled UPW hybrid joints?

Experimental Set-Up

Chapter 2 presents the applied materials, sample preparations and experimental set-up. An experimental study was performed to examine the application of displacement controlled UPW in the creation of joints between aluminium or steel and carbon fiber reinforced polyamide 6 (CFR-PA6).

In this study, AA5754 aluminium alloy was applied together with DC01 steel alloy as metal adherend materials. A black ULTRAMID B EXPERIMENTAL Polyamide 6 (PA6) from BASF was provided by Ten Cate Advanced Composites BV as a thermoplastic film of 0.14 mm thick. Thermogravimetric analysis, differential scanning calorimetry and dynamic thermomechanical analysis have been applied. A T_g around 57 °C was observed, with a melting temperature around 220 °C. More information is presented in Appendix A. PA6 is known to absorb moisture, which reduces the T_g. Therefore, drying of the thermoplastic is essential before performing tests. A carbon fiber reinforced thermoplastic, with the same PA6 as provided, was provided as well by Ten Cate Advanced Composites BV.

Composite samples were water jet cut, deburred and dried for at least 48 hours in a vacuum oven at 50 °C before attempting any tests. Energy directing films (EDs) are used as an interlayer between both adherends during welding. These were created by hot pressing three PA6 films at 210 °C in a hot platen press, and cutting these to a size of 27 by 29 mm. The surface of steel samples have been degreased by ultrasonic cleaning in acetone for 10 minutes, followed by grit blasting, air blasting and a subsequent same ultrasonic cleaning method for 10 minutes. This was also applied for aluminium adherends. In a number of series, this was followed by etching the surface in 65% nitric acid, subsequent rinsing in tap water and demineralized water, followed by drying in an air drying oven at 40 °C for 30 minutes. In the majority of welds, a thermoplastic coating was applied in a vacuum bagging treatment to 250 °C.

Adhesive reference samples were created as well. Here, 3M™ Scotch-Weld™ EC-9323 B/A was used as an adhesive. The CFR-PA6 surface was pretreated with UV/ozone for 5 minutes

to enhance bonding properties with the adhesive. Here, the aluminium surface was grit blasted and nitric acid etched as well. Curing of the adhesive was performed at 65 °C for 3 hours in an air circulating oven, where a vacuum bag applied pressure during the cycle. The resulting samples were milled according to size applicable to ASTM D1002-05.

Ultrasonic plastic welding (UPW) was performed with a Rinco Dynamic 3000 UPW device, with a welding frequency of 20.1 kHz, an amplitude of 36.3 µm and a pressure of 2.5 MPa (or a force of 800 N). The resulting welding overlap area was conforming to ASTM D1002-05. In general, welding was controlled by displacement. A multimeter was used to evaluate the electro-insulating behavior of the created joint.

The strength of the created joints has been evaluated by single lap shear testing, following ASTM D1002-05. The strain distribution has been assessed by differential image correlation for a number of welds. Resulting fracture was evaluated using SEM microscopy as well, using a JEOL JSM-7500F Field Emission Scanning Electron Microscope. Here, both low scatter and back scatter were used to identify contour and different materials. Further microscopy was used before fracture to assess the created interface and adhesive layer thickness after welding.

Results of Welding Process and Power & Displacement Feedback

In the following chapters, the results of this study are presented and discussed. In Chapter 3, the welding feedback and resulting particular results are presented. It was found, that non-hybrid welded joints showed welding behavior which conforms to the identified stages by Villegas et al. At the low amplitude and high force, the plateau in phase 4 was however not as pronounced as what has been identified before. The absence of a thermoplastic coating was found to result in no bond between the applied thermoplastic and pretreated metallic surface as the pretreated metallic surface was mechanically eroded by the welding procedure. This further resulted in a relatively high welding time and energy compared to the other series. When no coating was used, 1600 Joules were dissipated, whereas only 700 Joules were dissipated during welding with an applied coating. Application of a coating on the pretreated metallic surface enabled the successful creation of joints. When a layer of 0.14 mm was applied, welding was successful. With the applied welding settings, hybrid welds showed to dissipate the same amount of energy as non-hybrid welds, in the order of 700 Joules on average, at an average welding time in the order of 0.5 seconds. In case of welding hybrid joints with the CFR-PA6 adherend in contact with the sonotrode, an initial power peak was absent in the dissipated power feedback. These were however identified when the aluminium substrate was in contact with the sonotrode. In that case, a fretting-like damage was observed on the metallic surface in contact with the sonotrode. When steel adherends were welded, stress resulted in fracture of the ED during welding. Here, it is recommended to use an even lower amplitude during welding. For most welds, a large variability was observed in the dissipated welding energy and -time. The maximum and -average dissipated power during welding showed a positive correlation with the equivalent stiffness to height ratio of the used welding overlap.

With a vibration phase of on average 0.5 seconds and a solidification of 4 seconds, the total welding cycle took up about ten seconds. With these numbers, cycle times during assembly

can be reduced significantly compared to other welding techniques and adhesive bonding. However, considerable time was still spent in the pretreatment and coating process of the metallic adherend.

Electro-insulating Behavior

In Chapter 4, the resulting electro-insulating properties of the created hybrid joint are briefly evaluated. Welding resulted in an electro-insulating thermoplastic adhesive layer of about 200 μm thick between both adherends for hybrid welds. In the single case an electroconductive joint was created, the carbon fiber curled around the metallic during excessive thermoplastic outflow and created a joint outside the overlap area, with a resistance of 68.4 Ohm. The existence of an electro-insulating joint was considered to enhance the durability of the created joint. For non-hybrid welds, an electroconductive joint was created, with an electrical resistance of on average 10.2 Ohm. As an electro-insulating joint could be created, the durability of the created joints can be further evaluated. In following research, the long term durability in outside weather conditions should be further assessed. It has to be further assessed which conditions do result in an electroconductive joint. Further research is also needed on the calculated adhesive layer thickness from the welding feedback and initial data, and the actual measured adhesive layer thickness.

Mechanical Strength & Fracture

In Chapter 5 the mechanical strength tested for single lap shear specimens are presented and discussed. This is followed by an analysis of the resulting fracture behavior. The non-hybrid welded joints were found to have a single lap shear strength (SLSS) of 37.6 MPa on average with a coefficient of variation of 3.1 %. In this case, the deformation of carbon fiber bundles as a result of thermoplastic flow was limited. A symmetric strain distribution was observed in the joint overlap during testing, with mostly compressive normal strains and considerably higher shear strains in the overlap. Hybrid joints with coated steel adherends contained a SLSS of 8.5 MPa with a c.o.v. of 7.7 %. Here, the absence of a joint is observed at both sides of the overlap, which is thought to be a result of breakage of the ED during welding. The strain distribution showed to be greatly skewed to the side of the metallic edge. The peeling strain was considerably higher, up to 17.5 millistrains, compared to a shear strain of only 7 millistrains at the edge of the overlap. With grit blasted and coated aluminium samples, an average SLSS of 11 MPa could be reached. Single lap shear testing of welded samples with a grit blasted, nitric acid etched and coated aluminium surface resulted in a bond with an average SLSS of 16.5 MPa with a coefficient of variation of 2.2 %. This strength is up to 80 % of a tested adhesive reference. The resulting c.o.v. was significantly lower, when compared to the work of Krüger. The strain distribution was skewed as well, but showed a considerably higher shear strain at the metallic edge, of about 14 millistrains, with a maximum peeling strain of 14 millistrain at a load of 3.4 kN. Fracture of hybrid welded samples resulted in adhesive peel fracture on the metallic surface. This was initiated at both sides of the overlap. For the welds with 100 % displacement, a zone with adhesive/thermoplastic cohesive shear fracture was observed. It was evaluated what effect displacement had on the joint

strength, by lowering the controlling displacement to 66 % of the thickness of the energy director. Here, a strength of 15.1 MPa was observed with a c.o.v. of 7.5 %, with mostly adhesive peel fracture. The hypothesis was posted, that this was a result of a different strain distribution caused by the thicker adhesive layer. In fractured surfaces in a number of cross sections two layers could be observed. Further analysis on the microcrystalline structure is needed to assess whether these layers indicate a transition between a layer that did melt during welding and a layer which was cooled by the metallic adherend and did not reach its melting temperature. Cross sectional analysis further showed a difference in adhesion of the thermoplastic to the aluminium surface when grit blasted aluminium is compared to grit blasted and etched aluminium. In the former situation, a crack could be observed, which was not observed with grit blasted and etched aluminium. This was attributed to the difference in thermal expansion during cooling from the melting temperature.

Conclusion

In Chapter 6, the conclusions, implications, limitations and recommendations are presented. The results show that displacement controlled ultrasonic plastic welding can be used to create joints between metallic and carbon fiber reinforced thermoplastic structures. The application of a thermoplastic coating was found to be essential in the creation of such a joint. Assembly cycle times can be greatly reduced when UPW is applied in the creation of electro-insulating joints between metal and CFRTP structures, as the adhesive bonding process to the metal surface can be separated from the cohesive welding process of the thermoplastic itself. The created joint strength showed to be reliable and competitive with adhesive bonding.

Recommendations

The following main recommendations are given for following studies:

- Study the welding quality with coated steel adherends at an even lower welding amplitude.
- Evaluate the reliability of methods to apply a thicker coating on the metallic adherend which mitigates the usage of an energy directing film.
- Use more sophisticated surface treatments for the metallic surface, such as anodization.
- Evaluate the effect of amplitude and pressure on the welding displacement behavior, to assess the applicability of the displacement rate to find proper welding conditions.
- Evaluate the durability and galvanic corrosion behavior in outside weather conditions of the created electro-insulating joint. Further analyze the processing boundaries in which conditions actually do result in an electroconductive connection.
- Evaluate the microcrystalline structure of the adhesive layer after welding and its effect on the mechanical properties of the joint.

Table of Contents

List of Figures

List of Tables

List of Symbols

List of Symbols

Abbreviations

c.o.v.	Coefficient of variation
CFR-PA6	Carbon fiber reinforced polyamide 6
ED	Thermoplastic energy directing film
ESHR	Equivalent stiffness to height ratio
FRTP	Fiber reinforced thermoplastic
PA6	Polyamide 6
SLSS	Single lap shear strength
TP	Thermoplastic
UMW	Ultrasonic Metal Welding
UPW	Ultrasonic Plastic Welding

Latin Symbols

$\dot{Q}$	Heat flux as a result of ultrasonic plastic welding
a	Welding amplitude
E	Young's modulus.
f_a	Aliasing frequency
f_s	Signal frequency
G	Shear modulus
h	Height of layer in welding overlap
n	Positive integer
R	Sampling rate

Greek Symbols

ϵ	Strain
ν	Poisson's ratio
ω	Welding frequency

Preface

In September 2007, I freshly started a new part of my life. Great years have followed since, in which I could enjoy membership of an inspiring student society, even had the opportunity to take a year off to invest in extracurricular activities and flourish nice memories from a half year abroad. In all areas, and more, I felt supported by friends and family. As a closure to this period, the report in front of you is intended as a document which forms an essential part in the process of obtaining the title 'Master of Science in Aerospace Engineering' at the Delft University of Technology.

I deemed it fruitful to invest time in the field of reinforced thermoplastics, as this type of material results ultimately in faster production cycles and a broader applications of composite technology to reduce the energy consumption of moving vehicles. Already back in May 2012, a first contact was made with Irene Fernandez Villegas about conducting a thesis on the application of carbon fiber reinforced thermoplastics in the automotive industry. In the group of dr.ir. I. F. Villegas, currently much work is done on creating joints between carbon fiber thermoplastics by means of several fusion bonding methods. This provided an excellent combination with the intended direction of the research topic. Discussions however were set on hold as an internship was performed from October 2012 until March 2013, in Bavaria, Germany, in the field of production of thermoset composite structures. However, the discussion was reinitiated and a focus was on the current topic from September 2013 onwards.

Nowadays, automotive vehicles are responsible for a large part of greenhouse gas emissions. Therefore, weight reduction of such vehicles was deemed as an effective field of study. This should result in a fruitful application of knowledge to contribute in tackling the issues society is nowadays facing in aiming for a better future. More inspiration came about, as mentioned in the introduction, that the application of the automotive industry demands more knowledge about how to make hybrid structures between metals and carbon fiber reinforced thermoplastics. With this in mind, this study on the applicability of ultrasonic plastic welding in creating hybrid joints can be seen as applying a technique which is ready for a field which needs its application.

This report gives a brief overview of relevant literature about the field of fast joining of hybrid structures by means of adhesion. The methodology and experimental set-up are followed by information about data obtained which help in further controlling the portrayed welding process. The report presents opportunities of the displayed welding technique in increasing production cycles, while maintaining relatively high joint strengths, and enabling ways to control durability of the structure. It has been targeted to readers in the field of ultrasonic plastic welding and researchers who will work in the future on the presented topic of hybrid joining of metallic structures to carbon fiber reinforced thermoplastics on an industrial scale.

The report can be separated in several parts. The introduction is followed by a literature study which portrays the most relevant developments in applicable fields of ultrasonic plastic welding, adhesion and corrosion. In the following Chapter the applied research methodology is portrayed. The experimental set-up subsequently fills in the practical choices in this research, in which the information for reproduction of the current work can be found. Results are divided into three parts, which can be read separately. First, data obtained during and directly after the welding process are covered. Secondly, electrical insulation of created joints is presented and discussed. Mechanical results and fracture behavior are presented and discussed in the last results Chapter. Each Chapter with results contains a conclusion, of which an overview together with recommendations is presented in the final Chapter.

The performed research has been an inspiration to me. Due to the fact that not all test were flawless and not all experiments turned out the way they were expected to turn out, I learned to cope with situations that do not turn out how you want them to. The practical implication of research has been a great addition to the experience of conducting this thesis. Therefore, I do hope that readers will be as inspired as I became throughout the process.

Acknowledgments

The author would like to thank Dr. I. Fernandez Villegas for her expertise, patience and assistance during the process of conducting the work which has lead to this thesis. Without her work and effort, this thesis would not have been possible.

Also, the author would like to acknowledge Ten Cate Advanced Composites BV for supporting this research in the supply of materials.

Furthermore, the author would also like to thank the staff of the Delft Aerospace Structures and Materials Laboratory, for their effort in assistance during the performance of laboratory work. Especially the help of Frans Oostrum and Lijing Xue in performing surface treatments and microscopic analysis is worthy of mentioning.

Delft, University of Technology S. Bolt
18th of December, 2014

Chapter 1

Introduction

1.1 Motivation

As a result of increasing fuel prices and awareness on environmental pollution of traffic, a transition has started on the reduction of energy consumption of automotive vehicles. A major contributing factor in the consumption of energy of such vehicles during continuous acceleration and braking is the weight of the vehicle structure itself. In order to reduce this weight, an alternative for the applied materials, often steel and aluminium alloys, is sought in the application of fiber reinforced plastics. These composite materials have a high stiffness-to-weight ratio. Application of fiber reinforced thermosets results in long production cycle times, as a result of curing of the thermoset. With the high production rates of middle class automotive vehicles, application of such a material would be too costly to be applied for the vehicle used by the common user, as a lot of parts would have to be made concurrently. Therefore, the application of fiber reinforced thermoplastics (FRTPs) is preferred. Thermoplastics (TPs) can be deformed by increasing the temperature above the melting temperature, due to which products can be shaped, and regain stiffness as the product is cooled back to ambient temperature.

A recent survey [8] under staff members in the German automotive industry and composite industry revealed essential aspects needed in the development of the production of FRTP structures for successful implementation of this technology in the automotive industry. The fields in which most development for the FRTP technology is anticipated are the following [8]:

- Material cost reduction
- Industrialization and integration of composite manufacturing processes
- Waste management and recyclability of composites
- Repair methods & damage detection together with knowledge enhancement about repairs on these structures
- Increase in knowledge about hybridization and bonding technology

In this study the focus is on development in the last field, hybridization and bonding technology. Here, ultrasonic plastic welding is applied in the creation of hybrid joints. In this report, hybridization is interpreted as the ability to make structures that consist of both metallic and FRTP subparts. This will thus mainly focus on the application of joining technologies which enable the creation of such hybrid joints.

The current study adds to previous research in joining fiber reinforced thermoplastics (FRTPs) to metallic parts by fusion bonding. In the upcoming Sections, the most relevant literature to this research is presented. First, in Section 1.2, the advantages of fusion bonding over adhesive joining and mechanical fastening are assessed, followed by a brief overview of welding techniques which have been applied in joining FRTPs to metallic structures. In Section 1.3, attempts and developments in the last decades on ultrasonic plastic welding (UPW) are presented. First, fundamental research is presented on controlling and understanding the UPW process when applied to non-hybrid welds. This means welding between two similar FRTP adherends. After this, research is presented in the application of UPW for joints between metals and thermoplastic (TP) structures, which can be fiber reinforced. In Section 1.4 theory about adhesion between metallic structures and hot melt thermoplastic adhesives is presented together with ways to enhance such a bond by the application of surface treatments. The effects and consequences of galvanic corrosion are discussed in Section 1.5. The objective and research questions are presented in Section 1.6. In Section 1.7, the applied research methodology is presented. The outline of the upcoming chapters can be found in Section 1.8.

1.2 Developments in Joining Techniques for Thermoplastic Composites to Metals

For FRTPs, fusion bonding is preferred to mechanical fastening and adhesive bonding, as written by Stavrov et al. [1]:

> *"Traditional joining methods for metals and thermoset plastics (mechanical fastening and adhesive bonding) are feasible, but not ideal for TPCs [1]. Mechanical fastening has a number of disadvantages: introducing stress concentrations in the material, delamination during drilling, different thermal expansion of the fasteners relative to the composite, water intrusion into the joint, possible galvanic corrosion, weight increase and extensive labour and time requirements. Adhesive bonding, although more favourable than mechanical fastening because of avoiding stress concentrations, still presents some difficulties when applied on TPCs. It requires extensive surface preparation, generally difficult to control in industrial environment, and adhesives used (usually epoxies) have long curing cycles. It can also be difficult for the chemically inert thermoplastic matrix to bond."* [1], p.39

Clearly, there are limitations in the manufacturability of adhesive joints and the durability of mechanical fastening. Hence, joining by fusion of the TP seems to be an attractive candidate in the development of hybrid structures[2].

[1] Thermoplastic composites

[2] From the statement of Stavrov et al. it has to be recognized, that some of the limitations for mechanical fastening also count for joints between CFRTP structures and metals by fusion joining, like differences in thermal expansion and occurrence of galvanic corrosion, etc.

Welding techniques have been evaluated in the past to develop a technique which easily and quickly is able to weld FRTPs onto metallic structures. These developments have been performed into the fields of several welding techniques. For ultrasonic metal welding (UMW), the study has focused on the creation of an electroconductive joint between the carbon fibers and metal by mechanical interlocking as a result of plastic deformation of the metal [4, 9–11], which resulted in highly increased joint strengths. In induction welding, the hysteresis in a frequently reversed electrically induced magnetic field resulted in heating of carbon fibers and metal, which results in melting of the thermoplastic in contact with the carbon fibers and metal in the welding area [7, 12, 13]. In laser welding, a laser pulse heats the metallic surface locally, resulting in melting of the thermoplastic [14–20]. When amorphous thermoplastic is used, this laser pulse can be sent through the transparent thermoplastic. Finally, for resistance welding, an electroconductive metal mesh is placed between the two joining partners. The electroconductive metal is shielded off from this mesh, using a glass fiber weave [1, 21]. In the field of ultrasonic plastic welding (UPW) , research has been performed as well. This is presented in Subsection 1.3.2.

1.3 Ultrasonic Plastic Welding

Ultrasonic plastic welding (UPW) is a welding technique which consists of a vibration phase and a consolidation phase. In the first, vibration, phase, an ultrasonic vibration perpendicular to the joining interface is applied to heat up the thermoplastic by frictional- and viscoelastic heating beyond its melting temperature. After intermolecular diffusion, it is again passively cooled down to room temperature under applied pressure during the second, consolidation, phase. This entire process in general takes up to ten seconds in total.

The operation of UPW is similar to ultrasonic metal welding (UMW). For UMW, the vibration is however applied in the direction parallel to the joining interface, and thus perpendicular to the applied pressure during joining. An UPW device consists of a number of standard parts [22]:

- A pneumatic pressure actuator, which exerts a constant pressure through the welding stack onto the to be welded overlap.
- A piezo converter, which converts an ultrasonic electrical signal into a mechanical vibration.
- A booster, which amplifies this vibration.
- A sonotrode, or horn, which acts as the piece which concentrates and amplifies the mechanical vibration onto the welding overlap.

1.3.1 Developments in Understanding of the Welding Process

The heating process of UPW has been found to be a combination of interfacial friction heating and viscoelastic heating [23–25]. For amorphous and semi-crystalline thermoplastics, the frictional heating process through surface asperities results at the beginning in a large proportion of the heating process, whereas above the glass transition temperature viscoelastic heating plays a large role [24, 26]. The process of viscoelastic heating is described by Equation 1.1, as presented by Tolunay et al. [23]. Here, $\dot{Q}$ is the heat flux created by heating, ω the welding frequency, ϵ the induced strain in the material and E" the loss modulus of the thermoplastic at the present temperature. As the stiffness within the unreinforced TP is less, most strain is observed there, resulting in locally concentrated viscoelastic heating [25]. When joining two substrates, or adherends, between these substrates a layer of TP is often applied which has a lower stiffness. This layer experiences higher strains caused by the ultrasonic oscillation. This concentrates the frictional- and viscoelastic heating to this so-called energy director (ED). When the stiffness of the ED is equal to the transverse stiffness of the composite, there is no single preferential location of heating, resulting in uncontrolled melting.

$$\dot{Q} = \frac{\omega \epsilon^2 E^{"}}{2} \tag{1.1}$$

Because of the previously mentioned effect, for TP products, flat energy directors were not suitable [27]. High- and low stress sites were found in the product as a result of its geometry, which resulted in heating of the TP at these locations. It has been shown by Villegas et al. [28], that flat energy directing films (EDs) do concentrate melting in case of welding of FRTP substrates, because the stiffness in the FRTP is higher than the stiffness of the ED.

The welding pressure, or exerted force per overlap area, is used to clamp the substrates in the interface onto each other by exerting this pressure onto the sonotrode. It has been found to have effect on the dissipation of power at the initial welding phase and on the joint strength [22, 26]. The increased initial power is mainly a result of increased frictional heat dissipation. This results in more initiation sites of molten TP, which results in a faster melting of the entire welding interface [22]. Once the entire welding interface is molten and flow is possible, a high force results in faster flow of the TP [22, 28]. Due to the high force, however, flow is enabled somewhat earlier, resulting in a relatively colder molten TP than in the case when a lower force is used [25].

The welding amplitude is the amplitude of the tip of the sonotrode resulting from the UPW signal. This is induced by the piezo electric inducer. With a higher amplitude more power is dissipated into the welding interface as more stress is experienced [26] and higher strains are observed. The dynamic stress, caused by the amplitude of vibration, has been found to be far higher during welding than the static force (i.e. welding pressure) [29]. The used derived equation from the presented theory of Levy to calculate the absolute stress $|\sigma_n|$ caused by an amplitude a is defined as:

$$|\sigma_n| \approx a \cdot \left(\frac{h_{TP}}{E_{TP}} + \frac{h_{adh1}}{E_{adh1}} + \frac{h_{adh2}}{E_{adh2}} \right)^{-1} \tag{1.2}$$

Where h is the height of the layer in the welding overlap and E the stiffness of that layer in the transverse direction at a given frequency and temperature for either the ED or one of the adherends, respectively. The latter part of the right side of Equation 1.2 can be generalized, resulting in Equation 1.3. Here, the left side is called the equivalent stiffness to height ratio (ESHR) of the welding overlap, with the unit GPa/m.

$$\left(\frac{E}{h} \right)_{eq.} = \left(\sum_{i=1}^{n} \frac{h_i}{E_i} \right)^{-1} \tag{1.3}$$

Table 1.1: Typical values of thermal capacity, conductivity and density for thermoplastic, composite, aluminium and steel [31].

Description	Units	Symbol	PA6	CFR-PA6	AA5754	DC01
Density	kg/m^3	ρ	1150	1500	2700	7900
Thermal conductivity	$W/m \cdot K$	K	0.3	0.6	132	52
Thermal capacity	$J/kg \cdot K$	C_p	1500	1100	900	500

Following Equation 1.2, when a joint is welded at the same amplitude and a composite substrate is replaced by a metal adherend, which is stiffer in the transverse direction, the experienced stress in the transverse direction is expected to be higher. The experienced strains will be higher as a result, and using Equation 1.1, more heat is expected to be generated. The time until first melt in the interface has been found to be highly influenced by the welding amplitude as the dissipated power is linearly related to the experienced dynamic strain. In general, it has been advised to use an amplitude as high as possible, without causing excess damage on the to be welded parts [26].

Heat conduction plays a major role in the welding process. Within TPs, which have a low thermal conductivity, the heat stays concentrated around the welding interface [23]. For FRTPs, the heat conduction through the thickness is of the same order as for the TP. Typical values for PA6, CFR-PA6, steel and aluminium are presented in Table 1.1. For carbon fibers, in the fiber direction, however, generally the thermal diffusivity and conductivity is found to be an order of magnitude higher [29, 30]. This can be used as an advantage to distribute the generated heat over the welding interface. As volumetric capacity and thermal conductivity are higher, the surface of the metal stays relatively cool during welding. This was used by Potente et al. [27], to explain why there was no fused plastic found at the steel surface of the UPW sonotrode.

In controlling the welding process, for a long time the welding time or the welding energy has been used to control the process. This is the dissipated power integrated by time. However, van Wijk et al. [32] already found, that no correlation could be found between the weld strength and the time needed in energy based welds. Also, energy based welds result in a high scatter of resulting joint strength.

The interaction of welding pressure and amplitude and their effect on sonotrode displacement and dissipated power during welding was studied by Villegas et al. [5, 22, 33]. The aim of this study was to understand the influence of these parameters on the quality of the weld. In non-hybrid welds, the feedback of dissipated power showed 5 welding stages.

- In stage 1, an increase in power is found as the weld is initiated. This continues, until an initial peak is reached, from which stage 2 begins.
- Stage 2 is in general a stepwise decline of the dissipated power. In this stage, it is observed that local heating initiates melting spots throughout the welding interface, which are seen as a cause of the drop in dissipated power.
- In stage 3, an increase in dissipated power is observed caused by melting flow onset observed in displacement of the sonotrode.
- In stage 4, a plateau in dissipated power is observed, which is seen as a combination of the effects of flow of the energy director and onset of melting of thermoplastic within

the composite substrate. This can be observed together with a drop in the rate of displacement from that point onwards.

- Finally, in stage 5, the thickness of the thermoplastic layer has become practically zero as a result of the squeeze flow of molten thermoplastic. Further melt onset and even some flow is observed in the composite layers, which results in a decline in the dissipated power.

These stages are essential in finding the optimal moment in welding at which the welding is stopped. When the process is stopped too early, not the entire overlap is molten and only locally a bond is created. When the process is stopped too late, the thermoplastic in the composite melts excessively, resulting in an increased heat affected zone and flow of the carbon fibers together with the thermoplastic. This results in a reduction of the structural integrity of the composite close to the bonding zone. The optimum moment at which the vibration phase is stopped, results in a full bond over the intended joint overlap and a minimum of melting in the composite adherend away from the interface, which means a minimal heat affected zone outside the joining interface. This moment occurs for the stages identified by Villegas in stage 4. Villegas [22, 33] proposed to simplify the controlling of the welding process by using the displacement of the sonotrode[3] together with the dissipated power to quickly determine the ultimate welding settings for joining. At a given welding pressure and amplitude, it was found, that the joint strength could be optimized by selecting a proper welding displacement [5]. From a certain displacement onwards, a drop in joint strength is observed, as a result of the deformation of carbon fiber bundles resulting from thermoplastic flow in the composite. This effect is increased, when a higher welding amplitude is used. This deformation of the fiber bundles closest to the bondline results in a reduction in lap shear strength.

1.3.2 Application of Ultrasonic Plastic Welding in Fusion Bonding Thermoplastic to Metal

The UPW technique has been used in the past to weld TPs and FRTPs, with a fiber content up to 30%, onto aluminium. As presented in the review of Ageorges et al. [34], this hybrid joining technique has been applied and described by Wise et al. [2] and Ramarathnam et al. [3]. In 2004, Krüger et al. also presented the evaluation of this welding technique.

Ramarathnam et al. [3] performed an ultrasonic weld between a surface treated aluminum substrate and an oriented polypropylene sample, resulting in lap shear strength values as high as 14 MPa when 600 Joules of welding energy was used. In this research, so-called tie-layers of amorphous polypropylene were placed in between both samples which promote preferential melting and fusion at the interface. In other tests, a tie-layer was also hot pressed onto the pretreated metallic surface. The surface treatment performed in this study was done with sodium hydroxide etching, nitric acid cleaning and consecutive phosphoric acid anodization. After this, chemically modified polypropylene was used which should react with the aluminium oxide/hydroxide on the anodized aluminium surface. It was found here that a high energy input resulted in wide fusion in the sample and a heat affected zone. This reduced the

[3]In other studies, the terms penetration, collapse or travel have been used. In this study, the term (sonotrode) displacement will be used instead.

strength of the oriented polypropylene by disorienting the crystal structure during fusion. Testing further showed that the thickness of the welding affected zone was greatly dependent on the energy input during the UPW process. This ranged from 20μm at 400 Joules to 750 μm at 1000 Joules.

Wise et al. [2] showed in preliminary trials, that a butt joint with tensile strength of up to 19MPa was possible, using UPW between aluminium and thermoplastic polyethersulphone (PES) filled with 30% volume content of glass fibers. The aluminium specimens were pretreated with either phosphoric acid anodizing or silane coupling aging. After this pretreatment, a PES solvent solution was applied as a coating, to ensure a bond between the thermoplastic and the metal surface. This coating also preserves the pretreated metal surface before application of UPW. Between the fiber reinforced plastic substrate and the metal an additional plastic film material was placed which should prevent displacement of the coating on the metal surface during welding. In addition, in some welds a carbon fiber prepreg layer was placed in between, which should shield off the pretreated metallic surface during welding. Bonds with this inclusion resulted in the mentioned tensile strengths. Without this layer a tensile strength of only 15MPa was obtained, in which in general a lower welding time resulted in a higher tensile strength of the weld. This was thought to be caused by a damaged aluminum oxide layer as a result of the UPW process.

Further research has been performed by Krüger et al. [4]. A comparative study between untreated AA 5754 & Cu as metal and Polyamide-12/E-glass (GFR-PA12) as composite was performed for UMW and UPW. For the UPW technique, an amplitude of 30 μm was used, because higher amplitudes caused cracks in the 1 mm thick sheet metal during welding. The welding was optimized to the applied welding energy, which was found to be around 2000 Joules, although a large variance was found compared to the UMW technique, with a standard deviation as large as 50 % of the found single lap shear strength of about 12 MPa. This could only be attributed to the metal-to-plastic bonding. At lower welding energies, the contact was insufficient. At higher welding energies the metal sheets and glass fibers were damaged. By cross sectional analysis of welded joints with glass fiber reinforced thermoplastic, breakage of the glass fibers was found due to the ultrasonic vibration. In a trade off with UMW, it was found to result in a weaker joint, as no connection between the carbon fibers and metal was created.

1.4 Adhesion and Surface Treatments

In this Section, adhesion mechanisms and surface treatments are evaluated which are applicable in the creation of joints between metals and FRTPs by means of UPW. In Subsection 1.4.1, adhesion mechanisms are discussed. This is followed by surface preparation techniques for bonding for aluminium in Subsection 1.4.2 and steel in Subsection 1.4.3.

1.4.1 Adhesion Mechanisms

Several adhesion mechanism theories have been proposed to describe the adhesion between materials. Kinloch [35] mentions mechanical interlocking, diffusion theory and adsorption theory as viable theories to describe the mechanism of adhesion. For the adhesion mechanism for UPW of FRTPs, the diffusion theory describes the phenomenon in which upon melting the thermoplastic molecular strings diffuse and become entangled before solidification. This theory is however not applicable to the adhesion of TPs with metals.

Mechanical interlocking is an applicable adhesion mechanism for bonding dissimilar materials. Abrasion is mentioned to not result in a good mechanical interlocking, because the imprints do not restrict the out of plane movement of the adhesive. The treatment merely results in an increased bonding area, in degreasing of the surface and of increased wetting by increased roughness. Chemical roughening, by etching or anodizing, however results into holes in which the thermoplastic is allowed to interlock. The chemical treatment further results in removal of the weak natural metal oxide surface layers, improved interfacial contact and enhanced molecular bonding.

Adsorption is a dominant part of the bonding occurring between metal and thermoplastic and can be regarded as an attracting force between both materials. Bonds created by adsorption can in general be divided into primary bonds, donor-acceptor bonds and bonds by secondary forces, which are weaker in the presented order. Primary bonds can be described as ionic bonds, covalent bonds and metallic bonds, which are known for bonds in ceramics, molecules and metals, respectively. Donor-acceptor bonds are defined as Bronsted- and Lewis acid-base bonds, in which for Bronsted pairs protons are donated from the Bronsted acid to the Bronsted base, and for Lewis pairs electron pairs are donated from the Lewis acid to the Lewis base. The weaker bonds by secondary forces are divided into hydrogen bonds and 'van der Waals'-bonds. These van der Waals bonds are again divided into permanent dipole-dipole (polar) interactions, dipole-induced dipole interactions and dispersion (London) forces (both non-polar) and all occur as a result of materials within a minimal distance of nanometers.

Both mechanical interlocking and adsorption play a role in the adhesion of adhesives on the surface of metals. The surface structure of the metal can locally enable mechanical interlocking, whereas this surface can be chemically prepared to improve adsorption of adhesives on it. When a good adhesive bond is intended, prerequisites for a high adhesive strength are intimate contact, a high attraction and mechanically strong joining partners. In order to promote intimate contact and high attractivity of either joining partner, the surface of these materials must be prepared. The function of this treatment is the removal of contaminants, increasing the difference in surface free energy between the surface and adhesive and creating a controlled roughness. As in UPW TPs are used, those which can function as hot melt adhesive can be applied to adhere to the prepared metallic surface. However, a hot melt adhesive has a number of consequences on the applied joining process, as mentioned by Minford [36] for hot melt adhesives applied to prepared aluminium surfaces:

> *"The types of thermoplastics used also have considerable variety and the relative concentrations of polar groupings present in these resins undoubtedly have a distinct correlation with their abilities to bind to the polar aluminum oxide. (...) It should be clear that flow and wetting characteristics of hot-melts are directly correlatable with temperature change. Even in the elevated temperature state, however, the structural hot-melt compositions are viscous fluids, restricting ready flow and wetting of aluminum adherends. Also, the high heat conductivity of aluminum is an ever-present negative factor in achieving maximum flow and wetting. This relates to the fact that the hot-melt that is in immediate contact with the aluminum*

surface can readily lose heat in the interfacial area to the aluminum heat sink. The melt flow at the interface will accordingly diminish when it is most critical for wetting that the spread and flow be maximum. In effect, the hot-melt in the contacting layers will slide up the curve to higher modulus levels before intimate wetting has occurred. Thus, it is absolutely essential in bonding aluminum with hot-melts to monitor the surface temperature of the aluminum adherend throughout the manufacturing process to be sure optimum flow and wetting occurs. It should also be clear that any surface contamination that can adversely affect wettability needs to be removed before application of a hot-melt." [36], Minford et al., p. 135-136.

This mentioned effect of high heat conductivity of aluminum can generally be concerned in applying hot melt adhesives to metallic surfaces. Furthermore, the metallic surface needs to be prepared for the application of an adhesive. Such surface treatments will be covered in the upcoming Subsections.

1.4.2 Preparation of Aluminium Surfaces

For aluminium substrates, a number of steps are in general performed to prepare its surface for adhesion. The aluminium oxide surface itself is mentioned to be highly polar, which enhances bonding to polar adhesives, like the amino-group containing polyamide 6. On seemingly dry oxide surfaces, molecular water can still be found up to 20 layers thick [36] as a result of these polar forces. Further, gases like carbon dioxide, carbon monoxide and hydrogen have been found to adhere to the polar aluminium oxide surface. These contaminants result in shielding off the polar sites of the metal oxide to the adhesive during bonding. Contaminants are mostly removed in an initial step by degreasing the sample, which is often performed by ultrasonic cleaning with acetone.

Subsequently, often abrasion is applied, like sanding or grit blasting. A number of benefits are mentioned by Kinloch [35] for abrasion of the metal surface. It results into an increased joint strength. This is however not caused in general by mechanical interlocking. Abrasion results in an effective cleaning action of the surface and an increased surface area. Further, the wetting kinetics are improved and the chance of crack propagation is reduced. Corundum blasting of 200 µm large particles has been applied regularly as an easy and effective abrasion technique. This results in a uniform, rough, activated metal surface. The grit blasted surface is however prone to environmental attack after longer outside exposure [13].

After abrasion, the etching procedure is performed in order to enhance pits in the metal surface and etch away the weak natural aluminium oxide layer. Examples of etching treatments are chromium acid etching and phosphoric acid etching [35–37] or nitric acid etching [38]. After this procedure, the surface is rinsed in tap water and demineralized water. The tap water enhances the forming of a controlled, stronger, aluminium oxide surface.

When nitric acid etching is used for AlMg3 alloys, this mainly will dissolve the magnesium oxides out of the aluminium adherend surface [38]. The aluminium will oxidize further, resulting in a thicker aluminium oxide surface layer with a lower weight percentage of magnesium. This results in a lower sensitivity towards salty environmental attack. Emrich [38] found a surface free energy of about 60 mN/m of which 28 mN/m was dispersive. Emrich used a drying process for 30 minutes at 40 °C in an air circulating oven [38]. Properly dried material showed cohesive failure of the adhesive. Interestingly enough, although an etching procedure of 15 minutes results in a considerable growth of the cavernous [13] aluminium oxide layer to about 80 nm thick, hardly any further growth was found after exposure for 15 hours. This type of etching has been used successfully in combination with grit blasting in further research on UMW [6] and induction welding [7, 13] of joints between AlMg3 and FRTP. It resulted in a remaining strength of 65% after twelve months of outdoor environmental exposure.

After etching, often anodization is applied to improve the durability and strength of the bond. Here, the substrate is put in an acidic liquid, upon which an electric current is applied through substrate and liquid to enable an anodic corrosive reaction on the substrate surface. This electric current results in the creation of pores on the metallic surface, made of metal oxide. At the bottom of the pores, the distance from the liquid through the metal oxide to the metal is shortest, resulting in a path of least electrical resistance. This is therefore the preferred location of further corrosive reactions. The thermoplastic can mechanically interlock inside these pores [36], which also result in an increased surface area. Anodizing of aluminium is considered to be relatively complex and therefore not easily applicable outside the aerospace sector. In the field of creating welded joints between metal and (fiber reinforced) thermoplastic, of the existing types of anodization, phosphoric acid anodization has been applied for UPW [2, 3] and resistance welding [1]. This anodization technique has been developed as a replacement of Chromic Acid Anodization (CAA), after the hexavalent chromium in CAA was found to be environmentally unfriendly [37] and carcinogenic [3].

After chemical treatments, the adhesive surface needs to be dried properly before bonding. Exposure of the aluminium oxide layer to a RH of 50% for 30 minutes resulted in a decrease by 50% of the adhesive strength, due to forming of bayerite on the surface layer [36]. Therefore, the time between removal from dry conditions and bonding should be as short as possible. Especially for alloys with a high content of Mg, such as 5052 and the applied 5754 alloy, a strong growth in electrical surface resistance is found in the first days the material is exposed to humid conditions. Interestingly enough, on the longer run, a bond with a 5000-series alloy is more durable than a 6000- or 2000-series alloy, which show a lower initial oxide layer growth and a relatively higher continuous corrosion rate after 2 days.

The usage of primers on the aluminium surface might induce a longer durability of the aluminium surface before bonding [35]. The compatibility of such a primer with polyamide and the aluminium surface should be assured. Kwakernaak et al. [37] mention the usage of conversion coatings instead of anodization to improve bonding and durability of adhesive joints.

1.4.3 Preparation of Steel Surfaces

Because of their corrosive behavior, non-stainless steels should not be treated with etching treatments [37]. Mechanical roughening, like grinding or grit blasting are recommended as surface pretreatment before adhesive joining. To prevent warpage of thin specimens, often nitric-phosphoric acid is however applied instead.

1.5 Galvanic Corrosion

A direct joint between metal and carbon fibers appears mechanically attractive. However, on the longer run, this would result in enhanced corrosion, which means oxidation of the metallic adherend as a result of the higher corrosion potential of carbon fibers. When an electric circuit is enabled by water which contains electrolytes, a contact results in a reduction reaction at the surface of the, cathodic, carbon fibers with oxygen, together with an oxidation reaction on the exposed anodic metallic surface. This effect increases with increasing volume fraction of the graphite with respect to the metal [39]. Whether a metal is self-passivating is dependent on the structural properties of the resulting metal oxide after galvanic corrosion.

The reaction rate can be reduced by reducing the cathode-to-anode exposed surface area. The aim of weight reduction in the automotive industry would result in enhanced application of carbon fibers with respect to heavier anodic metals. This results in a conflict in such aims. A coating can be used to prevent exposure to humidity and ionic electrolytic pollutants. Damage on such a coating would however greatly reduce the service life. When the usage of corrosive metals is intended, a prevention of direct contact between the carbon fibers and these corrosive metals would be a best strategy to prevent increase of corrosion rate [40].

Further, the choice of suitable metallic alloys is a way to reduce the corrosion rate. Ferritic steels should in general be protected from exposure to humid environments. In the series of aluminium alloys, the 5xxx-series has a good corrosion resistance. However, heat tempers are needed to reduce the amount of intergranular corrosion.

Lastly, as mentioned by Jones [40], corrosion should be incorporated in material choice, design, inspection, service conditions and usage of the product.

1.6 Project Objective and Research Questions

The objective of the presented research is to study the applicability of UPW to make a joint between low cost alloying materials, like often applied steel and aluminium alloys, and advanced FRTPs. This study is intended to use UPW to enable reduction in time required to create joints between CFRTP and metal during assembly stages of hybrid structures. Furthermore, this study has the purpose to examine whether recent findings in research performed by Villegas et al. in the field of non-hybrid UPW can be translated to welding between CFRTP and metallic substrates. The used UPW technique is controlled by displacement of the sonotrode by reduction of the adhesive layer thickness. It is aimed in this study to use displacement controlled welding to create an electro-insulating adhesive layer between the metal and carbon fibers to prevent aggravated galvanic corrosive behavior. In literature, two types of metallic surface preparation before ultrasonic welding of joints between metal and (reinforced) thermoplastics have been proposed. First, there is the technique proposed by Wise et al. and Ramarathnam et al., which used UPW to create joints between metal and thermoplastic by means of a coating. In the current study, this is extended in applying a composite, CFR-PA6, which widens the applied field of UPW. Second, Krüger et al. performed welding in which no coating has been used, and found a coefficient of variation in lap shear strength close to 0.5. Both will be studied in this case. Being able to perform welds without the need of applying a coating would simplify the creation of joints between CFR-PA6 and aluminium or steel. Therefore, it will be evaluated whether the application of a coating can be avoided. Next to that, the aim is to reduce the amount of variation in the obtained single lap shear strength, as more sophisticated welding feedback will be used to interpret and control welding. Finally, it is intended to expose fields in which further research is needed.

The following research questions have been applied:

1. **How does the obtained welding feedback compare for different welding set-ups?**
   In this case, welding is compared for non-hybrid welded joints and for hybrid welded joints. For hybrid welded joints, the foreign adherend material will be either aluminium or steel. For aluminium, it will be assessed what the effect is of applying the aluminium adherend as either upper or lower joining partner during welding.
2. **Can the method as proposed by Villegas for controlling the UPW process for non-hybrid welded joints be applied in the creation of joints between carbon fiber reinforced thermoplastic and aluminium or steel as well?**
   The basis of this question lies in the aim of quickly finding the appropriate welding displacement, as several stages in the vibration phase are observed, as proposed by Villegas [5].
3. **Can the application of a coating be avoided?**
   As mentioned previously, being able to omit the usage of a coating on the metallic surface will reduce the complexity and length of the pretreatment process before welding.
4. **What processing times can be achieved with the application of UPW for the applied welding series?**
   As in the automotive industry, the reduction of cycle times during production and assembly is of greatest importance.
5. **Can an electro-insulating joint be achieved between aluminium or steel and carbon fiber reinforced thermoplastics by means of UPW?**
   It is known for UPW, that it can be controlled by the vertical displacement of the welding sonotrode as a result of the outflow of molten TP out of the joining overlap. This ultimately defines the thickness of the 'adhesive layer' between the joining partners. This ability can be used to be able to determine whether an adhesive layer can be made which is thick enough to result in an electro-insulating joint.
6. **What is the single lap shear strength of the created displacement controlled UPW hybrid joints?**
   The mechanical strength of the created joint should be competitive with the strength of joints created by other joining techniques. It should be determined how the joint mechanically behaves and to which extent the mechanical behavior of the joint is affected by the application of UPW. Also, in case of metal adhesive failure, it should be assessed whether the joint strength can be improved by the application of further surface treatments on the metallic adherend.

1.7 Methodology

The applicability of UPW to create joints for hybrid structures is evaluated by means of an experimental study. In such an experimental study, the welding process, the resulting joint and the mechanical behavior of that joint need to be assessed. How this will be evaluated, will be described per objective in the following Sections. First, the usage of a protective coating(Section 1.7.1) is described. After this, the way to further evaluate the welding feedback will be presented in Section 1.7.2. How research is performed on the ability of the joint to prevent an electro conductive connection and delay galvanic corrosion behavior is described in Section 1.7.3. Finally, the way to assess the mechanical behavior of the joint & application of surface treatments is discussed in Section 1.7.4.

1.7.1 Surface Preparation of Metallic Substrates

In the work of Ramarathnam et al. [3] and Wise et al. [2], welds have been performed both by applying a coating or so-called tie layer and by welding an oriented or reinforced thermoplastic on a pretreated bare metallic surface. Oriented thermoplastics possess a higher stiffness in certain direction as a result of stretching and extrusion procedures during manufacturing. In the work of Krüger et al. [4] no coating has been applied. Both concepts are evaluated and compared in this study. The applied coating technique is further elaborated in Subsection 2.2.4. The effect of surface treatments, i.e. grit blasting and etching, is evaluated in applying different surface treatments and assess their effect on the welding behavior, resulting strength and fracture of these joints.

1.7.2 Welding Feedback and Welding Time

Thus far, research on UPW at the TU Delft has been focused on the application to create a connection between two similar fiber reinforced thermoplastic (FRTP) substrates. In short, these welds are mentioned as welding of non-hybrid joints. It has been mentioned in Section 1.3.1, that vertical displacement of the sonotrode during the UPW process can be used as a controlling weld parameter for non-hybrid joints, resulting in highly reproducible joints. This is caused by the fact, that vertical displacement can be coupled directly to the outflow of molten thermoplastic (TP) out of the welding interface. In these previous studies, changes in dissipated power during the vibration phase have been linked to simultaneous events in the heating, melting and flow of TP material. In this study, this will be evaluated as well. Welding in this study is generally stopped after reaching a provided sonotrode displacement. It is attempted to optimize this welding parameter on basis of either identified stages in welding or on the observed displacement rate, to reduce the deformation of carbon fiber bundles and maintaining higher joining strengths.

In hybrid welds (i.e. between substrates of dissimilar materials) the usage of materials with different physical properties might result in different welding behavior, for instance a different dissipated power feedback. By example, metals are generally stiffer than FRTPs in the transverse direction. Further, metallic materials have a high thermal conductivity and capacity and might with that influence the heating process. This might result in higher, or at least different, feedback of dissipated power. The applicability of feedback of dissipated power to quickly determine the proper welding conditions has to be evaluated for hybrid welded joints as well. To verify whether welds result in similar power feedback, the power feedback curves of several substrate configurations are presented and discussed. The effect of the metallic adherend as the substrate in contact with the sonotrode is evaluated and compared with those in which the FRTP adherend is the closer substrate. The effect of using a stiffer and denser steel instead of an aluminium substrate is assessed as well. The maximum service temperature and melting temperature of steel substrates are considerably higher. Also, as ultrasonic welding ultimately is a mechanical way of heating, the effect of improved bonding by the usage of surface treatment of the metal on the welding behavior is evaluated.

Welding time is an indirect parameter in ultrasonic welding. It however indicates potential cycle times in welding structures in assembly. Therefore, the resulting welding time for the selected controlling weld displacement of the sonotrode is presented as well. The welding process is further elaborated in Subsection 2.3.1.

1.7.3 Electro-insulating Behavior of Welded Joints

It has been mentioned in Section 1.5 that an effective way to prevent galvanic corrosion between corrosive metals and carbon fibers is to prevent the electroconductive connection. This means, UPW should result in an electro-insulating joint. UPW is based on joining parts by local active melting of the TP. Therefore, this could be used to prevent an electroconductive contact in the joint. A good way to assure such an electro-insulating joint is by testing whether an electrical resistance through the welded joint can be measured. Also, the resulting TP 'adhesive layer' is evaluated by cross sectional analysis. This is further elaborated in Subsection 2.3.2. Sonotrode displacement as a result of TP flow is first regarded as a controlling variable on the quality of the joint. Therefore, welds have been presented in which the welding time is controlled by the amount of sonotrode displacement as a fraction of the thickness of the energy director.

1.7.4 Mechanical Behavior of Created Joints

Applying UPW in the creation of joints between metals and carbon fiber reinforced thermoplastics will introduce the question what the strength of the created joints will be. Understanding is needed on what mechanisms act in the failure of the joint in order to be able to propose improvements of the design and joining process, and find the applicability of UPW in certain conditions. As different adherends are used, the effect of the introduction of these adherends in assessing the mechanical behavior needs to be evaluated as well. In order to evaluate the mechanical behavior, the following tests are performed.

- The strength of the welded joints is determined by means of single lap shear testing according to ASTM D-1002-05. This is done in order to value the applicability of UPW in the assembly of load bearing structures. The used welding jig is designed for the production of sample which conform to this standard.
- The strain distribution of a series of welded joints during single lap shear testing is assessed by means of Digital Image Correlation (DIC). This is done in order to determine the effect of the used adherends on the resulting lap shear strength as a result of the distribution of load over the joint overlap.
- The physical process of fracturing of welded samples is evaluated by means of fractography and cross sectional analysis of the broken samples. This is mainly convenient as such analyses result in the identification of weakest areas within the created joint

as possible areas of improvement. Also, this helps in comparing the resulting type of fracture as a result of the stress state in the joint overlap.

In Subsection 2.3.3 the mechanical test is further elaborated. The applied microscopic analysis is further presented in Subsection 2.3.4.

1.8 Outline

This report can be divided into several parts. First, the experimental set-up is presented in Chapter 2. Results for several welding series are presented and discussed in the subsequent Chapters. First, this is done for the welding power and displacement feedback and consumed time & energy during welding in Chapter 3. This is data which is retrieved during welding and used to predict the quality of the joint. The effect of the application of a coating on the metallic adherend is evaluated in this Chapter as well. Also, possible cycle times for the welding procedure are determined. The first four questions presented in Section 1.6 will be evaluated in this chapter. After this, the electro-insulating behavior of the created adhesive layer is evaluated in Chapter 4, answering question five. Results of mechanical analysis and fracture behavior is presented in Chapter 5, which answers question six. Conclusions and recommendations are presented in Chapter 6.

Chapter 2

Experimental Set-Up

In this Chapter, the experimental set-up is presented as applied in this research. This is divided into, firstly, Section 2.1 about the applied materials, and subsequently the sample preparation in Section 2.2, followed by applied experimental techniques in Section 2.3.

2.1 Materials

In this Section, relevant properties of the used materials are described. In Subsection 2.1.1 the properties of the used metals, i.e. steel and aluminium alloy, in substrates are discussed. Properties of the presented thermoplastic (TP), polyamide 6 (PA6) , and composite are presented in Subsection 2.1.2 and Subsection 2.1.3, respectively.

2.1.1 Metals

In order to be able to compare results of the current study with that of other studies in the field, it was chosen to look at frequently used materials within the creation of hybrid joints for welding methods which application are close to the field in which ultrasonic plastic welding is applied. Both Balle et al. [6] and Mitschang et al. [7] used AA5754 as aluminium, DC01 as steel and polyamides as TP in ultrasonic metal welding (UMW) and induction welding, respectively. As both techniques would ultimately be traded off against the technique of ultrasonic plastic welding (UPW), a logical step is to use the same materials in the current study. Therefore, AA5754 was used as an aluminium and DC01 as a steel alloy in this study. Both metals are widely used in the automotive industry.

AA5754, or AlMg3, is an aluminium alloy with Magnesium as major alloying material and is used as well in the current study. As mentioned in Section 1.5, it has a higher resistance against corrosion. The material experiences a phase change resulting in recrystallization above its maximum service temperature between 197 and 215 °C, and melts around 620 °C [31]. It must be mentioned, that in this research the effects of treatments and welding above the service temperature of aluminium has not been evaluated. The effects of viscoelastic heating in the polycrystalline aluminium adherend itself above these temperatures is neither assessed.

As a steel, a cold rolled high strength low alloy steel was applied, indicated as DC01. It has been mentioned by Balle [41], that steel currently makes up about 40 % of the weight of general car structures. The mentioned steel type is, as a relative soft metal mostly used as a metal for platings. It has a melting temperature of about 1500 °C.

For both metals, 2 mm thick plates were ordered at Salomon's Metalen B.V. Upon arrival, these metallic plates were cut and milled to size of 1 by 4 inches (i.e. 25.4 by 101.6 mm) of which the latter size was in the rolling direction.

2.1.2 Thermoplastic

As mentioned in Section 2.1.1, materials were selected to be able to compare the results in this study with the results in the study of other innovative welding techniques applied in the automotive industry. Therefore, a PA6 was selected as the used TP material. It is known as a semi-crystalline thermoplastic, which has, compared to its price, relatively high mechanical properties.

The used TP for coating the metal samples and creating the energy directors was equal to the TP which has been used as a composite matrix. This is a black ULTRAMID B EXPERIMENTAL PA6 material from BASF, provided as a 0.14 mm thick film material by Ten Cate Advanced Composites BV.

In order to determine the physical properties of the used PA6 during further experiments and treatments a number of analyses were performed. These were thermogravimetric analysis (TGA), differential scanning calorimetry (DSC) and dynamic mechanical thermal analysis (DMTA). From the TGA, serious loss of mass was observed to start from 300 °C onwards, with ignition around 385 °C. When DSC was applied, a melting onset around 210 °C was observed with a melting temperature of about 220 °C. A T_g of around 57 °C was observed as well by means of DSC for dry material. DMTA results showed a storage modulus of 3.3 GPa at room temperature in dry conditions. The glass transition temperature, T_g was found with a maximum loss modulus for dry materials around 66, 71 and 79 °C for testing rates of 0.1, 1.0 and 10 Hz, respectively. Further elaboration and accompanying figures can be found in Appendix A.

PA6 does, however, adsorb water readily because of its polar nature. As this results in a reduction of the glass transition temperature, weight gain and potential disbonding on the adhesion surface, such water intrusion should be incorporated into the design process. Samples were dried in a vacuum oven for 48 hours at 50 °C before performing the coating operation of metals, welding procedures or mechanical tests.

2.1.3 Composite

The selected composite in this case is a carbon fiber reinforced PA6 (CFR-PA6) provided by Ten Cate Advanced Composites BV. The type of TP is equal to what has been described in Section 2.1.2. A plain weave has been used, of which about 89% of the fibers lay in warp direction in 12k bundles and the rest lies in weft direction in 3k bundles. A 5 layer, about

2.1 mm thick, UD-like stacking has been used, with a resulting fiber volume fraction of about 50%.

Of this material, the stiffness in the warp direction is mentioned to be higher than 85 GPa. The flexural stiffness in warp direction lies around 75 GPa, in weft direction about 15 GPa [42].

2.2 Sample Preparation

In this Section, the applied procedure of preparation of samples is described. In Subsection 2.2.1, the preparation of composite substrates is presented. This is followed by an elaboration of the hot press fabrication of energy directing thermoplastic films (EDs) in Subsection 2.2.2. In Subsection 2.2.3 the applied surface treatments are presented. The method of applying a PA6 coating is presented in Subsection 2.2.4. The production of reference samples which were adhesively bonded is presented in Subsection 2.2.5.

2.2.1 Preparation of Composite Samples

Upon arrival, composite laminates were inspected by applying a C-scan. No significant shortcomings were found, except for some small disturbance created within 1 cm of the edge of the composite laminate. Samples were cut out of the panel by water jet cutting, performed by an external company. Upon receiving, the edges of the samples were deburred with Scotch Brite. After this procedure, the material was dried in a Heraeus VTR5036 vacuum oven at 50°C for at least 48 hours before applying further tests or treatments.

2.2.2 Hot Press Fabrication of Energy Directors

A film of polyamide 6 (PA6) has been applied between the two substrates which were welded together. The function of this thermoplastic film, which stiffness is lower than the transverse stiffness of the carbon fiber reinforced adherend, is to result in most deformation during the applied welding procedure, resulting in a preferred location of melting. Such a film has been referred to as a thermoplastic energy directing film (ED).

EDs have been produced in the following way: Film of PA6 with a thickness of 0.14 mm has been cut to size of 45 by 45 cm and stacked, spot welding the corners using an ultrasonic spot welding device. EDs used in welds presented in this report consisted of three layers, resulting in a thickness of 0.42 mm. This stack was put between two stainless steel plates, which were cleaned with PT technologies PF-SR sealant remover and waxed with Marbocote releasing agent. The stack was then put in a JOOS hot press, which was heated at a rate of 7 °C per minute to 210 °C, the melting onset temperature of the used PA6. This temperature is used to promote bonding between the PA6 film layers. After holding the program at this temperature for ten minutes, the pressure was increased from 0.1 MPa to 2 MPa in one minute. After this, the temperature stayed on 210 °C temperature for another ten minutes before cooling back down to 40 °C at a rate of 7 °C per minute. After staying an additional seven minutes at this temperature, to provide enough time for the press to cool down locally, the pressure of 2 MPa was removed. Subsequently, the film was dismounted from the press. The cohered 0.42 mm thick films were then cut in EDs of 27 by 29 mm to function as energy directing

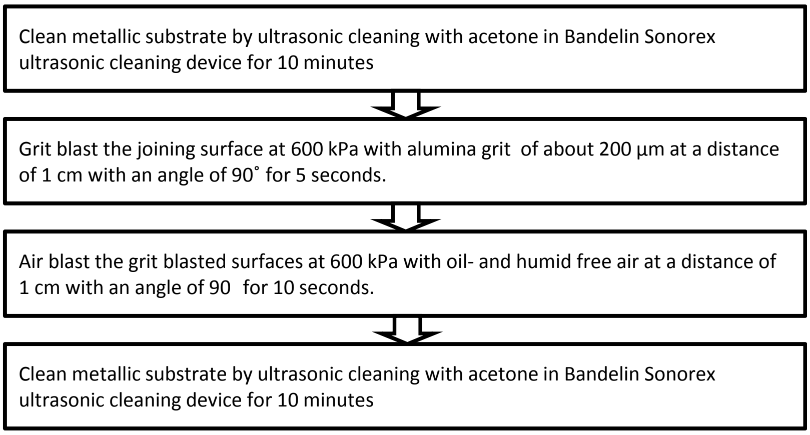

Figure 2.1: The applied acetone degreasing and grit blasting procedure.

films during welding. These EDs were dried for at least 48 hours in a vacuum oven at 50 °C before performing subsequent tests.

In some of the presented welding series, an ED with a thickness of 0.28 mm was used. These were used in initial trials, at for instance the presented series with uncoated aluminium adherends and a series of non-hybrid welded joints for which the electrical resistance was measured. In order to reduce the equivalent stiffness to height ratio (Equation 1.3) to reduce the induced stresses as a result of the applied amplitude, it was chosen to apply thicker EDs of 0.42 mm for other series. It is indicated in the text when the 0.28 mm thick EDs are used. It can be assumed in other cases, that 0.42 mm thick EDs have been applied.

2.2.3 Metallic Surface Preparation

Before using the metallic samples in ultrasonic welding, the surface of the samples was pretreated and coated. As the aim of this study is to be able to understand the process and be able to compare the results of this process, the used surface treatments are comparable to the used surface treatments in the work of Mitschang et al. [7] and Balle et al. [6].

After removing surplus of grease with a wiping paper, acetone degreasing and grit blasting was performed in the joining zones as presented in Figure 2.1. In the case that no nitric acid etching was performed on these samples, they were stored in a vacuum oven at 50 °C until the procedure to apply a coating of PA6 film on the treated surface. This was done to prevent exposure to moisture of the prepared surface during this time interval. Metallic samples which have been treated in the aforementioned way are in this report further referred to as grit blasted substrates.

In case etching was performed, the aluminium surface was etched after earlier degreasing- and grit blasting treatments according to Figure 2.2. As immediate preparation of these samples for the coating treatment could not be performed, the samples were stored in a vacuum oven at 50 °C to prevent exposure to moisture of the pretreated surface in the mean time. Metallic samples which have been treated with the aformentioned grit blasting treatment and the etching procedure are further referred to as grit blasted & etched samples.

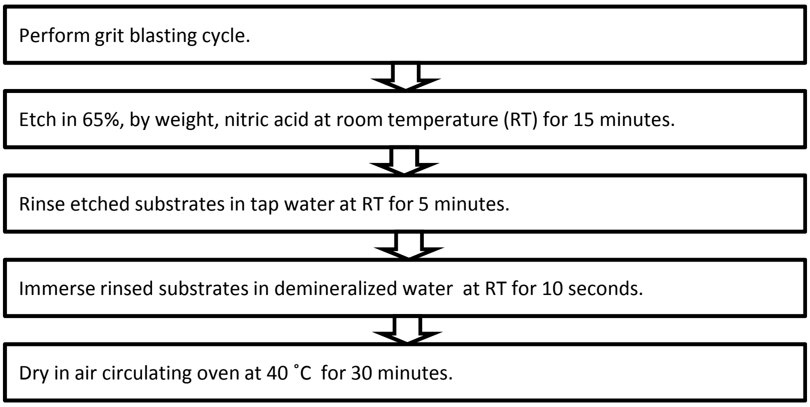

Figure 2.2: The applied nitric acid etching procedure [38].

2.2.4 Method of Applying Thermoplastic Coating

A PA6 coating was applied on several series of metallic samples at the location where the composite samples were intended to weld onto. This was done in order to protect the metal bonding surface and assure intimate contact between the thermoplastic and pretreated metallic surface. This coating was applied by means of a hot oven cycle, in which vacuum bagging was used in order to assure intimate contact throughout the treatment. This vacuum bagging was performed as presented in Figure 2.3. The used materials were all able to cope with temperatures higher than 250 °C. A metallic spring was inserted into the silicon tubing to prevent closure of the tubing by the applied vacuum. The steel mold itself was waxed with Marbocote 227CEE release agent. A PA6 film was cut to size and placed on top of the treated surface of the metal and taped at the edges to the metallic pieces which acted as a mold. An example of the vacuum bagging package is shown in Figure 2.4. It should be mentioned, that indeed six samples per series were prepared. It is acknowledged, that the resulting quality of the coated samples might differ from series to series in the time needed for vacuum bagging the produced samples. Moreover, the varying ambient air conditions, where surface treated samples were exposed to before completion of this vacuum bag, might influence the joint quality as well. In producing larger series it was found, that preventing wrinkles in the vacuum bagging foil was harder. Therefore, the amount of samples per series were limited with the used technique.

A heating cycle was performed in which the Heraeus UT6200 oven was heated to 250 °at about 3 °C per minute and stayed at that temperature for at least 20 minutes. After this, the oven was cooled down slowly with an average cooling rate of 1.8 °C per minute. The oven door was opened at around 70 °C to enhance the cooling rate from that temperature onwards to about 2.8 °C per minute. Vacuum was applied throughout the oven cycle until the oven was cooled back to 40 °C. Then, the coated metallic samples were removed from the oven. An example of the resulting coated metal specimens is shown in Figure 2.5.

Whereas in the presented results, only a coating was applied from a film with a thickness of 0.14 mm, trials were also performed in which a thickness of 0.42 mm was applied. With the application of a thicker coating the usage of an ED was not needed. However, with the currently applied technique of applying a coating, a thermoplastic bulge was created on the metallic surface. This focuses welding on the center of the overlap where a physical contact

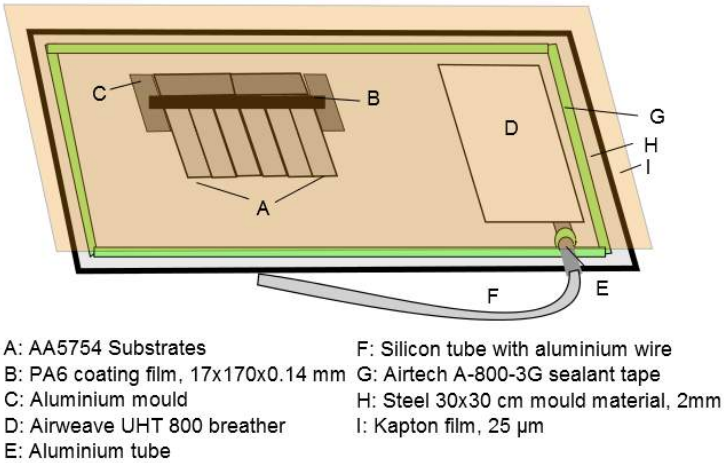

Figure 2.3: Scheme of vacuum bagging set up as applied in application of a thermoplastic coating on the metallic surface.

was created. To prevent that, other coating techniques, like using a hot platen press, can be applied.

2.2.5 Production of Adhesive Reference Samples

In order to validate performed hybrid welds, a reference process has been applied, in which a grit blasted and etched aluminium plate was adhered on a plate of carbon fiber reinforced PA6 (CFR-PA6) by means of a slow curing 3M™ Scotch-Weld™ EC-9323 B/A. This adhesive is known to result in at least 28 MPa of single lap shear strength for carbon fiber reinforced epoxies and results in comparable or higher bond strengths when applied to pretreated aluminium. It further is known to bond well with thermoplastics like PMMA. In the adhesive, 200 to 300 µm in diameter large glass beads were applied, in an amount of 8.9% by weight of the B-part of the adhesive. These were applied in order to assure an adhesive layer thickness and prevent excessive outflow of adhesive out of the joint overlap under application of pressure through vacuum bagging. Limited outflow resulted in the creation of fillets at both sides of the overlap.

The laminate of CFR-PA6 was pretreated by means of exposure to UV/Ozone for five minutes. This was done, as nylons themselves are known to be hard to adhesively bond. The used surface treatment is known to be an applicable technique to chemically prepare the thermoplastic surface by controlled local oxidation. Through the created sites, the adhesive can chemically bond with the surface. An aluminium, AA 5754, plate of 11.5 by 19 cm was degreased, grit blasted and etched in the same way as described in Section 2.2.3 and stored in a vacuum oven at 50°C before adhesive bonding.

The vacuum bagging has been performed as presented in Figure 2.6. All applied materials were able to cope with temperatures higher than 100 °C. A metallic spring was inserted into the silicon tubing to prevent closure of the tubing by the applied vacuum. The mold itself was

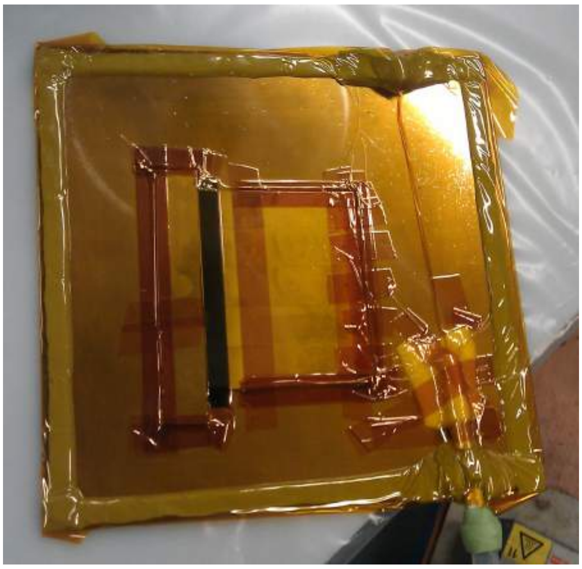

Figure 2.4: Vacuum bagging concept for coating of metal surface with PA6.

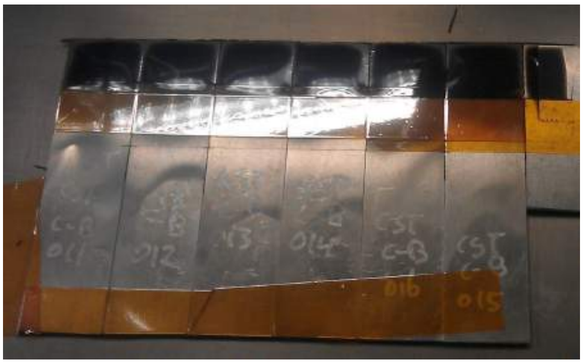

Figure 2.5: Metallic samples after applying a thermoplastic coating on the pretreated zones, intended for welding.

waxed with Marbocote 227CEE release agent. The aluminium substrate was put as bottom substrate and aligned against a wooden plate, in order to prevent movement throughout the oven cycle. The adhesive was applied in the joining zone, and excess adhesive was removed before application of a vacuum. A joint overlap of about 12.7 mm was created. Throughout the placement of each substrate or plate, these plates where firmly attached to the steel mold by means of the used tape. After testing of air tightness, the vacuum bagged package was cured in a Heraeus UT6200 oven at 65 °C for 3 hours.

Samples were milled out of the substrate with a width of 25.4 mm by an external company and dried in a vacuum oven at 50 °C for at least 48 hours before single lap shear testing.

2.3 Applied Experimental Techniques

This Section is focused on the applied techniques in the presented research. In Subsection 2.3.1, the applied process of ultrasonic plastic welding (UPW) is elaborated on the used welding device, a description of the welding process and the used welding settings. This is followed in Subsection 2.3.2 by the applied technique in measuring the electro-insulating behavior of the joint. The technique of evaluating the mechanical behavior in single lap shear testing is presented in Subsection 2.3.3. Finally, the used technique of microscopic analysis is presented in Subsection 2.3.4.

2.3.1 Ultrasonic Plastic Welding

Ultrasonic plastic welding is presented in three parts. First, the used device and jig is presented. After this, the welding process is presented. Finally, the applied welding settings are presented.

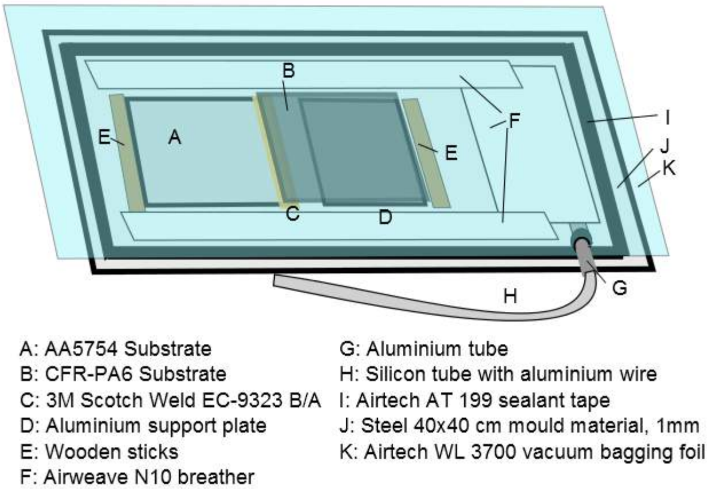

Figure 2.6: Scheme of vacuum bagging set up as applied in curing of adhesively bonded joints.

Welding Device

A Rinco Dynamic 3000 UPW device was used in this study, which is shown in Figure 2.7a. Basically, the functioning of this machine has been described by Villegas et al.:

> *"Pressure and vibration are exerted simultaneously by a sonotrode, connected through a booster to a piezoelectric generator, which converts a high-frequency alternating current into high-frequency vibrations. Likewise, this ultrasonic stack (converter/booster/sonotrode) is connected to a pressure actuator."* [22]

The mentioned high frequency lies around 20.1 kHz. Compared to other devices, the Rinco Dynamic 3000 is able to control the process by means of vertical displacement of the sonotrode during the process as a result of reduced thickness of the welding stack. This displacement is generally caused by outflow of molten thermoplastic (TP) during the welding process. Throughout the process, every millisecond the experienced force, power and vertical displacement is recorded. The force is measured and displayed in Newton, the displacement in mm and the power in percentage of the maximum consumable power of 3000 Watts. After welding, the total used welding time and -energy, together with the total vertical displacement from the start of the welding process until the end of consolidation is recorded. The welding process can be controlled by a given consumed amount of energy, power, and vertical displacement. A titanium alloy sonotrode with a rectangular contact surface of 1.5 by 3.0 cm and an amplification of 1:2.75 was applied, together with a booster with an amplification of 1:2. As welding has been applied with the mentioned device, from these tests it is not clear whether the obtained results can be translated when another device or sonotrode is used.

Welding Process

The performed welding procedure is as follows. The thickness and width of samples are measured, after which the substrates and energy director samples were cleaned with PT

(a) **(b)**

Figure 2.7: Rinco Dynamic 3000 UPW device (left) and used set-up of sample jig.

technologies PF-QD Quick Drying Cleaning Solvent. The polyamide 6 (PA6) coatings of the coated metal substrates were cleaned as well with PF-QD. In case of uncoated grit blasted metal substrates, the surface was not cleaned after removal from the vacuum oven, as this procedure would only contaminate the surface. The thermoplastic energy directing film (ED) was taped onto the lower substrate, which was put in the lower part of a metal welding jig, shown in Figure 2.7b. After that, the ED was further attached to the bottom of the jig with some more tape. The upper substrate was then installed as well in the upper part of the jig. This upper jig is guided by four metal vertical cylinders which enables freedom in vertical movement to prevent unwanted flexural stresses on the joint during welding. Springs are installed, such that the upper jig is prevented to press the upper substrate onto the lower substrate before welding.

When welding starts, the sonotrode of the UPW device pushes the upper substrate down, due to which it makes full contact with the ED on top of the joining area of the lower substrate. The force with which the sonotrode is pushed onto the welding area is increased with 500 N/s until the provided welding force is reached. At that moment, the vibration phase starts and the sonotrode vibrates with the given amplitude and a frequency of 20.1 kHz onto the joining surface of the upper substrate. This amplitude results in compression of both the substrates and the ED. As a result of the frictional- and viscoelastic heating of the ED caused by the vibration, the thermoplastic starts to melt and flow. Upon contact with other molten thermoplastic, diffusion takes place. This flow results in vertical displacement of the sonotrode. Ultrasonic vibration is applied on the interface by the sonotrode until the desired amount of time, energy or displacement is reached. At that moment, the vibration is stopped and the solidification phase begins, in which the interface cools down under the application of an equal or increased pressure force for several seconds.

In the attached welding controller is configured whether welding is stopped at a certain reached amount of energy, time or displacement. In the presented set of welds, in general the amount of displacement of the sonotrode is used as the controlling parameter for the duration of the vibration phase. In practice, the displacement is also expressed in percentage of the thickness of the ED.

After welding and consolidation, the welded substrates were removed from the welding jig, dried for at least 48 hours upon which mechanical tests or other analyses could be performed.

Welding Settings

To be able to determine the differences in welding feedback when different material systems are used, the welding pressure and used amplitude is equal for all performed welds. As the equivalent stiffness-to-height ratio of a given welding overlap is set, it has been decided to use an as low as possible amplitude with the given welding sonotrode and booster, to prevent excessive damage when metallic samples were welded. A welding amplitude of 36.3 µm, i.e. a peak-to-peak amplitude of 72.6 µm, was generally used in the results presented in this report. A welding pressure of 800 N, or 2.5 MPa, has been applied to the welding interface. This pressure has also been applied in the work of Krüger [4] and is somewhat higher than the pressure used in other studies. This is done to assure more contact surface area during welding at a lower amplitude. The welding behavior is analyzed, and if the stages described by Villegas (see Section 1.3.1) are recognized, the controlling sonotrode displacement according to displacement found in stage 4. If this is not the case, a controlling displacement is based on the displacement at which the rate of displacement starts to decline from a maximum value. In the presented study, an additional series of grit blasted, etched and coated aluminium substrates has been welded until a relative displacement of 66 % of the thickness of the ED to validate the resulting lap shear strength at 100 % displacement. Once welding finishes, a consolidation time of 4 seconds has been applied at an equal pressure of 2.5 MPa, i.e. 800 N. This has been done to mitigate any potential secondary effects of increasing the welding pressure. A welding overlap of 12.7 by 25.4 mm was welded, conforming to ASTM D1002-05.

2.3.2 Measurement of Electro-insulating Behavior of Welded Joints

Electrical conductivity of the welded joint is measured using an electrical multimeter, from which the electrical resistance is measured. In this case, contact points of the measuring device are placed onto an electroconductive location of either adherend. It has been assured for these locations, that they result in an electroconductive throughout the entire adherend. The absence of a measurable electroconductive connection with the used measuring device suffices in this research. Next to this, the thickness of the electro-insulating thermoplastic adhesive layer is determined for a number of welds by means of cross sectional analysis.

2.3.3 Mechanical Testing of Joints

Mechanical tests were performed following the ASTM D1002-05 standard using a Zwick 250 kN tensile testing device. Samples were removed from the vacuum oven and cooled down back to room temperature.

A joint overlap length of 12.7 mm was used for the 25.4 mm wide samples. This overlap with an area of 322.58 mm^2 was used in the calculation of the resulting shear strength of the overlap. Here, the maximum experienced load in Newton was divided by the overlap area in square millimeter, resulting in the shear strength of the overlap in MPa. Used samples had a thickness of about 2 mm. A distance of 60.0 mm was set between both gripping ends at the start of each test. For clamping, first the upper clamp was closed, upon which for the lower clamp was assured, that the clamp did not bend the sample upon closing. After the test started, first, the clamping pressure was increased. After this, force was put onto the joint by increasing the distance between both grip ends with 13 mm per minute until the joint failed. This failure was set as 20 % of the maximum load.

In a number of tests differential image correlation has been applied to evaluate the strain distribution. Welded joints were sanded at the side of the overlap and cleaned by air blasting. Subsequently, a white paint was sprayed on the side, which dried for 1 hour. With a paint brush, black fine speckles were applied on this white paint. During mechanical testing, every 250 ms a picture was made. Pictures were correlated by means of VIC-2D™ software. Here, a subset of 29 pixels was used with a step size of 5 pixels.

2.3.4 Microscopic Analysis

Samples for microscopic analysis, either fractography or cross section analysis, were prepared by cutting them by means of a Struers Secotom 10, using a silicon carbide blade, meant for soft non-ferrous alloying materials. In case of cross sectional analysis, these samples were embedded in Technovit® 4071. Subsequently, the embedded materials were sanded and polished using a Struers Rotopol and Pedemat automated polisher.

Spectral electron microscopy was performed on a JEOL JSM-7500F Field Emission Scanning Electron Microscope. In general, low secondary electron images and backscatter electron images were taken to observe texture and composition, respectively. The former results in a better sight on the relief of the structure and is indicated by "LEI", whereas the latter, indicated by "COMPO" on the images, results in a clear difference in electron reflection, resulting in metallic material to appear lighter compared to thermoplastic material. All specimens were sputtered with gold particles before analysis with an electron microscope was performed.

Chapter 3

Results of Welding Process and Dissipated Power & Displacement Feedback

In the previous Chapters, the objective, methodology and experimental set-up were presented. Several welding series were welded and analyzed of which results is presented in the upcoming Chapters. In the current Chapter, the objective is to present feedback and findings of the ultrasonic plastic welding (UPW) process itself. Examples of welded samples are presented in Figure 3.1. The obtained welding feedback was evaluated for several series of welds with different pretreatments and adherend stacking orders. Furthermore, particular optical observations during welding are presented. Next to that, the usage of different controlling parameters is discussed. Obtained welding times are presented as well.

In Section 3.1 the welding power and displacement feedback from non-hybrid welds is presented and discussed. This is presented for hybrid welds between aluminium and carbon fiber reinforced polyamide 6 (CFR-PA6) substrates with several different preparations of the metallic adherend in Section 3.2. Here, welds without the application of a coating, and welds with the application of a polyamide 6 (PA6) coating on the aluminium adherend are discussed with this adherend as either upper or lower joining partner during welding in the latter case. Welding feedback in which steel was used as the metallic adherend is presented in Section 3.3. Steel was only used as lower joining partner during welding. A comparison of several aspects of the welded series is presented in Section 3.4. The discussion is presented in Section 3.5.

3.1 Reinforced Thermoplastics on Reinforced Thermoplastics

As a reference, non-hybrid welds, between two CFR-PA6 adherends, were performed. For the welds performed between two composite substrates, the welding feedback is presented in Figure 3.2 by means of dissipated power and resulting vertical displacement of the sonotrode. Only in weld 4, the power feedback followed the stages as described by Villegas et al. [22].

Figure 3.1: Welded samples: non-hybrid (top), aluminium without coating to CFR-PA6 (middle) and aluminium with coating to CFR-PA6 (bottom).

This means, both an initial and secondary peak could be observed during this weld cycle. The identified stages are demarcated in the Figure. For the other welds in this series, only the initial peak in dissipated power could be clearly observed, demarcating the end of stage 1. A variety in the height of this peak could be observed. Next to weld 4, a smaller secondary peak in dissipated power was only observed in weld 3. For all the welds of which stages 3 and 4 were not recognizable in the feedback of dissipated power, the same displacement behavior was recognizable, however.

The shape of the displacement curves showed to be similar for all performed non-hybrid welds. A drop in displacement rate was observable after a displacement of 0.25 mm. Hyptoheses about this drop in displacement are elaborated in Section 3.4. It is thought to be affected by either the deformation of fiber bundles or the reduction of the average temperature in the overlap as a result of squeeze flow.

The single lap shear strength (SLSS) of non-hybrid welded joints, whose welding process were presented in Section 3.1, were found to be 37.6 MPa on average with a coefficient of variation (c.o.v.) of 3.1 % when a displacement of 100 % of the thickness of the ED was applied during welding. A resulting fracture surface is presented in Figure 3.3. Contrary to what was found at both higher and lower amplitudes [5] by Villegas, only limited deformation of the fiber bundles was observed at 100 % displacement at the low amplitude used in this study. Welding was also performed at a lower displacement. It was chosen to use a displacement of 66 % (i.e. $\tilde{0}.28$ mm), because from this displacement onwards the displacement rate drops. In the work of Villegas [5], such a drop in displacement rate could be observed at the displacement at which onset of deformation of fiber bundles could be observed. This deformation has been identified to negatively affect the resulting SLSS. When the welds were performed until a displacement of 66 % of the thickness of the ED is reached, a SLSS of 33.2 MPa with a c.o.v. of 9.5 % was measured. This average strength was a reduction of 8.8 % compared to the welds with 100 % displacement. When the fracture surface of both series was compared, it was observed,

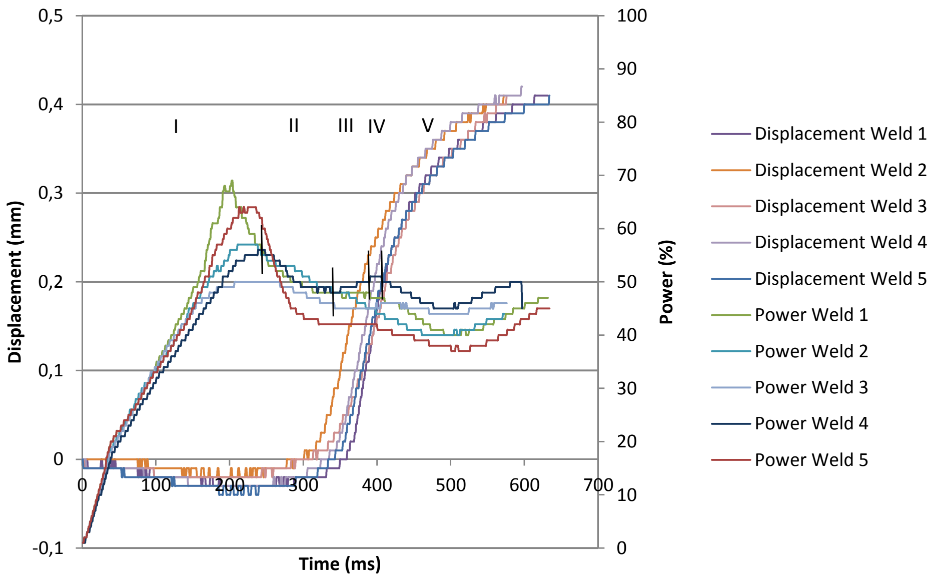

Figure 3.2: Power and displacement curves for ultrasonic welds between composite and composite substrate. Around 0.24 mm displacement, phase 4 is observed, in which the welding is preferably stopped [5]. From that point onwards, a drop in the displacement rate was observed.

that slightly more sideways deformation of the carbon fibers occurred as a result of flow of the thermoplastic when 100 % displacement was applied. This weft fiber deformation was however restricted by the warp fibers.

The welded series at 100 % displacement showed the highest SLSS, and only a limited amount of fiber deformation was observed in that case. Therefore, it was decided to apply 100 % displacement for hybrid welded joints as well. The vibration (or heating) time for both series were 0.5 and 0.6 seconds, respectively. So, although the welding time increased with 100 % displacement with respect to 66 %, still a very low amount of time was consumed during the vibration phase. As 100 % displacement is used in that case, the analysis of the electro-insulating behavior of the created joints is evaluated with a less conservative approach. If an electroconductive joint is obtained, the displacement is intended to be lowered until electro-insulation is obtained. From the work of Gleich et al. [43], it is known that a lower adhesive layer thickness results in lower peel stresses, by which a higher single lap shear strength (SLSS) can be obtained. A higher displacement can with that result in a higher SLSS. It is more clearly assessed, how the stages develop for hybrid welded joints and how that compares to what has been obtained for non-hybrid welded joints, as presented by Villegas et al [5].

3.2 Reinforced Thermoplastics on Aluminium Substrates

Several series were welded to create joints between carbon fiber reinforced polyamide 6 (CFR-PA6) and aluminium alloys. These series are presented in the following Subsections. In Subsection 3.2.1, welds are presented, in which the aluminium surface has been prepared by grit blasting, but no coating has been applied. These welds were performed with the CFR-PA6 adherend in contact with the sonotrode. Welds were performed with and without using

Figure 3.3: Fracture surfaces of a non-hybrid joint after single lap shear testing, welded until a displacement equal to 100 % of the thickness of the ED.

Figure 3.4: Fracture surfaces of a non-hybrid joint after single lap shear testing, welded until displacement equal to 66 % of the thickness of the ED.

an ED between the adherends. This set-up also resembles more closely the work performed by Krüger [4]. In Subsection 3.2.2, welds are presented in which a coating was applied after performing surface treatments on the metallic substrate. Here, the CFR-PA6 substrate was in contact with the sonotrode. In Subsection 3.2.3, the same preparations were applied as in Subsection 3.2.2. Here, however, the aluminium adherend was in contact with the sonotrode during welding.

3.2.1 Non-coated Aluminium as a Bottom Joining Partner during Welding

In Figure 3.5 an overview is presented of power and displacement feedback during welding for welds in which no coating was applied on the metallic surface. In this series, an ED with a thickness of 0.28 mm was applied instead of 0.42 mm. Next to a clear peak at the beginning of the vibration phase, no clear pattern could be observed in the dissipated power, compared to non-hybrid welded joints. The displacement curves showed three phases after displacement onset onwards. Until a displacement of 0.08 mm, an initial high displacement rate was observed. After this, a drop in the rate of displacement could be identified. The rate of displacement increased again from a displacement of 0.15 mm onwards. A vibration could be observed as well in these curves.

After welding, no bond was created. The surface of both adherends after welding are presented in Appendix D.1. In Figure 3.6, the thermoplastic surface after welding is presented by SEM microscopy. Metallic particles in several sizes were observed on the thermoplastic surface. The roughened metallic surface was mechanically abraded by the thermoplastic of the ED, and

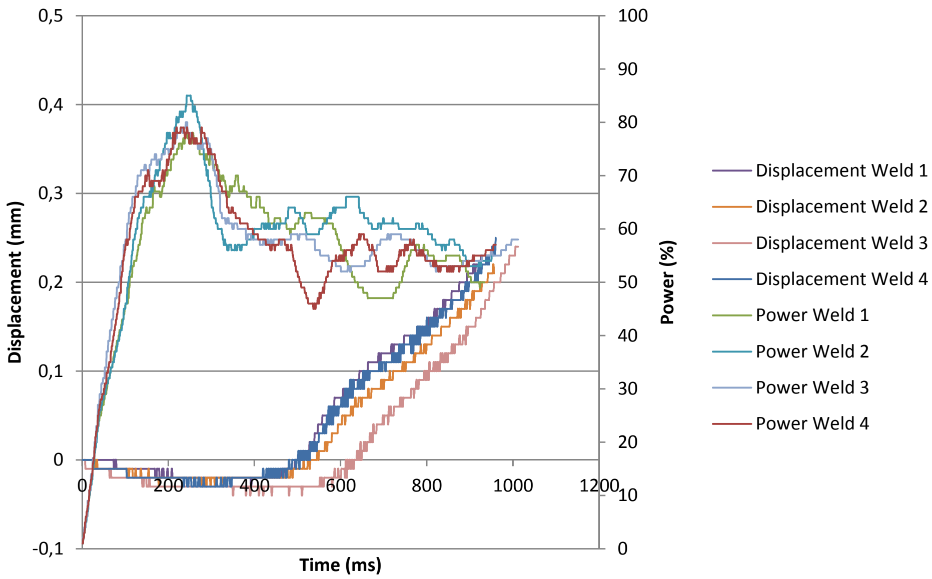

Figure 3.5: Power and displacement curves for ultrasonic welds between grit blasted, non-coated, aluminium and CFR-PA6 substrate, with the latter as top adherend.

broken off particles were imprinted into the thermoplastic surface. It was therefore thought, that troughout the entire welding cycle no bond was created between the thermoplastic and metallic surface. From this observation, the vibration in the displacement in Figure 3.5 was attributed to the absence of a bond between both substrates during welding. The absence of a bond does not correspond with what has been presented by Krüger et al [4]. Main differences in this case were the fact, that a higher peak-to-peak amplitude was used of 72.6 µm, i.e. a peak amplitude of 36.3 µm, and that the CFR-PA6 substrate was in contact with the sonotrode during welding instead of the metallic adherend. Krüger et al. used a peak amplitude of 30 µm.

Attempts were performed as well in which no ED was used during welding of CFR-PA6 onto a grit blasted metallic substrate. Only more aggravated results were found, with higher dissipated power and a more eroded surface. In these applied welds, no bond was created either. The resulting appearance of the substrates after welding is presented in Appendix D.1. In those welds the erosion induced by welding on the grit blasted aluminium surface created a pattern equal to the weave structure in the surface of the composite adherend. Further, heating in the thermoplastic was not concentrated to the interface between both adherends. Melting of thermoplastic could also be observed on the side of the composite adherend which was in contact with the sonotrode. Attempts have also been performed with EDs with a thickness of 0.42 mm in this series. However, also in that case, no bond could be created between the metallic surface and the thermoplastic.

3.2.2 Coated Aluminium as a Bottom Joining Partner during Welding

In Figure 3.7 the feedback of dissipated power is presented of the UPW process obtained during welding between coated grit-blasted metal adherends and CFR-PA6, together with the resulting vertical displacement of the sonotrode. After an initial rise in dissipated power,

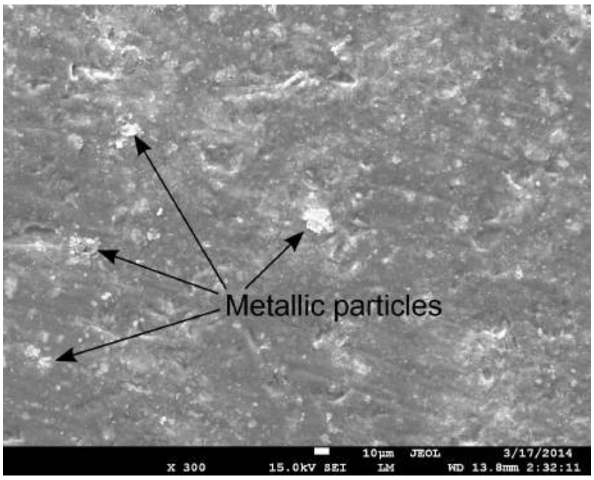

Figure 3.6: Thermoplastic surface after welding with uncoated aluminium adherend. Particles were eroded from the aluminium surface and impressed into the thermoplastic surface.

beyond 60% of the maximum dissipated power of 3000 Watt, no clear pattern in the dissipated power feedback could be recognized. The displacement curves of the welds performed in this series showed a low variety in the shape of the displacement curve after onset of the displacement phase. A drop in the rate of displacement from a displacement of 0.30 mm onwards was observed.

The feedback of dissipated power and vertical displacement of welds with grit blasted, etched and coated metal adherends, is presented in Figure 3.8. The initial rise in dissipated power was found to be rather constant for all welds, i.e. no initial peak in dissipated power was observed. A maximum in dissipated power was only observed around the time of onset of displacement. During the time span in which the displacement took place, a drop in the dissipated power could be observed. In the series presented in Figure 3.8, the rate of displacement reduced from a displacement of 0.30 mm onwards. For Weld 1 and Weld 4, a sudden increase around 60 ms was observed in the measured displacement. From further examination, the cause of this increase could not be identified. Where displacement behavior in Figure 3.7 was observed to follow the same pattern, some scatter was found in this series.

In both series of welds presented in this Subsection, an initial peak in the power curves was absent. No significant differences between power curves in both series could be observed. The initial peak which was observed in Figure 3.5 was not observed in the power curves in this Subsection. As in this case no significant abrasion on the rear surface of the metallic adherend was observed, this supports the hypothesis, that the initial peak in the previous Subsection was caused by abrasion.

3.2.3 Coated Aluminium as a Top Joining Partner during Welding

Dissipated power and sonotrode displacement are presented in Figure 3.9 for welds with an aluminium substrate as upper welding partner, and therefore in direct contact with the sonotrode during welding. These welds resulted in dissipated power feedback which was more similar to the power feedback observed for non-hybrid welds. In Weld 1, welding was

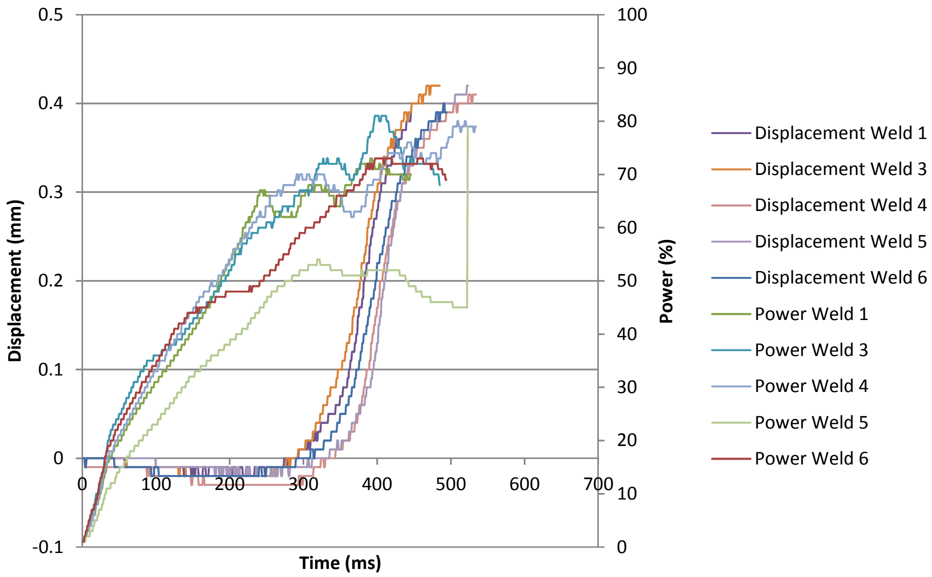

Figure 3.7: Power and displacement curves for ultrasonic welds between grit blasted & coated aluminium and CFR-PA6 substrate, with the latter as top adherend.

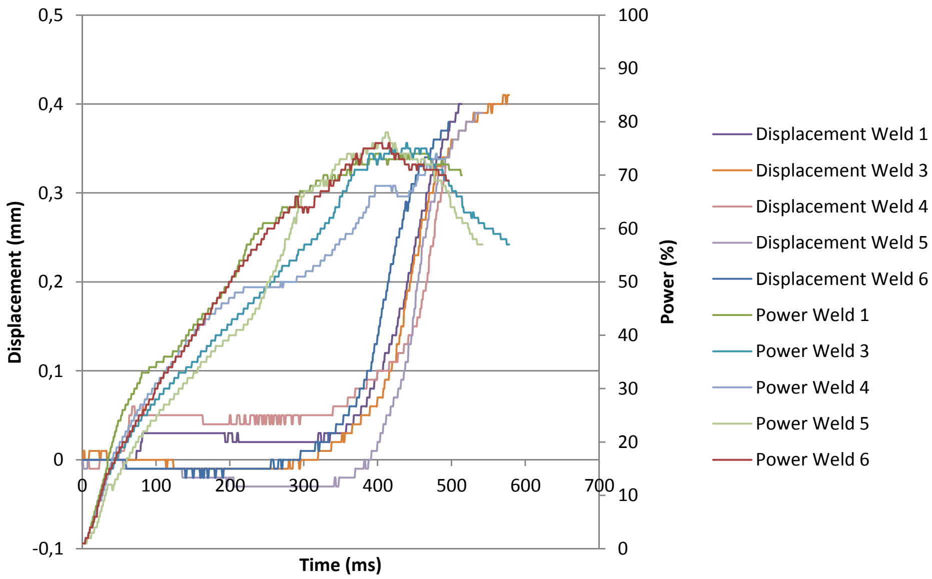

Figure 3.8: Power and displacement curves for ultrasonic welds between grit blasted, etched and coated aluminium and CFR-PA6 substrate, with the latter as top adherend.

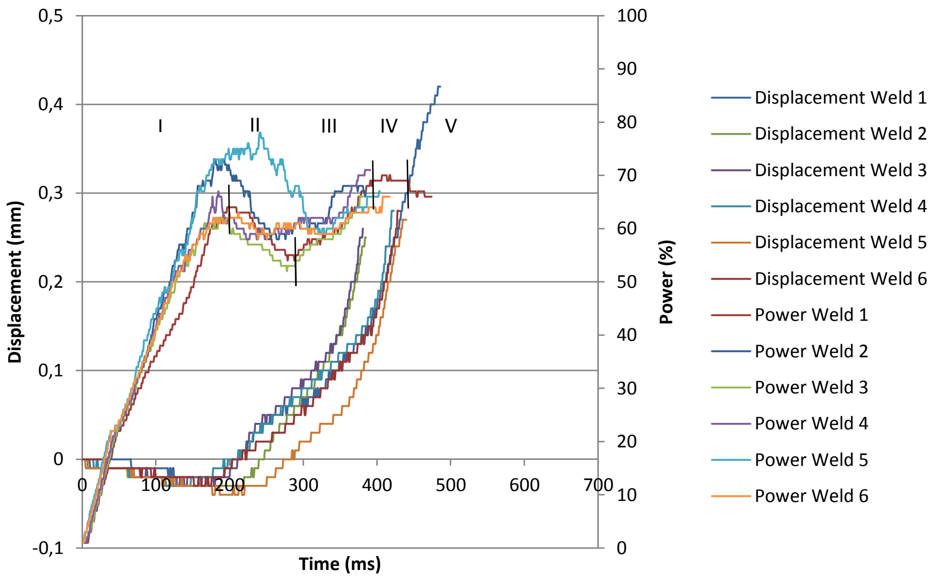

Figure 3.9: Power and displacement curves for ultrasonic welds between CFR-PA6 and aluminium substrate, with the latter as top adherend. The Roman numerals indicate the different stages as described by Villegas throughout the vibration phase for Weld 1. The transition of each stage to the next is indicated with the vertical line.

continued until a displacement was reached equal to 100 % of the thickness of 0.42 mm of the ED. Only a slight drop in rate of displacement was observed from a displacement of 0.35 mm onwards. The peak in feedback of dissipated power at the beginning of the welding cycle was clearly pronounced. After this, a second peak in dissipated power was observed during the phase in which displacement of the sonotrode was observed. The initial rate of displacement after displacement onset appeared to be low. Only late in the vibration phase, this rate of displacement increased. This behavior shows a great similarity to the displacement curve presented in Figure 3.5. For Weld 1, the stages as identified by Villegas and discussed in Subsection 1.3.1 could be recognized and are marked with Roman numerals in Figure 3.9. In the work of Villegas [22], stage 4 (IV) was identified as the welding stage in which the welding displacement resulted in the highest joint single lap shear strengths.

A fretting like abrasional damage was observed on the metallic surface, which is presented in Figure 3.10. For welds which were welded in the same series, the pattern on the metallic surface of the fretting like damage showed a great similarity, because the pattern was found to be a result of small irregularities on the surface of the sonotrode. Such indentations were not found when the metallic sample did not have direct contact with the sonotrode and acted as the lower adherend.

When the power and displacement curves are observed in Figure 3.9, a great similarity is observed compared to welding without a coating in Subsection 3.2.1. As in this case an abrasional effect also occured during welding, the hypothesis was supported, that the initial high peak in both cases was a result of abrasion of the metallic surface during welding. This abrasional effect was also thought to affect the initial displacement for both welds, compared to the displacement as observed for welds presented in Subsection 3.2.2.

Figure 3.10: Aluminium surface after welding, which was in direct contact with the sonotrode throughout welding. The darker area is identified as fretting like abrasional damage on the aluminium surface as a result of the frequent impact of the sonotrode on its surface.

3.3 Reinforced Thermoplastics on Steel Substrates.

In Figure 3.11, power and displacement are presented against time for welds with coated steel to CFR-PA6, where the CFR-PA6 substrate was in contact with the sonotrode during welding. Here, similar behavior in dissipated power was observed as for aluminium to CFR-PA6 welds in the same configuration. However, both time of displacement onset and the rate of displacement after displacement onset of the sonotrode showed a lot of scatter up till a displacement of 0.17 mm. After this, the curves are observed to continue in a similar displacement rate for all displayed welds. Here as well, with the absence of a clear pattern in the dissipated power feedback, variation in the dissipated energy at a given displacement can be expected. During welding of hybrid joints between coated steel adherends and CFR-PA6 adherends, the 3-layer, 0.42 mm thick energy directors (ED) broke in the initial stages of the vibration phase. An example is shown in Figure 3.12. This phenomenon was hardly observed in non-hybrid welding and only limited in welds between aluminium adherends and CFR-PA6 adherends. It was thought, that this breakage is a result of higher stress concentrations during welding, resulting in breakage of the ED. These stress concentrations are thought to occur as the thermoplastic of the ED in the welding overlap starts to melt, and are thought to occur as the steel adherend is stiffer. More on that in Section 3.4. Further research on this phenomenon is needed in order to provide a more thorough explanation. Caution in providing an explanation is needed, however, as several effects play a role and occur simultaneously. A selection of these effects which are thought to play a role are the induced pressure and vibration during welding by the welding device, the complex temperature profile, melting and expansion of the thermoplastic and internal stresses in the ED. A lower welding amplitude should be applied to reduce stresses and mitigate such an effect [30]. Breakage of the ED during welding results into a locally reduced amount of thermoplastic in the overlap, which might result in a reduction in bonding area. For most welds, an increase in rate of displacement could be observed from a displacement of about 0.15 mm onwards.

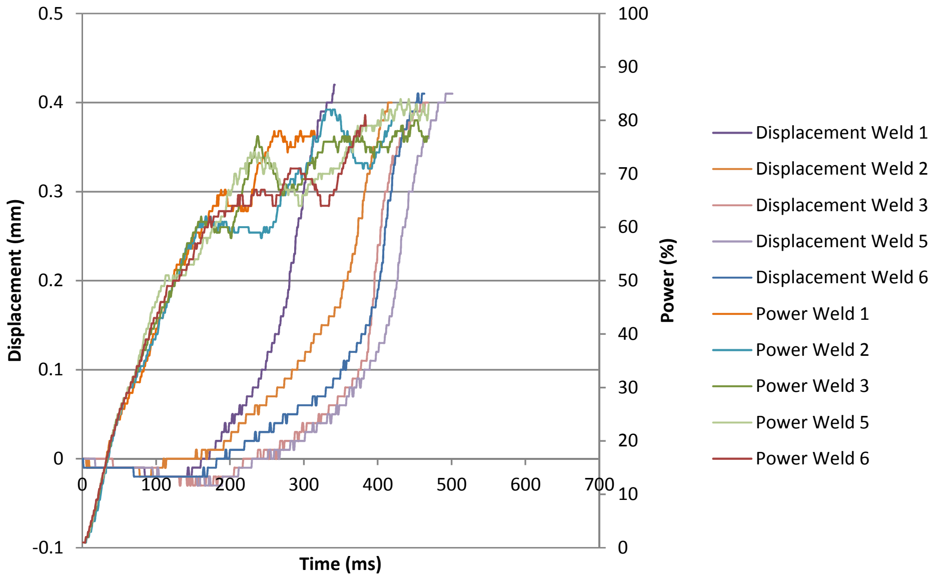

Figure 3.11: Power and displacement curves for UPW between steel and CFR-PA6 substrate, with the latter as top adherend.

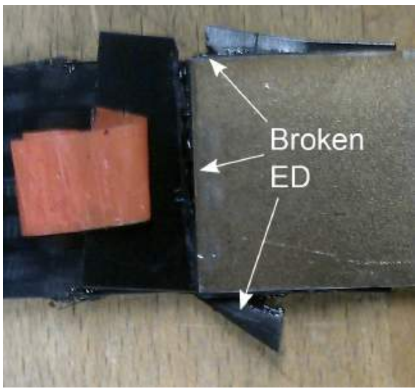

Figure 3.12: Top view of overlap after UPW of CFR-PA6 to steel. The used, 0.42 mm thick, energy director showed local fracture as a result of welding.

3.4 Comparison of Presented Welding Series

In earlier studies, relations between energy, time and quality were made. In this Section, welding time and welding energy are compared for a series of welds in Figure 3.13. The time of vibration until onset of displacement for welds with coated metallic substrates was on average around 0.3 seconds. However, welds with uncoated metallic adherends showed a significantly higher time until onset of around 0.6 seconds. For this phase, the dissipated energy was on average 400 Joules and 1000 Joules, respectively. With uncoated metallic adherends, the higher amount of dissipated energy is attributed to first a longer vibration phase and, second, a higher dissipated power during welding. Between the presented non-hybrid welded series and hybrid welded series with coated metallic adherends a low variation in dissipated welding energy is observed, all ranging between 700 and 850 Joules. A decrease in welding time is here attributed to an increase in dissipated power. For the performed successful welds, with coated metallic adherends or non-hybrid welded joints, the entire vibration phase took up about 0.5 seconds on average. This was in the same order of magnitude as what has been found for non-hybrid welded joints. With a solidification phase of 4 seconds, cycle times during assembly can be reduced significantly compared to induction welding and adhesive bonding. However, considerable time was still spent in the pretreatment and coating process of the metallic adherend as presented in Subsections 2.2.3 and 2.2.4, respectively. This agrees with theses of Ramarathnam et al. [3] and Wise et al. [2].

In Figure 3.13 the welding time appeared to be shorter for welds with joining partners which are stiffer in the through-the-thickness direction. This is considered to be mainly a result of increased average power for these stiffer joining partners. This was further supported, when the results in Figure 3.14 were observed. Here, the average and maximum dissipated power during welding showed a positive correlation with the equivalent stiffness to height ratio of the welding overlap. This ratio is, when multiplied by the welding peak amplitude, related to the induced stresses in the welding overlap, as described in Equation 1.2. The average dissipated power was obtained by dividing the total amount of energy during welding by the total amount of time. The equivalent stiffness to height ratio was calculated by applying Equation 1.3. The used stiffness and heights of the materials are presented in Table 3.1. For the transverse stiffness of the CFR-PA6 of 5.0 MPa, the inverse rule of mixtures was applied with a fiber volume fraction of 0.5 and a fiber stiffness of 240 GPa. Here, a linear trend for both maximum and average dissipated power could be observed. The series of welds with steel adherends deviated from the presented trend for welds with an aluminium adherend, although not significantly. With the presented data, no clear cause of this deviation could be identified.

3.5 Conclusion

This Chapter was intended to evaluate the following four questions. Firstly, how does the obtained welding feedback compare for different welding set-ups? Secondly, can the method proposed by Villegas be applied in the creation of hybrid welded joints? Thirdly, can the application of a coating be avoided? And fourthly, how much time does the process take?

First, the third question is discussed. For welding with or without an applied coating clear differences were observed. The absence of a coating resulted in damaging of the metallic

Table 3.1: Stiffness at room temperature and height used in the calculated equivalent stiffness to height ratio. The stiffness of carbon fibers, DC01 and AA5754 were obtained from CES Edupack.

Part	Material	Transverse stiffness (GPa)	Height (mm)
Substrate	CFR-PA6	5.0	2.10
Substrate	AA5754	70	1.90
Substrate	DC01	210	1.95
ED (with uncoated substrates)	PA6	3.0	0.28
ED (coated substrates)	PA6	3.0	0.42
Coating	PA6	3.0	0.14

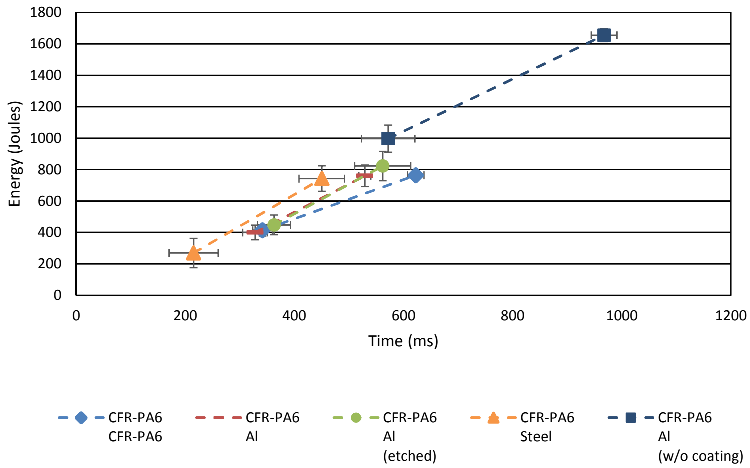

Figure 3.13: Comparison of welding time and welding energy in several series until onset of displacement and from that point until the end of the weld at 100 % displacement. The first mentioned substrate was in contact with the sonotrode during welding.

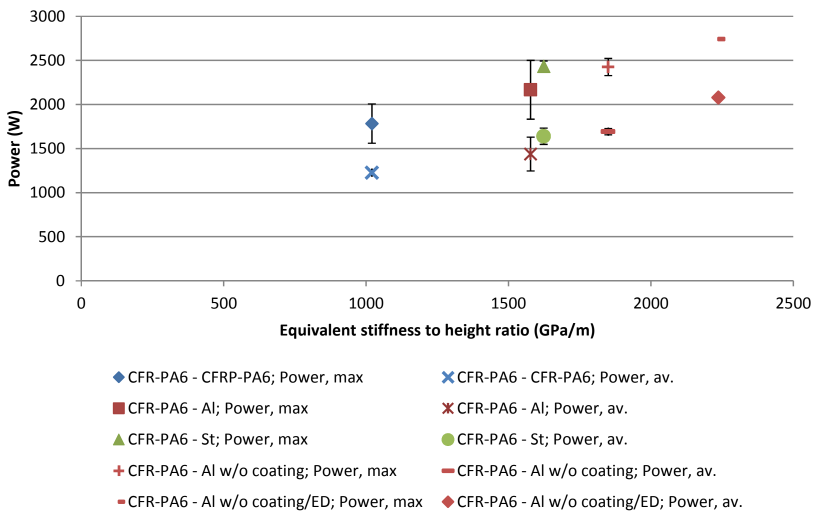

Figure 3.14: Average and maximum power during welding of the presented series against the equivalent stiffness to height ratio (ESHR).

surface and the absence of a bond between the thermoplastic and metallic surface. Not applying a coating resulted furthermore in more dissipation of energy. In the used set-up the application of a coating to create a joint could therefore not be avoided. This means an increase in surface preparation time of the metallic surface before welding.

Comparing the different welding set-ups showed interesting aspects which will be summarized as follows. Firstly, for the successfully created welds, about the same amount of energy was consumed. A range in welding times were obtained as a result of difference in average dissipated power. A correlation of the average and maximum dissipated power with the equivalent stiffness to height ratio could be made. The power feedback of hybrid welded joints showed to change between the different welding set-ups. Both when no coating was applied and when the coated aluminium adherend was used as upper joining partner, a clear initial peak in dissipated power vs. time was observable. A fretting like damage was observed on the aluminium surface in the latter case. The initial peak is thought to be a result of abrasion of the metallic adherend during welding. Next to this also in the displacement behavior for both welds three stages could be distinguished. A secondary peak could in this case be observed as well, and could be used to identify a displacement as proposed by Villegas et al. When the coated metal adherend was not in contact with the sonotrode during welding, the initial peak in dissipated power could not be observed. The dissipated power increased until displacement onset occurred. After this, no clear plateau could be observed in dissipated power. Rather an irrelegular pattern was observed. This was the case for both aluminium and steel adherends. With both metals in this set-up, the displacement showed only an increase in displacement rate uptill a maximum displacement rate. After this, the displacement rate dropped with displacement until 100 % displacement was reached. As no clear secondary plateau in the power feedback was created in this set-up, the technique as proposed by Villegas could not be applied to quickly assess an ideal displacement. As mentioned, the applied sonotrode could as well play a role in the obtained power feedback. Further study is needed to evaluate whether a change in displacement rate can be applied to find an optimum displacement, but also whether the applied sonotrode affects the obtained results.

The welding time were used as an indication of possible cycle times obtained during this method. With vibration times around 0.5 seconds and solidification times of four seconds, cycle times in the order of ten seconds can be obtained.

Chapter 4

Results of Assessment on Electro-insulation of Welded Joints

In the previous Chapter, the welding process itself was evaluated. In this Chapter, the electro-insulating behavior of hybrid welded joints is assessed. As mentioned in Section 1.5, prevention of an electroconductive connection between carbon fibers and aluminium or steel is essential in reducing galvanic corrosion in the metallic structure. This enhances the durability of the structure. In this case, both the electroconductive behavior of the joint and the welded cross section was evaluated.

In Section 4.1, the joint interface cross section after welding of non-hybrid welding is presented. This is done for hybrid welds between coated aluminium substrates and composite in Section 4.2. The discussion can be finally found in Section 4.3.

4.1 Welded Non-Hybrid Joints

For joints welded to 60% of an 0.28 mm thick ED, an average electrical resistance of 10.2 Ohm with a standard deviation of 2.4 Ohm was found. In that series, a force of 500 N with a peak amplitude of 42.3 µm had been applied, however, and both peaks identified by Villegas could be identified and applied, enabling a quick selection of optimum welding settings. Further information about this thinner ED is presented in Section 2.2.2. The fact, that an electrical resistance could be measured, supported the conclusion, that an electroconductive connection has been created. This was further supported by cross sectional analysis, as shown in Figure 4.1. Here, a contact between the fibers of both adherends through the welding interface was observed. Further potential on the application of this electroconductive joint was not evaluated.

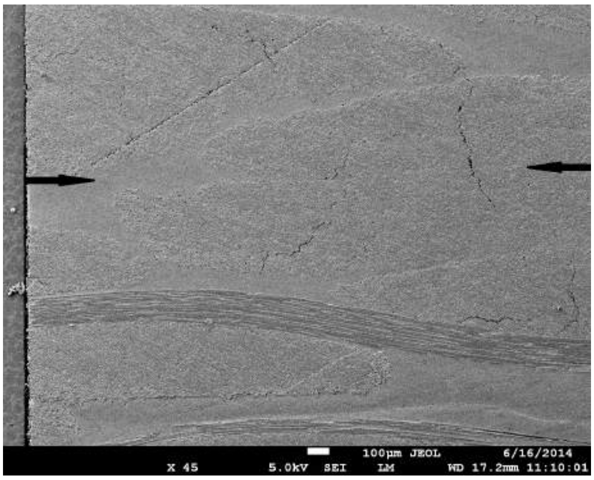

Figure 4.1: Interface between two composite substrates after welding, indicated by the two black arrows in the image. The interface was viewed in the same direction as the direction of the warp fibers.

4.2 Welded Hybrid Joints

After testing the electroconductive behavior of successfully welded hybrid joints, all presented joints were found to be electro-insulating, even when a welding displacement was used equal to 100 % of the thickness of the ED. A number of welded specimens were examined after welding by cross sectional analysis. An example is shown in Figure 4.2, for a weld with a grit blasted aluminium surface. For this joint, a PA6 layer of about 0.2 mm thick was observed between the carbon fibers and the metal adherend surface. This thickness agrees with what was calculated when for this weld the total displacement of 0.43 mm was subtracted from the combined thickness of the ED, 0.42 mm, and the measured added thickness of the coating on the metal substrate of 0.21 mm. The adhesive layer thickness was measured as well on other locations of the overlap and ranged from 0.09 to 0.25 mm.

On the cross section in Figure 4.2, cracks could be observed between the grit blasted aluminium adherend and the polyamide 6 after welding. Such a crack already was observed between grit blasted aluminium and the applied coating before welding. However, this was hardly observed in welds in which the aluminium surface was etched after grit blasting. It was thought, that this crack is a result of difference in thermal expansion coefficient between the thermoplastic and aluminium, which overcome the adhesive strength upon cooling. As the existing crack was a result of a loss in adhesion, it can be expected that this affected the strength of the created joint, resulting in a lower single lap shear strength. As the loss in connection results in an interface on which friction is possible, this might also result in increased local melting on the interface between the thermoplastic and metal. This same effect is thought to mitigate the application of this welding technique to metals with surfaces which have not been grit blasted, as no mechanical interlocking can take place of the thermoplastic in the metallic surface. In Section 5.2 is further elaborated on this matter.

In earlier attempts, for one weld between grit blasted & coated steel and carbon fiber reinforced PA6 (CFR-PA6), however, an electroconductive connection was found with an electrical resistance of 65.4 Ohm. In this case, the electroconductive connection was further analyzed.

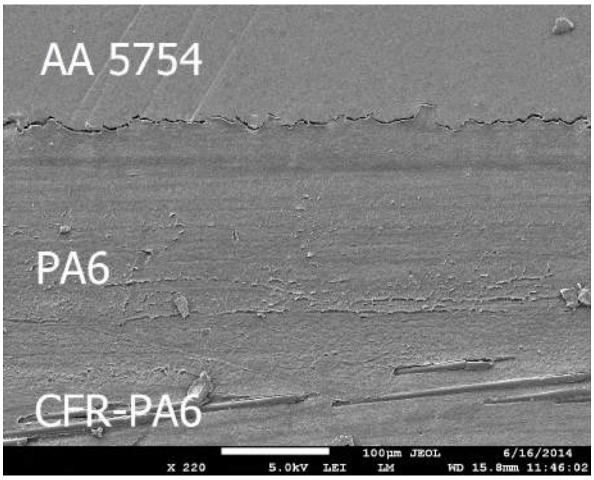

Figure 4.2: Cross section of joint after ultrasonic welding, showing a 270 µm thick adhesive layer between the grit blasted metal and composite substrate. A crack was observed between the thermoplastic and metal surface.

It was found for this weld, that after prolonged welding, carbon fibers flowed with the molten PA6 outside of the welding interface. In this case, the fibers curled around the edges of the metallic substrate and formed a contact with the side of the metallic adherend. At this location, for the hybrid weld with a steel adherend, the ED was found to have broken during welding at the side where later the electroconductive connection was found. Of that weld, after single lap shear testing, the welding interface was inspected and was found to solely consist of PA6 material and was electro-insulating. This means, also in that case no electroconductive joint was created through the adhesive layer itself, but was indeed created outside the joint overlap.

4.3 Conclusion

The goal of the experiments presented in this Chapter was to determine whether the welding method resulted in an electro-insulating joint between carbon fibers and metals to mitigate this as an enhancing factor in galvanic corrosion. No previous studies were found which evaluate the electroconductive behavior of ultrasonic plastic welded joints between CFRTP and metallic substrates. Therefore, the findings presented in this Chapter could not be compared to existent work. Whereas in the work of Krüger et al. [4], the existence of a thermoplastic layer between the used glass fibers and metallic substrate was presented as a disadvantage, in the current study this thermoplastic layer was considered as a necessity in the mitigation of galvanic corrosion. With the presented data it was shown, that with the used set-up an electro-insulating joint could be achieved between CFR-TPs and metals such as steel and aluminium, even when a welding displacement was used equal to 100 % of the thickness of the ED. It was observed that the outflow of carbon fibers can result in the creation of an electroconductive joint outside the joint overlap. For non-hybrid welded joints an electroconductive connection was found. Further potential on the application of this electroconductive joint was not evaluated.

As a conclusion, an electro-insulating joint could be achieved as long as the outflow of carbon fibers was controlled properly. Therefore, the presented UPW technique is applicable in the creation of joints in which these conditions are preferred. However, further research is needed to evaluate how the long term durability of the joint is affected by outside weather conditions. Research has to be performed as well on what minimum adhesive layer thickness is needed and can be controlled in order to assure an electro-insulating joint. Next to that, it needs to be evaluated when outflow of carbon fibers results into the creation of an electroconductive joint. Lastly, further research is needed on the remaining calculated thermoplastic adhesive layer thickness and the actual resulting adhesive layer thickness for a given substrate and ED combination. In such a way, the actual adhesive layer thickness might be calculated from the displacement obtained during welding. This can be used to control the mechanical behavior of the joint [43] and, if affected, the durability.

Chapter 5

Results of Mechanical Behavior and Fracture of Welded Joints

The objective of this Chapter is to present the mechanical behavior of joints created by means of ultrasonic plastic welding (UPW) using single lap shear testing. The single lap shear strength was evaluated as a standard way to compare welded and adhesively bonded joints. Here, ASTM D1002-05 was applied. All presented series were welded at a peak-to-peak amplitude of 72.6 µm, with a clamping force of 800 N.

In order to determine whether the single lap shear strengths of welded joints can be compared, the strain distribution during single lap shear tensile tests was analyzed by means of digital image correlation. This was assessed for the presented non-hybrid welded joints, joints in which coated grit blasted aluminium was used as a metallic adherend, and joints in which coated grit blasted steel was used as metallic adherend.

Fractography was applied in order to further understand the effects of the performed joining process on the failure behavior. Fractography and cross sectional fracture analysis were performed for non-hybrid joints, welded joints with coated and grit blasted aluminium as metallic adherend, and joints with coated, grit blasted and etched aluminium as metallic adherend.

This Chapter is divided into four parts. First, a comparison is made in the strain distribution during single lap shear testing for non-hybrid welded joints and hybrid welded joints with either aluminium or steel metallic adherends. This is followed by results for hybrid welding joints with aluminium substrates in Section 5.2 and steel substrates in Section 5.3. The discussion of this Chapter can be found in Section 5.4.

5.1 Comparison of Strain Distribution during Single Lap Shear Testing

In this research, ultrasonic plastic welding is applied in the creation of hybrid joints between carbon fiber reinforced thermoplastics and metals such as aluminium and steel. As the technique is developed for the thermoplastics industry and research has recently been performed on the application of joining carbon fiber reinforced thermoplastic structures, the question arose whether bonding in non-hybrid structures can be compared to hybrid structures. Especially, the question arose, whether the strengths obtained in the creation of hybrid joints could be compared to the obtained strength of non-hybrid welded joints. In this Section, the strain distribution is compared for the three types of adherend combinations. Namely, for non-hybrid welded joints, for hybrid welded joints with aluminium adherends, and for hybrid welded joints with steel ahderends. The obtained strain distribution shows how stresses are distributed in the overlap, and at what load failure stresses are reached locally. First, all strain distributions for the used adherend combinations are presented subsequently. After this, a discussion follows in which the results are compared.

Results of the strain distribution, as analyzed by digital image correlation of non-hybrid welded joints at a load of 9.6 kN, 80 % of the failure load, are presented in Figure 5.1 for welds performed to 100 % displacement. In this series, the single lap shear strength was found to be 37.6 MPa on average with a coefficient of variation (c.o.v.) of 3.1 %. For these joints, relatively low normal strains (in x-direction) were observed, as shown in Figure 5.1a. Rather, the normal strains were found to be mostly compressive in the joining overlap. The strains in the tensile direction, in Figure 5.1b, increased closer to the edge of the welding overlap. Increased tensile strains were observed where the substrates were connected with fillets created by squeezed out PA6 during welding. The shear strain was higher on the edges of the overlap than in the center, as expected for single lap shear tests. When the shear strain was compared to the normal strain in Figure 5.1d, the shear strain dominated during the application of tensile shear loads. For both a bathtub-like shape appeared. For isotropic PA6, the proportion of the peel stress could be compared to the shear stress, as for isotropic materials Equation 5.1 holds. Here, E is the Young's modulus, ν the Poisson's ratio and G the shear modulus.

$$G = \frac{E}{2(1+\nu)} \tag{5.1}$$

When the ratio between tensile modulus and shear modulus was incorporated for isotropic materials with a Poisson's ratio of about 0.3, such as PA6, the resulting peel stress and shear stress were found to be about equal around the edges of the overlap. In the center of the overlap, the shear stress was found to be higher than the peel stress. It could be concluded, that for non-hybrid welds, a shear dominated fracture is found.

Results of the strain distribution, as analyzed by digital image correlation of CFR-PA6 to aluminium welded joints, are presented at a load of 3.4 kN in Figure 5.2, at 95 % of the failure load. The experienced strains were found to be non-symmetric over the overlap length. Peel strains were mostly compressive, as shown in Figure 5.2b. However, at the edge of the metallic adherend in the joint overlap, considerable positive peel strains were observed. The distribution of in plane strains, in the direction of the applied loads, in Figure 5.2b showed comparable behavior to the non-hybrid welded joints. A high tensile strain was found between the edge of either adherend and the PA6 fillet-like structure. The shear strain, in Figure 5.2c was higher on the edges of the overlap than in the center, as expected for single lap shear tests. At the edge of the metallic adherend significantly larger shear strains were observed. The results over the overlap length were presented in Figure 5.2d. For isotropic PA6, the

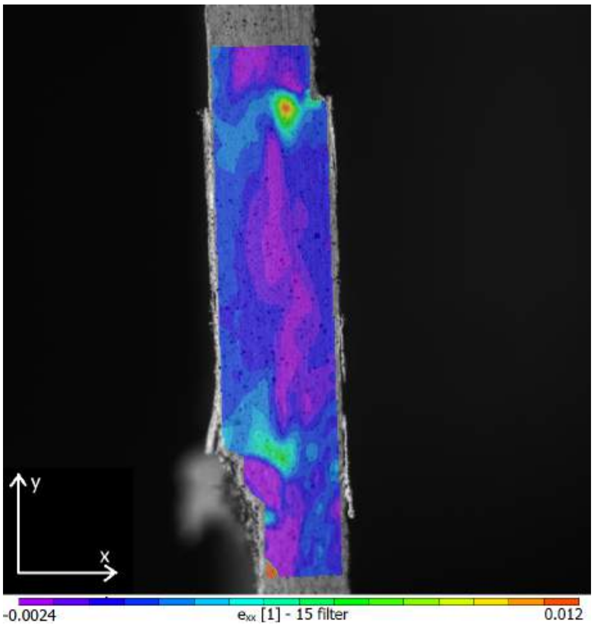

(a) Strain in the x-direction.

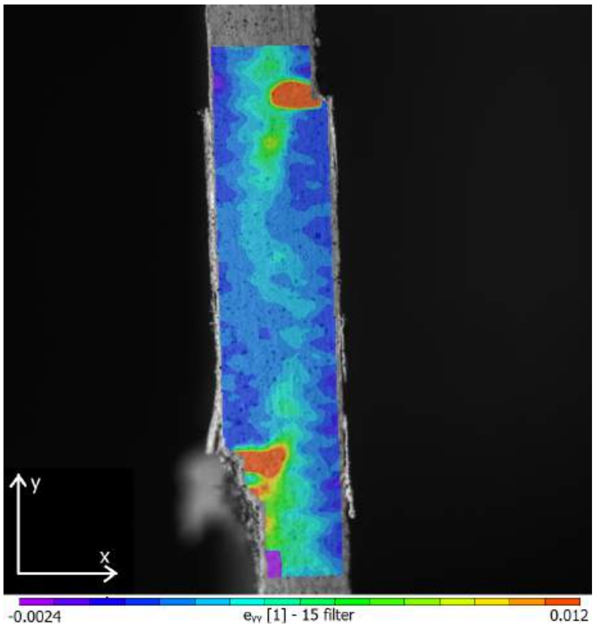

(b) Strain in the y-direction.

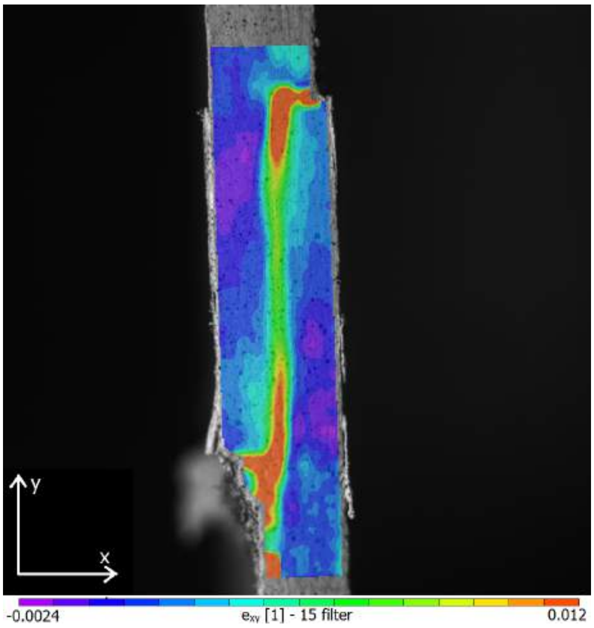

(c) Shear strain.

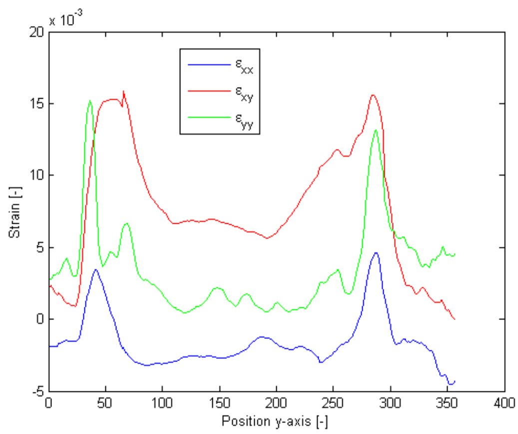

(d) Strains along the overlap length. The edges of the welding overlap are indicated by the two peaks in ϵ_{yy}.

Figure 5.1: Strain measurements by digital image correlation of a composite to composite ultrasonic welded joint at a load of 9.6 kN.

proportion of the peel stress could be compared to the shear stress, applying equation 5.1. At an equal strain value, the peel stress was found to be significantly higher at the edge of the metallic adherend, what was the case in Figure 5.2d.

Results of the strain distribution as analyzed by digital image correlation of ultrasonic welded joints of CFR-PA6 to Steel are presented at a load of 2.5 kN in Figure 5.3. Fracture was not observed in the analyzed picture. Again, compressive normal strains were observed in the center of the welding overlap in Figure 5.3a, with high tensile peel strains at the edge of the steel adherend. In Figure 5.3b, hardly any deformation was observed in the in plane direction. As the steel samples fractured at a relative low load, hardly any transition could be observed between the composite adherend and the thermoplastic fillet on top of it in tensile strains. Shear strains, presented in Figure 5.3c, showed to be higher at the edges of the joint overlap, what should be expected. The resulting strains were compared in Figure 5.3d. The highest peel strains were observed at the metallic edge.

When strain distributions for the three adherend combinations were compared, it was observed that the strain distribution showed to be non-symmetric in hybrid welded joints, as opposed to non-hybrid welded joints. The peel strains at the edge of the metallic adherends showed to be far higher when compared to the peel strains observed in the non-hybrid welded joints. These were regarded as a major cause of fracture at lower loads. This can be further evaluated by the application of finite element modeling. As a result, the failure mode was influenced by the substrate stiffness and constituents. Therefore, as a result of the strain distribution during single lap shear testing, influenced by the used adherends, the three types of substrate combinations showed to be incomparable and should therefore be assessed independently.

5.2 Hybrid Welded Joints with Aluminium Adherends

In this Section, the SLSS and fracture of hybrid welded joints with aluminium adherends are presented. The SLSS of substrates tested according to ASTM D1002-05 were compared in Figure 5.4. Fracture surfaces can be found in Appendix D. Welds with aluminium either as top or bottom adherend resulted in a similar fracture strength. Joints which were welded with grit blasted and etched metallic adherends showed lap shear strengths of 16.5 MPa on average with a c.o.v. of 2.2 %. This was a considerable improvement, as compared to what was found by Krüger et al. In the work of Ramarathnam et al. [3] and Wise et al. [2], the standard deviation was omitted in the presentation of mechanical results and could not be compared. Moreover, in the work of Wise et al. peel tests were performed. The presented adhesive reference resulted in a SLSS of 20.5 MPa with a c.o.v. of 11.9 %. Here, an adhesion peel fracture was observed on the surface of the CFR-PA6 adherend. A relatively high coefficient of variation was observed. The length of the created fillets differed, which might have affected the SLSS of each sample. As spew fillets were created in the adhesively bonded samples, it should be taken into account that these significantly reduce the shear- and peel stresses in the joint overlap [44]. It was evaluated whether at a higher displacement the same effect was obtained as found in Section 3.1, where it was found that a lower displacement in this case did not result in a higher joining strength. Therefore, tests with grit blasted, etched and coated aluminium adherends, welded until 66 % displacement, were performed as well. In this case, as presented in Figure 5.4, a lower SLSS was found, on average 15.1 MPa, with a c.o.v. of 7.5 %. As mentioned in Section 3.1, it is anticipated that the higher adhesive

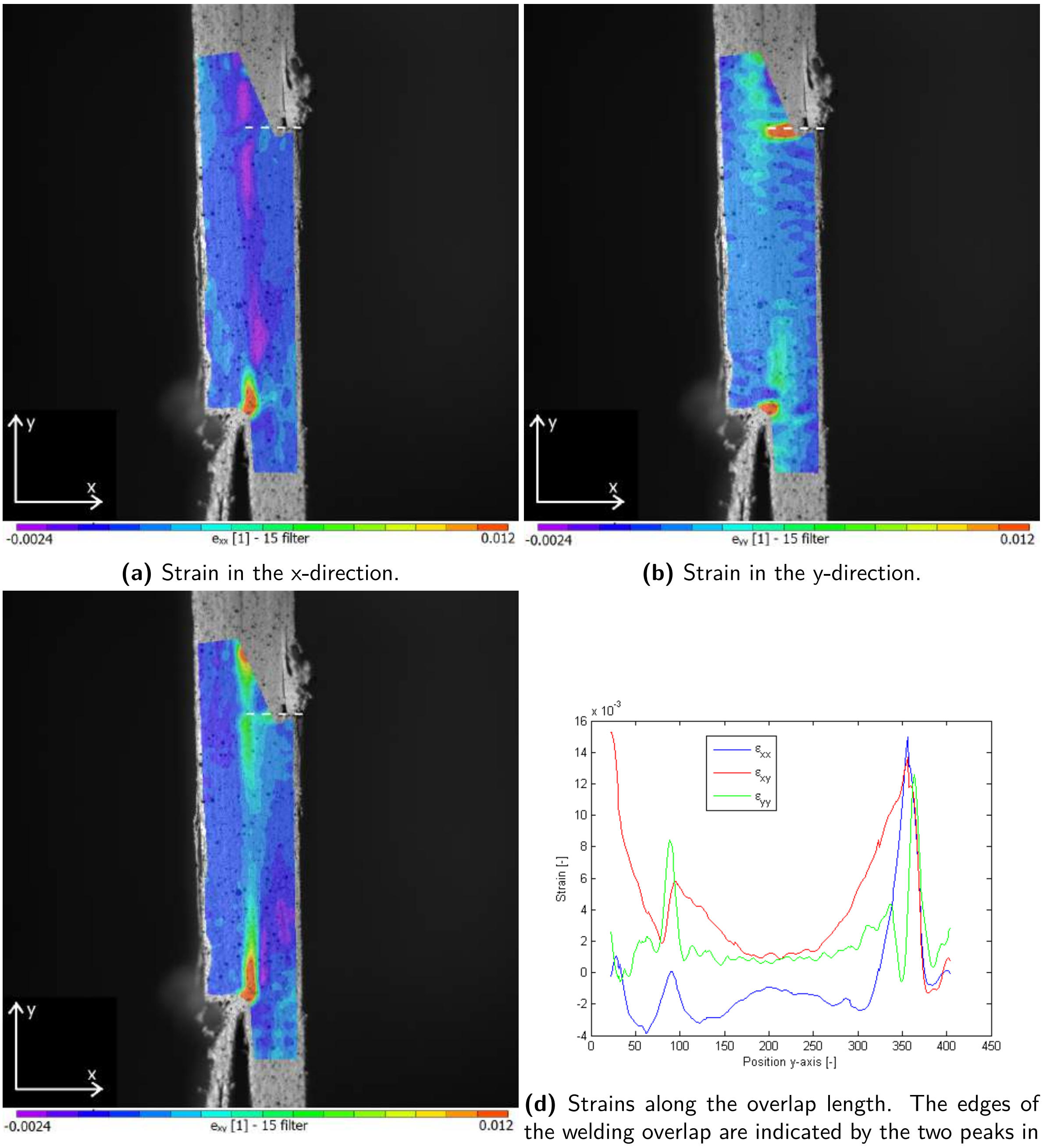

(a) Strain in the x-direction.

(b) Strain in the y-direction.

(c) Shear strain.

(d) Strains along the overlap length. The edges of the welding overlap are indicated by the two peaks in ϵ_{yy}.

Figure 5.2: Strain measurements by digital image correlation of a composite (right) to aluminium (left) ultrasonic welded joint at a load of 3.4 kN just before fracture. The edge of the CFR-PA6 adherend is demarcated with a local peak in Figure 5.2b.

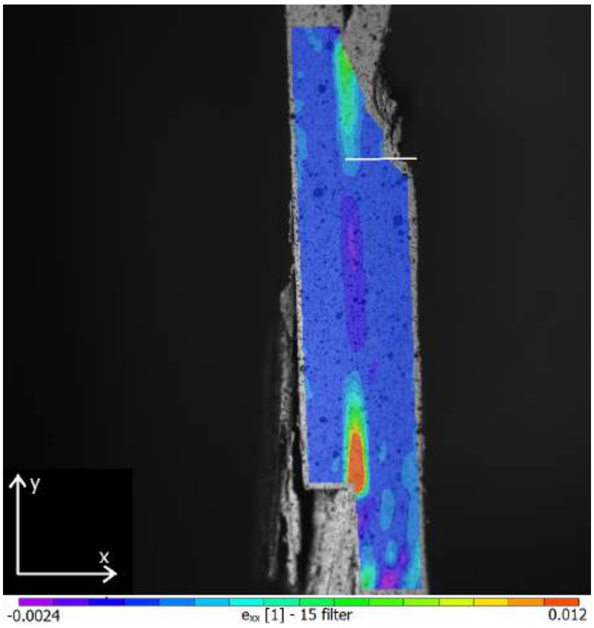

(a) Strain in the x-direction.

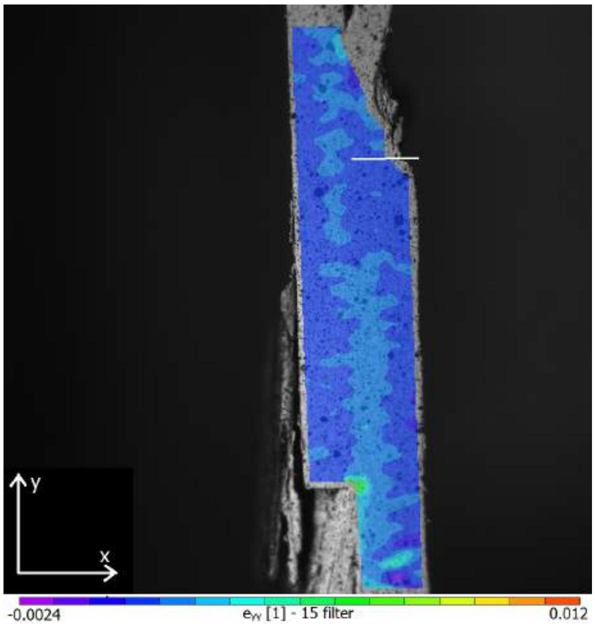

(b) Strain in the y-direction.

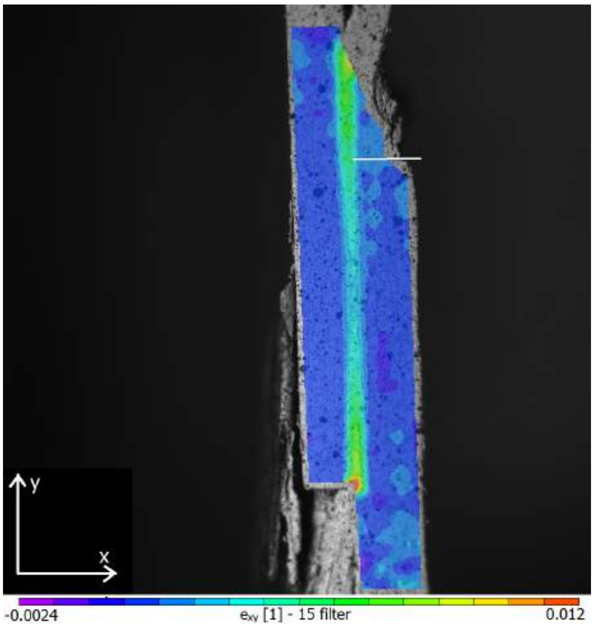

(c) Shear strain.

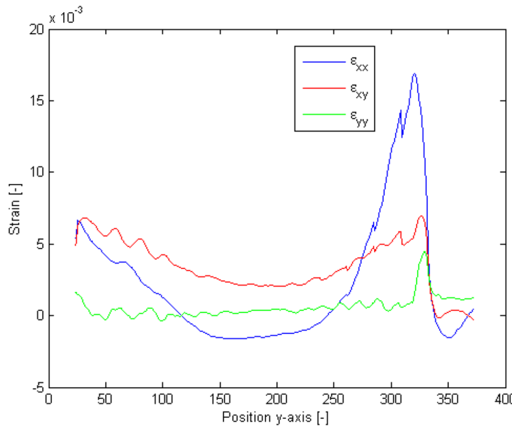

(d) Strains along the overlap length. The joint overlap is from around the 120th datapoint on the y-axis until the displayed end around the 330th datapoint on the y-axis.

Figure 5.3: Strain measurements by digital image correlation of a composite (right) to steel (left) ultrasonic welded joint at a load of 2.5 kN just before fracture. Here, the edge of the composite adherend is indicated by the white line.

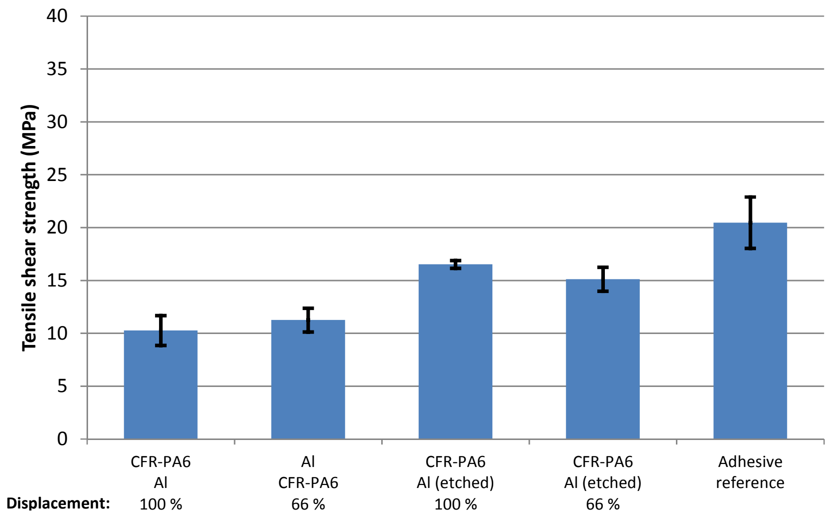

Figure 5.4: Lap shear strengths in MPa of the tested joints. Dimensions of welding substrates according to ASTM D1002-05. Testing speed: 13.0 mm/min. Grip-to-grip distance: 60 mm. The top mentioned adherend was in contact with the sonotrode during welding.

layer thickness results in higher peel stresses, which was found by Gleich et al. [43]. Further research is needed to evaluate the significance of these results.

All metallic samples in the welding series were produced in separate batches. It was not verified whether and how the conditions during the treatment of the grit blasted metallic samples influenced the adhesive strength of the created joints.

5.2.1 Fractography and Cross Sectional Analysis

The fractography of hybrid welded joints with aluminium adherends after single lap shear testing is presented in this Subsection. In Appendix D the fracture surfaces of all presented joints in this report are presented. In Figure 5.5 an example is presented of a fractured joint after single lap shear testing. At the lower left edge of the metallic adherend on Figure 5.5, a small edge of dark PA6 coating did not melt and adhere to the composite sample. Next to that, the edge of the metallic showed a zone at which less thermoplastic could be found left on the aluminium surface. Such a lighter zone with less PA6 residues could be found on the right side of the aluminium adherend. In the center, in between these lighter zones, a darker zone could be observed, with fracture which resulted in more PA6 staying adherent to the metallic surface. Next to that, larger pieces, referred to as patches, of PA6 showed to have stayed adherent, sometimes accompanied with a layer of carbon fibers which had broken off the composite adherend. Also, darker stripes of PA6 perpendicular to the tensile direction were observed on the metallic in that greyer area. On the CFR-PA6 adherend, the negative markings of the described fracture surface for the metallic adherend were found.

The fracture surface of welded joints with aluminium that was grit blasted, etched and coated and then welded until a displacement of 66 % of the thickness of the ED, was analyzed as well. This has been presented in Figure 5.6. Here, less thermoplastic stayed on the metallic surface and the metallic fracture surfaces shows to somewhat whiter overall. In this case,

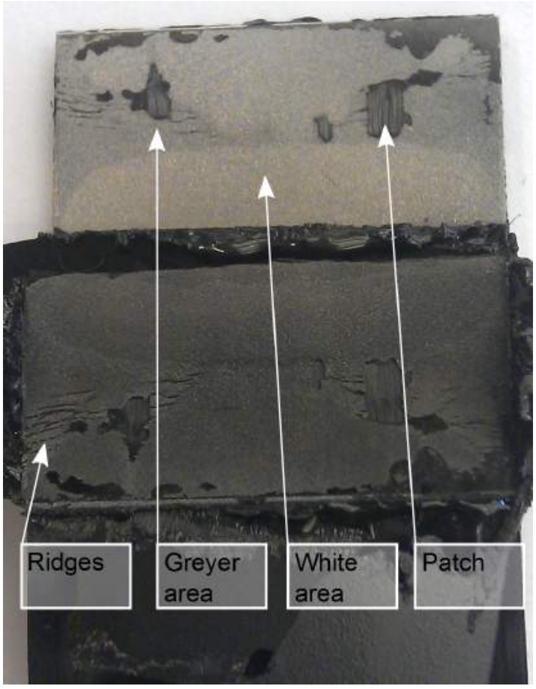

Figure 5.5: Fracture surface after welding between a grit blasted and etched aluminium and a composite adherend, welded until a displacement equal to 100 % of the ED thickness. On the aluminium surface, a lighter, white zone was observed, correlated to peeling, mode I failure. In the middle of the overlap length, a greyer area was observed, which was correlated with a shear, mode II, type of failure.

Figure 5.6: Fracture surface after welding between a grit blasted and etched aluminium and a composite adherend, welded until a displacement equal to 66 % of the thickness of the used ED. Failure was dominated by peeling, mode I failure. Towards the edge of the metallic adherend in the overlap, some shear fracture was observed.

more thermoplastic stayed on the metallic surface close to the edge of the metallic adherend. On the fracture surface, color gradations were observed on the metallic adherend. These were not further evaluated.

To further study the fracture phenomena, a scanning electron microscopy analysis was performed. In the following paragraphs, both peel fracture and shear fracture dominated areas are individually discussed.

White Area

In the lighter fracture zone on the metallic adherend, hardly any PA6 was found on the metal surface, except from that which were mechanically interlocked into the grit blasted surface, as shown in Figure 5.7. On the fracture surface of the CFR-PA6 adherend, metallic residues could be found, as presented in Figure 5.8.

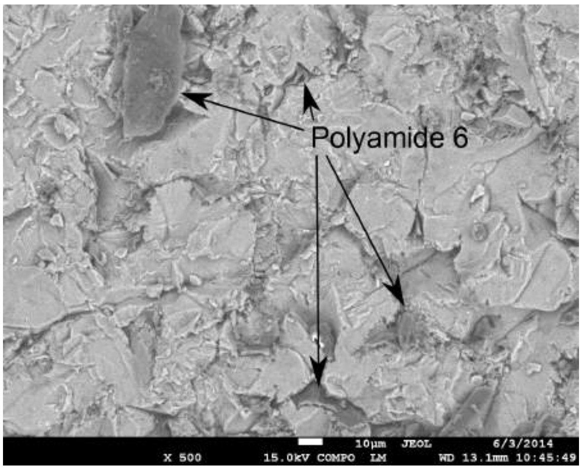

Figure 5.7: Grit blasted metal surface after fracture. The surface was practically clean from thermoplastic residues, although locally some darker thermoplastic could be observed which is thought to be mechanically interlocked into local cavities in the aluminium surface.

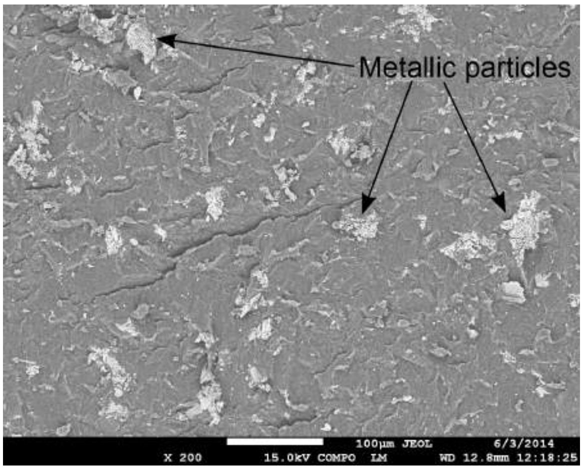

Figure 5.8: Thermoplastic surface after fracture with grit blasted metal surface from the same area as Figre 5.7. Metallic particles could be found on the thermoplastic surface after fracture.

Greyer Area

In the darker fracture area, as mentioned, more diverse fracture was observed. More PA6 was left on the metallic surface as observed in Figure 5.9. A cross section of the adhesive layer across the identified darker stripes is shown in Figure 5.10, where the fracture showed to propagate diagonally away from the metallic surface into the adhesive layer, perpendicular to the tensile component of an induced shear load. Such diagonal crack propagation is seen as an indication of mode II, shear, fracture in this greyer fracture area. A transition could be found in this cross section in the adhesive layer, about 70 µm away from the metallic adherend. It was thought, that this transition could be a result of two different causes. The first hypothesis is that the layer closer to the metallic adherend did not melt during welding and was initially part of the coating, resulting in a higher crystallinity and more dense structure. Another hypothesis is that this is the transition between the initial coating and the thermoplastic of the ED. The crystallinity of both layers can be determined in order to get more insight in this matter.

When the crack propagation at the tip of a diagonal crack in the horizontal direction was continued, more PA6 stayed attached to the metallic surface. This thermoplastic sometimes even contained carbon fibers which have broken off the CFR-PA6 surface. An example of the crack in the adhesive layer is presented in Figure 5.11. In other cases, it was found, that the fracture could propagate through less healed PA6 interfaces, as presented in Figure 5.12. Fracture through the layer close to the metallic surface showed to be different from fracture in the other layer of PA6 closer to the composite which did melt and flow during the welding process. This was especially observed, when the fracture propagation receded from the surface of the composite adherend back to the surface of the metallic adherend. This behavior was observed in Figures 5.13 and 5.14. In the former figure, close to the metallic grit blasted and etched surface, the fracture surface showed a finer, more granular-

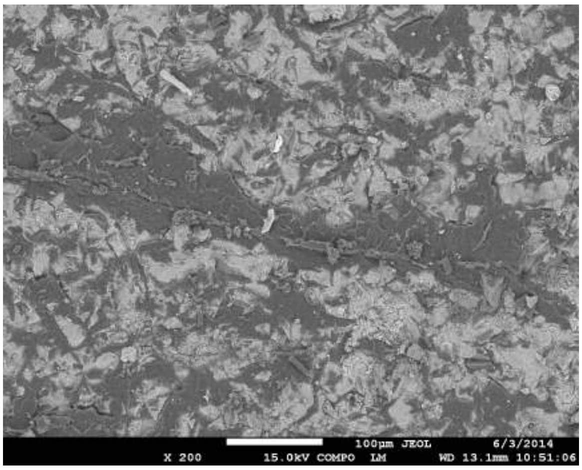

Figure 5.9: Fracture surface in darker area of aluminium substrate which was welded after grit blasting and coating. As shown in this figure, the greyer color was a result of more PA6 staying adherend to the metallic surface. Here, as a result of backscattered electron analysis, the composition is demarcated, with PA6 appearing to be darker on the image than aluminium.

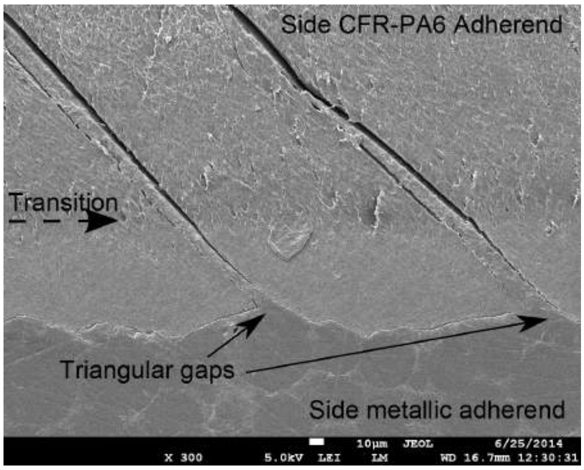

Figure 5.10: Cross section of PA6 in greyer shear fracture area after UPW with a grit blasted aluminium sample. Diagonal cracks propagated from the metallic surface trough the thermoplastic adhesive layer. The triangular gaps were a result of ridges which stayed adherent to the aluminium surface. A transition in the PA6 was found about 70 µm away from the fracture surface, as a result of thermal history.

like structure. As the fracture was not found to be continuous in this case between two identified layers, further research is needed whether this fracture is a result of the possibility that a part of the thermoplastic on the metallic surface did not melt during welding.

The effect of etching could best be analyzed by cross sectional analysis of coated grit blasted surfaces without and with etching. Both are presented in Figure 5.15 and 5.16. When etching was not applied, a crack of a few micrometers was found between the metallic surface and the PA6. It was thought that the observed crack was a result of the difference in thermal expansion between the aluminium and thermoplastic material. Here, local mechanical interlocking was thought to form the most contributing factor in adhesion. When the etched surface was analyzed, the PA6 adhered to the metallic surface without an observable crack. In the current study, the aluminium adherend was again ultrasonically cleaned in the acetone after grit blasting. This was performed in order to enable further removal of metallic particles from the grit blasted surface. This treatment might have resulted in the reattachment of some grease on the aluminium surface. Tests in which this second ultrasonic cleaning step is omitted have to be conducted in order to further support such a statement. The observed crack might support the findings by Didi et al. [13], which found a remaining SLSS of 5% after 12 months of outside weather exposure. This was for induction welded joints with grit blasted aluminium adherends on carbon fiber reinforced PA66.

Discussion

The dominating failure mechanism in the performed tests with hybrid welded joints was adhesive peel failure on the aluminium surface. As a result, the cohesive strength of the

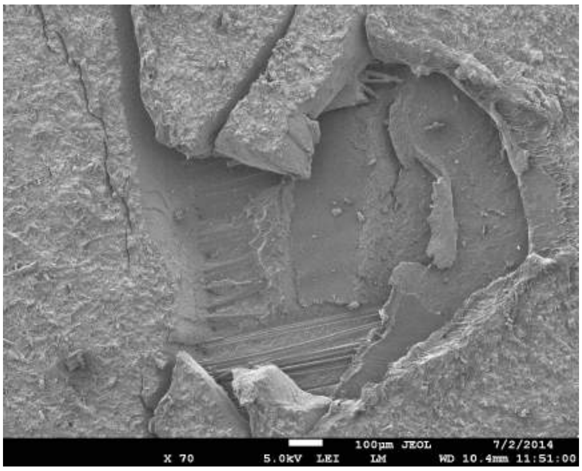

Figure 5.11: PA6 surface from which locally a patch was removed which stayed adherend to the metallic surface after fracture. The CFR-PA6 composite substrate was pulled to the left. The composite substrate was welded to a grit blasted and etched aluminium substrate.

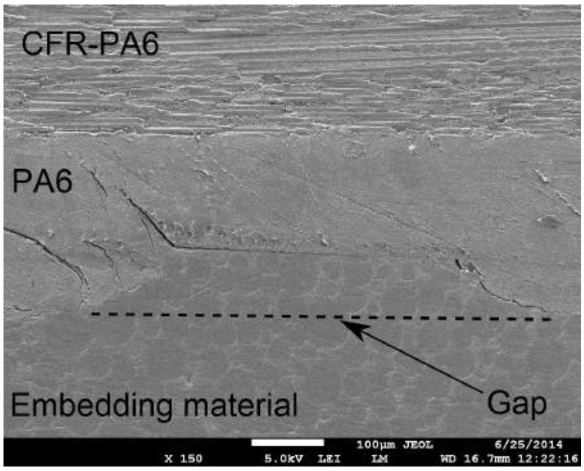

Figure 5.12: Remaining gap of a patch of PA6 which stayed adherent to the metal surface. The horizontal crack line follows an already apparent imperfection on that level. The composite substrate was welded to a grit blasted substrate which was used as upper joining partner and was pulled to the left during lap shear testing.

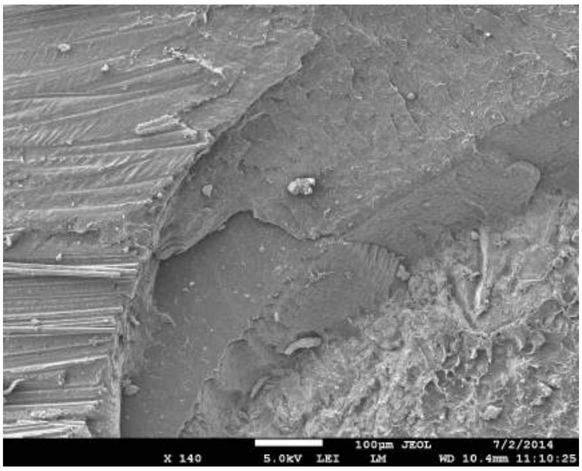

Figure 5.13: Edge of a patch of PA6 which stayed adherent to the grit blasted and etched metallic surface. Top layer fibers of the composite locally were broken off the composite. Two distinct layers could be observed in the thermoplastic fracture surface. As an indication of the occurring stresses during fracture, the aluminium substrate was pulled to the left during lap shear testing, just as in Figure 5.14.

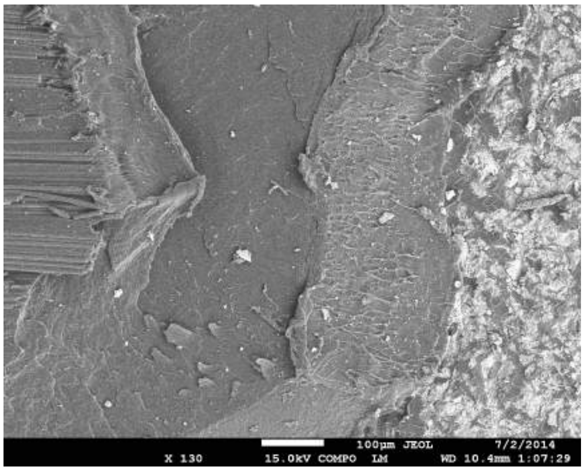

Figure 5.14: Top view of a patch of PA6 staying adherent to the metal surface. Two distinct layers could be identified in the adhesive layer. The one closest to the metal showed a location of final fracture, where PA6 filaments lay disentangled on the diagonal fracture surface in the adhesive layer. On the right, carbon fibers were broken off from the surface of the surface of the CFR-PA6 adherend.

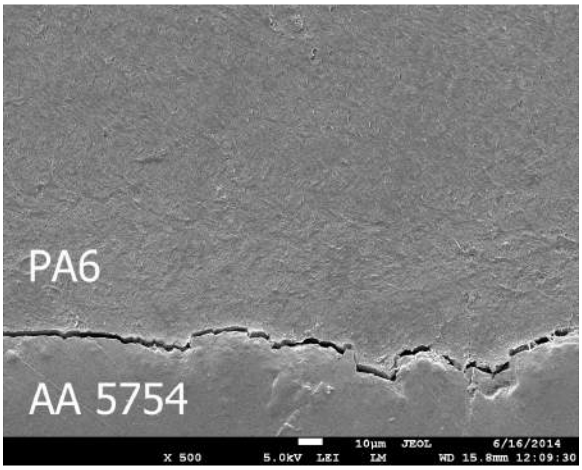

Figure 5.15: Interface between grit blasted metal surface and PA6 coating, before welding.

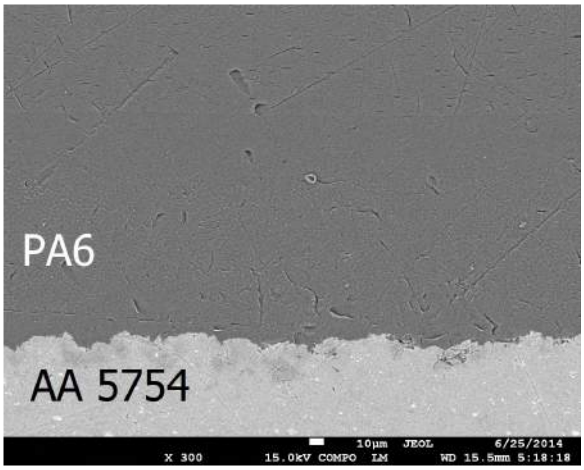

Figure 5.16: Interface between grit blasted and etched metal surface and PA6 coating, after welding.

welded adhesive layer could not be determined when the used surface treatment was applied. The peel fracture agreed with what was found in the research on the application of induction welding in the creation of such hybrid joints [12]. In that case, 1 mm thick aluminium adherends were used, however. As adhesion peel fracture occurred, improvement of the SLSS can be attempted in following studies by the application of anodization treatments. In this technique, metaloxide pores are created on the metallic surface, in which the adhesive is allowed to interlock, next to acting adherend forces between the metallic oxide surface and the polar polyamide. Anodization is especially developed and applied in the aerospace sector.

5.3 Hybrid Welded Joints with Steel Adherends

For steel as a joining partner, a SLSS of 8.5 MPa on average was observed with a c.o.v. of 7.7 %. A typical fracture surface is presented in Figure 5.17. At the edge of the metallic adherend, no bond was created between the ED and the thermoplastic coating. This could be observed by the reflection of light on thermoplastic of another adherend in Figure 5.18. The fracture for welded joints with grit blasted steel adherends showed adhesive peel fracture at an average SLSS of 8 MPa. However, at the edges of the joint overlap it appeared that no bond was created. It is thought that this might be caused by the breakage of the ED during welding. In further studies it has to be determined whether the prevention of such a breakage results in a higher SLSS.

5.4 Conclusion

In this Chapter the mechanical behavior of the UPW joints was evaluated when tested in single lap shear. Further, the effect of applying both grit blasting and nitric acid etching was assessed. These tests were performed in order to evaluate what single lap shear strengths can be obtained with ultrasonic plastic welding.

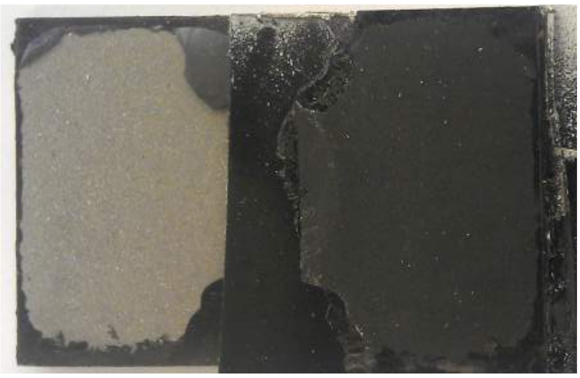

Figure 5.17: Fracture surface after single lap shear test of a steel substrate (left) welded to composite (right).

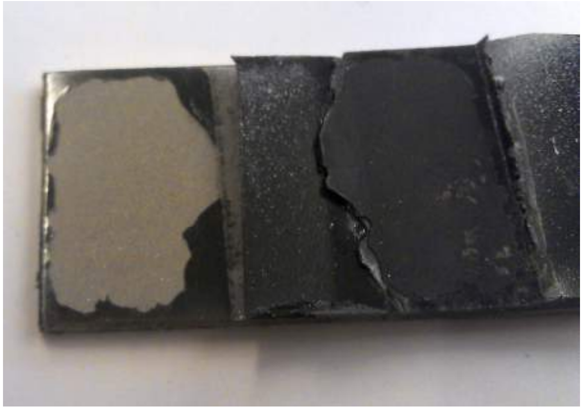

Figure 5.18: Side view of fracture surface after single lap shear test of a steel substrate (left) welded to composite (right).

The strain distribution between non-hybrid welded joints was evaluated. This was done to determine whether the obtained mechanical results can be compared. The performed cross sectional analysis and fractography was used to further determine the type of fracture and identify further ways to improve the bond quality.

The dominating failure mechanism in the performed tests with hybrid welded joints was found to be adhesive peel failure on the metallic surface. As a result, the cohesive strength of the welded adhesive layer could not be determined when the used surface treatment is applied. The peel fracture agreed with what was found in the research on the application of induction welding in the creation of such hybrid joints [12]. In that case, 1 mm thick aluminium adherends were used, however. As a result of the strain distribution during single lap shear testing, influenced by the used adherends, the three types of substrate combinations could not be compared. This was because the failure mode was influenced by the substrate stiffness and constituents. The strain distribution showed to be non-symmetric in hybrid welded joints, as opposed to non-hybrid welded joints. The peel strains at the edge of the metallic adherends showed to be far higher when compared to the peel strains observed in the non-hybrid welded joints. These were regarded as a major cause of fracture at lower loads. This can be further evaluated by the application of finite element modeling.

For grit blasted specimens, an average SLSS of 11 MPa was found. No significant difference could be observed when either of the adherends was in contact with the sontrode during welding. The SLSS was significantly improved by the application of welded specimens with the usage of grit blasted and etched metallic adherends. A SLSS of 16.5 MPa was achieved, which is a strength of about 80% of the adhesively bonded specimens. For these welded joints a coefficient of variation of 2.2 % was measured. This was a considerable improvement, as compared to a coefficient of variance around 0.4, what was found by Krüger et al. In the work of Ramarathnam et al. [3] and Wise et al. [2], the standard deviation was omitted in the presentation of mechanical results and could not be compared. Moreover, in the work of Wise et al. peel tests were performed.

For the adhesively bonded joints, an adhesion peel fracture on the CFR-PA6 surface was observed. A relatively high coefficient of variation was observed. The length of the created fillets differed, which might have affected the SLSS of each sample. However, the adhesively bonded samples with grit blasted and etched aluminium surface resulted in a SLSS of 20.5 MPa, with a c.o.v. of 10.6 %. The present spew fillets are known to reduce the apparent stresses significantly. Obtaining 16.5 MPa of joint strength for the welded samples is therefore considered as a result which is considered competitive with adhesively bonded samples.

It was assessed whether the SLSS was affected by applying a lower displacement, as found by Villegas [5]. In this case, when for grit blasted, etched and coated aluminium substrates the welding displacement was set at 66 % of the thickness of the ED, a SLSS of 15.1 MPa was reached with a c.o.v. of 7.5 %. This was a reduction of 8 % over welded joints up till 100 % displacement. It is anticipated that the lower displacement of 66 % results in a thicker bond line. This was found to result in increased interface peel stresses from a minimum adhesive layer thickness onwards [43]. A further assessment on the effect of the bond line thickness in welding is needed, however.

For welded joints with grit blasted steel adherends an average SLSS of 8 MPa was obtained. Further studies are needed to improve such results.

The major conclusion is that the SLSS of the created joint by UPW of CFR-PA6 substrates to grit blasted and etched coated aluminium is competitive with what was found for adhesive bonded joints.

Chapter 6

Conclusions and Recommendations

The objective of this study was to research the applicability of ultrasonic plastic welding (UPW) to result in a joint between carbon fiber reinforced thermoplastics and aluminium or steel alloys. With the identified need for further hybridization of structures at lower production cycle times, UPW was considered to be a suitable candidate to be applied in this study. Earlier studies in this field either were focused on the application of UPW between coated metals and thermoplastics [2,3] or between uncoated metals and glass fiber reinforced thermoplastics [4]. All these studies were performed, controlled by either dissipated energy or time. When the coefficient of variation of the joint strength was presented, this was found to be around 0.4, indicating a low level of reproducibility. In the current study, it has been evaluated whether controlling the welding process by means of power and displacement data, as proposed by Villegas [22] for non-hybrid welded joints, results in more consistent weld quality. As an electroconductive connection between carbon fibers and aluminium or non-stainless steel alloys results in aggravated galvanic corrosion it has been assessed whether the application of UPW can result in an electro-insulating joint. In this study, the following research questions have been asked:

1. How does the obtained welding feedback compare for different welding set-ups?
2. Can the method as proposed by Villegas for controlling the UPW process for non-hybrid welded joints be applied in the creation of joints between carbon fiber reinforced thermoplastic and aluminium or steel as well?
3. Can the application of a coating be avoided?
4. What processing times can be achieved with the application of UPW for the applied welding series?
5. Can an electro-insulating joint be achieved between aluminium or steel and carbon fiber reinforced thermoplastics by means of UPW?
6. What is the single lap shear strength of the created displacement controlled UPW hybrid joints?

Firstly, it has been evaluated whether and how the obtained power and displacement feedback is affected by the application of UPW in the creation of hybrid joints. At a fixed welding pressure of 2.5 MPa and a peak-to-peak amplitude of 72.6 µm, welds have been performed based on sonotrode displacement. Series with the aluminium adherend with and without a thermoplastic coating on the metallic adherend have been welded. Furthermore, welds with the coated aluminium adherend as either the bottom adherend or in contact with the sonotrode during welding have been assessed. Also coated steel alloy substrates have been applied as bottom adherends. For these series, the dissipated power and displacement during the vibration phase have been evaluated on whether stages as observed by Villegas [22] could be identified. Also, optically observable differences in the welded samples have been reported. The effect of the mentioned welding configurations on the welding time, energy, displacement and maximum & average dissipated power have been presented as well.

Secondly, it has been assessed whether UPW could be used in creating joints with an electro-insulating adhesive layer. For non-hybrid welded joints and the successfully created joints with coated metallic adherends, the electroconductivity has been measured. Also the adhesive layer thickness of selected samples has been measured.

Thirdly, the mechanical behavior of the created joints has been evaluated and compared with standard joining processes like adhesive bonding. The single lap shear strength (SLSS) of successfully welded samples has been assessed for joints with CFR-PA6, aluminium or steel as secondary joining partner material. For joints with aluminium adherends, the effect of nitric acid etching next to grit blasting has been evaluated as well. The strain distribution as a result of the usage of different adherend materials have been examined by digital image correlation. By scanning electron microscopy, the fracture behavior of non-hybrid substrates and hybrid substrates with an aluminium adherend has been evaluated.

In the following sections, the main conclusions are presented. Firstly, a conclusion on data obtained during welding and process duration is presented in Section 6.1. This is followed by Section 6.2, which covers conclusions in the electro-insulating behavior of welded joints. Conclusions of the mechanical behavior of welded joints are presented in Section 6.3. The implications of the presented conclusions are presented in Section 6.4, research limitations are given in Section 6.5 Finally, recommendations are presented in Section 6.6.

6.1 Welding feedback, process times and the effect of a coating

The absence of a coating on the metallic surface showed to result in damaging of the pretreated metallic surface at the selected welding force and amplitude. Next to that, no bond could be created between the metallic surface and the thermoplastic. When a coating is applied, a successful joint is created, however.

At the used welding amplitude and pressure, the obtained power and displacement have been studied for both hybrid and non-hybrid welded joints. When the CFR-PA6 adherend was in contact with the sonotrode during welding for these hybrid joints, the obtained power feedback did not result in the characteristic stages as found by Villegas [22] and described in Subsection 1.3.1. When the aluminium adherend was in contact with the sonotrode during welding, these stages were identified, however. Here, the welds were stopped at a welding displacement which occurred at the stage at which the thermoplastic in the CFR-PA6 adherend is known to start melting. A relatively high standard deviation in welding energy for individual welding series was observed when the welded joint was observed at the selected final sonotrode displacement. Therefore, if welding would have been performed based on energy, the displacement after welding would differ significantly. The maximum and average dissipated power shows to correlate with the equivalent stiffness to height ratio used at a given welding amplitude and pressure. As indicated in Section 1.3.1, this complies with existing theory.

As was mentioned in the previous paragraph, the stages could not be identified when the CFR-PA6 adherend was in contact with the sonotrode during welding. Especially, an initial peak in dissipated power could not be identified. Therefore, the proposed method by Villegas et al. [5] to identify ideal welding settings cannot be readily applied in this case. The absence of the initial peak is sought in the absence of abrasion of the aluminium adherend in that case. Next to that, it is thought, that the used sonotrode resulted in this different power feedback. Further research is needed, however.

For the performed welds, the welding time was determined in order to indicate possible cycle times. For the performed successful welds, with coated metallic adherends or non-hybrid welded joints, the vibration phase shows to take up about 0.5 seconds on average, as presented in Section 3.4. With a solidification phase of 4 seconds, cycle times during assembly can be reduced significantly compared to induction welding and adhesive bonding. However, considerable time has been spent in the pretreatment and coating process of the metallic adherend. For instance, etching itself takes up about 15 minutes. This agrees what has been found by Ramarathnam et al. [3] and Wise et al. [2].

6.2 Electro-insulating behavior and durability

The application of a coating on the pretreated metallic surface resulted in a successful joint. The electro-insulating behavior of both hybrid and non-hybrid welded joints were examined in Chapter 4. For non-hybrid welded joints the adhesive layer was minimized, resulting in an electroconductive joint with an average measured minimal electrical resistance of 10 Ohm. For hybrid welded joints an adhesive layer of 0.09 to 0.25 mm was found between the carbon fibers and aluminium after welding. This layer was found to be electro-insulating. An electroconductive connection showed to be possible when carbon fibers flowed out during the welding process and made contact outside the overlap area. When this outflow is prevented, an electro-insulating joint can be achieved. With this, galvanic corrosion is effectively reduced by preventing an electro-conductive connection.

6.3 Mechanical and fracture behavior

In case no coating was applied on the metallic surface, no bond could be created. The created bonds in which a coating had been applied on the pretreated metallic surface could successfully be tested by single lap shear testing. Where load and fracture in non-hybrid joints were found to be shear dominated, high peel strains were observed at the metallic edge of the hybrid welded joints. These different strain distributions indicate that the resulting SLSSs of the joints with the different adherend combinations cannot be compared. The fracture of the hybrid welded joints were found to be peel adhesion fracture dominated on the metallic surface. The hybrid welded joints at 100 % displacement with grit blasted and etched aluminium adherends resulted in an average joint strength of 16.5 MPa with a coefficient of variation (c.o.v.) of 2.2 %. This means, by using displacement controlled welding, a relatively low c.o.v. can be achieved, which confirms to what has been found for non-hybrid welded joints by Villegas [5]. This result is considered to be competitive with adhesively bonded joints, of which on average a SLSS of 20.5 MPa was observed with a c.o.v. of 11.9 %, with adhesive failure on the surface of the CFR-PA6 substrate. Therefore, the obtained SLSS from these welded joints is 80 % of what has been obtained for adhesively bonded joints. Here, it should be taken into account that the created spew fillets in adhesively bonded joints results in considerable reduction of the apparent stresses in the weld overlap compared to the welded joints, in which no spew fillets are created. It was evaluated how lowering the welding displacement to 66 % of the thickness of the ED would affect the SLSS. The SLSS was found to reduce to 15.1 MPa with a c.o.v. of 7.5 %. It is thought, that in the current welding set-up the fiber bundle deformation in the composite adherend is limited, and the effect of reducing joint strength with increased displacement [5] does not apply with the used materials and welding settings. The hypothesis is posted that rather increased interface peel stresses with a thicker bond line thickness is the cause of such a reduction in joint strength [43].

For welded hybrid joints with coated grit blasted steel substrates, at the used welding settings, the resulting SLSS was found to be 8.5 MPa with a c.o.v. of 7.7 %. The hypothesis is posted, that a lower welding amplitude would result in lower dissipated power and less excessive damage during the welding process. This is thought to result in a better joint strength.

6.4 Implications

The results presented in this study show, that displacement controlled ultrasonic plastic welding, as proposed by Villegas [22], can be used to create joints between metallic and CFRTP structures. The welding stages, as presented by Villegas, are however found not to be applicable in a hybrid welding process, when the CFRTP substrate is in contact with the sonotrode during welding. Further research is needed in this case on what causes the absence of these stages in the dissipated power. In this field, as the welding displacement is proposed to be used as controlling parameter, also further research is needed on how the welding displacement behavior is affected by welding pressure, amplitude and dissipated power.

As found by Ramarathnam et al. [3] and Wise et al. [2] with thermoplastic structures, the application of a thermoplastic coating on the metallic substrate results in the successful application of this welding technique. In the manufacturing of a structure, such a coating process should be implementable. Likewise mentioned by them, the assembly cycle times can be greatly reduced, as the adhesive joining process between thermoplastic and metal after surface treatments can be separated from the cohesive welding process in assembly. The resulting joint strength is in the meantime found to be competitive with the adhesive joining technique, especially when the welding time is considered. As the electro-insulating behavior in the performed tests is found to be guaranteed as long as excessive outflow of carbon fibers is prevented, the durability of the joint might be positively affected.

6.5 Limitations

Although this research has been performed with care, limitations of this study do exist and have to be acknowledged.

In this study, welding has not been stopped per welding stage. A physical comparison what happens per stage could therefore not be made. Also, no relation has been created between the amount of displacement during welding and the resulting single lap shear strength. Only at selected displacements the SLSS has been measured. Results presented by Krüger et al. [4] could not be reproduced. Likewise, the results found in the welding power and displacement feedback have not been reattempted with the usage of another welding device or sonotrode and thus cannot be directly translated to another experimental set-up. As welding has only been performed for individual single lap shear samples, the results in dissipated power and displacement behavior cannot readily be translated to other joint configurations.

The coating technique was applied by vacuum bagging in oven cycles in series of six samples. It should be acknowledged, that the resulting quality of the coated samples might differ from series to series in the time needed for vacuum bagging the produced samples. Moreover, the varying ambient air conditions, where surface treated samples were exposed to before completion of this vacuum bag, might influence the joint quality as well. In producing larger series it was found, that preventing wrinkles in the vacuum bagging foil was harder resulting in an inferior coating surface quality. Therefore, the series were limited. As mentioned, thicker coating layers can be applied on the pretreated metallic surface to mitigate the usage of a separate ED. The usage of a hot platen press can support further research in the prevention of a created bulge on the surface when such a thicker coating is applied.

In the application of grit blasting before coating of aluminium specimens, a crack was observed between the aluminium and thermoplastic after the coating treatment. No tests have been performed in which the surface free energy of the prepared metallic surface has been measured. In welding steel samples, the resulting quality of the welded joints was found to be insufficient. Further tests have to be applied in order to evaluated whether, and how, this can be improved.

6.6 Recommendations

Recommendations of research in the nearby future for the studied ultrasonic plastic welding process are the following:

- Apply even lower welding amplitudes in the current adherend combination when steel samples are applied in UPW. In the performed research, the lowest possible amplitude was applied in the used set-up. The breakage of the ED during welding resulted in a smaller joint area. When no breakage occurs, a clear reference condition can be assessed.
- Apply methods in which a thicker coating can be applied with a flat surface. In such a case, the application of an ED can become obsolete, as mentioned in Section 2.2.2, which is expected to make the process more convenient for further industrialization. This method should be able to be applied in larger series such that several series can be welded with an equal pretreatment history.

- Apply more sophisticated surface treatments on the metallic surface, like anodization, to further improve the adhesive strength after welding.
- Evaluate further how welding pressure and amplitude affect the displacement behavior and whether the displacement rate can be used to more quickly determine welding conditions resulting in improved mechanical behavior. Next to this, evaluate how a selected sonotrode affects the dissipated power feedback throughout welding. This is needed, because no clear pattern in dissipated power was observed for a number of series. It is suggested to identify controlling parameters by analyzing the welding displacement behavior.
- Evaluate whether and how the adhesive layer thickness correlates to the displacement at a given welding force and amplitude. The displacement during welding is measurable, and is a result of the outflow of thermoplastic from the adhesive layer. When the adhesive layer thickness can be obtained by analyzing the welding displacement, an electro-insulating joint can be further guaranteed, and the optimal adhesive layer thickness for the stress distribution through the joint can be further assessed.
- Assess how the long term durability of the created joints is affected by outside weather conditions. Because an electro-insulating joint is created, galvanic corrosion as a result of contact between carbon fibers and aluminium or steel should be reduced. To further determine the processing boundaries to obtain a durable connection, also research has to be performed on what conditions actually do result in an electroconductive connection trough the adhesive layer.
- Further evaluate the resulting morphology of the adhesive layer after ultrasonic welding. After welding, two distinct layers could be observed in the adhesive layer. To be able to determine how the mechanical behavior is affected by welding itself, the crystallinity in the thermoplastic between the metallic and CFRTP part needs to be further evaluated.

6.7 Conclusion

Concluding, the research shows that the application of ultrasonic plastic welding in the creation of joints between carbon fiber reinforced polyamide 6 and aluminium or steel offers prospect to the successful implementation in an industrial environment. The durability and reliability of the process and resulting joints need to be further evaluated. This would further enable application of carbon fiber reinforced thermoplastic in, for instance, the automotive industry.

References

[1] D. Stavrov and H. E. N. Bersee. Resistance welding of thermoplastic composites-an overview. *Composites Part A: Applied Science and Manufacturing*, 36(1):39–54, 2005.

[2] R. J. Wise and A. D. H. Bates. Ultrasonic welding of PES to aluminium alloy. In *54th Annual Technical Conference ANTEC '96*, volume 1, Dallas, 1996. Society of Plastics Engineers.

[3] G. Ramarathnam, T.H. North, M. Libertucci, and R.T. Woodhams. Ultrasonic bonding of high strength polypropylene to aluminium. In *48th Annual Technical Conference ANTEC'90*, volume 1, pages 1778–1782, Dallas, 1990. Society of Plastics Engineers.

[4] S. Krüger, Guntram Wagner, and D. Eifler. Ultrasonic welding of metal/composite joints. *Advanced Engineering Materials*, 6(3):157–159, 2004.

[5] I. F. Villegas. Strength development versus process data in ultrasonic welding of thermoplastic composites with flat energy directors and its application to the definition of optimum processing parameters. *Composites Part A: Applied Science and Manufacturing*, 65:27–37, 2014.

[6] F. Balle, G. Wagner, and D. Eifler. Ultrasonic metal welding of aluminium sheets to carbon fibre reinforced thermoplastic composites. *Advanced Engineering Materials*, 11(1-2):35–39, 2009.

[7] P. Mitschang, R. Velthuis, and M. Didi. Induction spot welding of metal/CFRPC hybrid joints. *Advanced Engineering Materials*, 15(9):804–813, 2013.

[8] R. Laessig, M. Eisenhut, A. Mathias, R. T. Schulte, F. Peters, T. Kuehmann, T. Waldmann, and W. Begemann. Series production of high-strength composites perspectives for the german engineering industry. Technical report, Roland Berger Strategy Consultants, 2012.

[9] C. Born, G. Wagner, and D. Eifler. Ultrasonically welded aluminium foams/sheet metal - joints. *Advanced Engineering Materials*, 8(9):816–820, 2006.

[10] F. Balle, G. Wagner, and D. Eifler. Ultrasonic spot welding of aluminum sheet/carbon fiber reinforced polymer - joints. *Materialwissenschaft und Werkstofftechnik*, 38(11):934–938, 2007.

[11] G. Wagner, F. Balle, and D. Eifler. Ultrasonic welding of aluminum alloys to fiber reinforced polymers. *Advanced Engineering Materials*, 15(9):792–803, 2013.

[12] P. Mitschang, R. Velthuis, S. Emrich, and M. Kopnarski. Induction heated joining of aluminum and carbon fiber reinforced Nylon 66. *Journal of Thermoplastic Composite Materials*, 22(6):767–801, 2009.

[13] M. Didi, S. Emrich, P. Mitschang, and M. Kopnarski. Characterization of long-term durability of induction welded aluminum/carbon fiber reinforced polymer-joints. *Advanced Engineering Materials*, 15(9):821–829, 2013.

[14] J. P. Bergmann and M. Stambke. Potential of laser-manufactured polymer-metal hybrid joints. *Physics Procedia*, 39:84–91, 2012.

[15] A. Roesner, S. Scheik, A. Olowinsky, A. Gillner, U. Reisgen, and M. Schleser. Laser assisted joining of plastic metal hybrids. *Physics Procedia*, 12:370–377, 2011.

[16] A. Cenigaonaindia, F. Liébana, A. Lamikiz, and Z. Echegoyen. Novel strategies for laser joining of polyamide and AISI 304. *Physics Procedia*, 39:92–99, 2012.

[17] A. Fortunato, G. Cuccolini, A. Ascari, L. Orazi, G. Campana, and G. Tani. Hybrid metal-plastic joining by means of laser. *International Journal of Material Forming*, 3(S1):1131–1134, 2010.

[18] K. W. Jung, Y. Kawahito, M. Takahashi, and S. Katayama. Laser direct joining of carbon fiber reinforced plastic to zinc-coated steel. *Materials & Design*, 47:179–188, 2013.

[19] K. W. Jung, Y. Kawahito, M. Takahashi, and S. Katayama. Laser direct joining of carbon fiber reinforced plastic to aluminum alloy. *Journal of Laser Applications*, 25(3), 6 March 2013 2013.

[20] P. Amend, S. Pfindel, and M. Schmidt. Thermal joining of thermoplastic metal hybrids by means of mono- and polychromatic radiation. *Physics Procedia*, 41:98–105, 2013.

[21] C. Ageorges and L. I. N. Ye. Resistance welding of metal/thermoplastic composite joints. *Journal of Thermoplastic Composite Materials*, 14(6):449–475, 2001.

[22] I. F. Villegas. In situ monitoring of ultrasonic welding of thermoplastic composites through power and displacement data. *Journal of Thermoplastic Composite Materials*, 2013.

[23] M. N. Tolunay, P. R. Dawson, and K. K. Wang. Heating and bonding mechanisms in ultrasonic welding of thermoplastics. *Polymer Engineering & Science*, 23(13):726–733, 1983.

[24] Z. Zhang, X. Wang, Y. Luo, Z. Zhang, and L. Wang. Study on heating process of ultrasonic welding for thermoplastics. *Journal of Thermoplastic Composite Materials*, 23(5):647–664, 2009.

[25] A. Levy, S. Le Corre, and A. Poitou. Ultrasonic welding of thermoplastic composites: a numerical analysis at the mesoscopic scale relating processing parameters, flow of polymer and quality of adhesion. *International Journal of Material Forming*, 7(1):39–51, 2012.

[26] A. Benatar, R. V. Eswaran, and S. K. Nayar. Ultrasonic welding of thermoplastics in the near-field. *Polymer Engineering and Science*, 29(23):1689–1698, 1989.

[27] H. Potente. Ultrasonic welding - principles & theory. *Materials & Design*, 5(Octaber/November):228–234, 1984.

[28] I. F. Villegas, M. Barroso-Romero, and H. E. N. Bersee. Analysis of the effect of the welding parameters in ultrasonic welding of CF/PEI composites. In *SAMPE 2012*, Baltimore, 2012. SAMPE.

[29] A. Levy, S. Le Corre, and I. F. Villegas. Modeling of the heating phenomena in ultrasonic welding of thermoplastic composites with flat energy directors. *Journal of Materials Processing Technology*, 214:1361–1371, 2014.

[30] A. Benatar and T. G. Gutowski. Ultrasonic welding of peek graphite apc-2 composites. *Polymer Engineering & Science*, 29(23):1705–1721, 1989.

[31] Granta Design Limited. *CES EduPack 2013 Version 12.2.13*. Granta Design Limited, Cambridge, United Kingdom, 12.2.13 edition, 2013.

[32] H. v. Wijk, G. A. Luiten, P. G. v. Engen, and C. J. Nonhof. Process optimization of ultrasonic welding. *Polymer Engineering and Science*, 36(9):1165–1176, 1996.

[33] I. F. Villegas. High-speed spot welding of continuous fibre reinforced thermoplastic composites. In *International CFK-Valley Stade Convention*, Stade, 2012.

[34] C. Ageorges, L. Ye, and M. Hou. Advances in fusion bonding techniques for joining thermoplastic matrix composites: a review. *composites Part A: Applied Science and Manufacturing*, 32:839–857, 2001.

[35] A. J. Kinloch. *Adhesion and Ahesives - Science and Technology*. Chapman and Hall Ltd, London, 1987.

[36] J. D. Minford. *Handbook of Aluminum Bonding Technology and Data*. Marcel Dekker, Inc., New York, 1993.

[37] A. Kwakernaak, J. Hofstede, J. Poulis, and R. Benedictus. Improvements in bonding metals (steel, aluminium). In D. A. Dillard, editor, *Advances in structural adhesive bonding*, volume 1, chapter 8, pages 185–236. Woodhead Publishing Limited, Cambridge, 2010.

[38] S. Emrich. *Untersuchungen zum Einfluss von Oberflächenchemie und -morphologie auf die Langzeitbeständigkeit geklebter Aluminiumverbunde*. PhD thesis, Universität Kaiserslautern, Kaiserslautern, 21-07-2003 2003.

[39] K. A. Lucas and H. Clarke. *Corrosion of Aluminium-Based Metal Matrix Composites*. Research Studies Press Ltd., Taunton, Somerset, 1993.

[40] D. A. Jones. *Principles and prevention of corrosion.* Prentice-Hall, Inc., Upper Saddle River, 2 edition, 1996.

[41] F. Balle. *Ultraschallschweissen von Metall / C-Faser-Kunststoff (CFK) - Verbunden.* PhD thesis, Technische Universitaet Kaiserslautern, Kaiserslautern, 02-02-2009 2009.

[42] TenCate Advanced Composites BV. Personal communications. Nijverdal, The Netherlands, 2014.

[43] D. M. Gleich, M. J. L. van Tooren, and A. Beukers. Analysis and evaluation of bondline thickness effects on failure load in adhesively bonded structures. *Journal of Adhesion Science and Technology*, 15(9):1091–1101, 2001.

[44] M. Y. Tsai and J. Morton. The effect of a spew fillet on adhesive stress distributions in laminated composite single-lap joints. *Composite Structures*, 65:123–131, 1995.

[45] S. C. Tjong and S. P. Bao. Preparation and nonisothermal crystallization behavior of polyamide 6/montmorillonite nanocomposites. *Journal of Polymer Science Part B: Polymer Physics*, 42(15):2878–2891, 2004.

Appendix A

Analysis of the Used Thermoplastic

The used thermoplastic has been tested on several physical properties, which were used in the experimental phase. The outcome of these tests for the used PA6 are presented in this Appendix.

In Section A.1, the results of thermogravimetric analysis are presented. For differential scanning calorimetry, the results are presented in Section A.2. Results of dynamic thermo-mechanical analysis are presented in Section A.3.

A.1 Thermogravimetric Analysis

TGA was performed using a Perkin Eimler . A thermogravimetric analysis has been performed in which air was used as heating gas to analyze the thermo-oxidative behavior of the thermoplastic material. A sample was heated from room temperature up to 450 °C with a heating rate of 10 °C per minute. Results are shown in Figure A.1. DTG μg/min is the loss of material per minute as a result of the heating. DTA (μV) is the amount of heat needed to keep a constant heating rate as a function of the temperature.

Around 100 °C, a local peak of relative weight loss can be observed. This has been attributed to the evaporation of water around it's boiling point at standard pressure in the outside air. A weight percentage of 1.5% is attributed to the loss of water until around 140 °C. A second peak in the DTG-curve can be observed around 350 °C, which can be attributed to thermo-oxidative behavior in air. Ignition can be observed in the DTG-curve from around 385 °C, which results in burning of the PA-6 material above that temperature. In the DTA curve, around 220°C, a local dip can be observed, which can be attributed to the melting temperature of the material, as indicated in the DSC-curves of the material.

A.2 Differential Scanning Calorimetry

A Differential Scanning Calorimetry (DSC) analysis was performed to further analyze the glass transition temperature, melting temperature and crystallization temperature was analyzed.

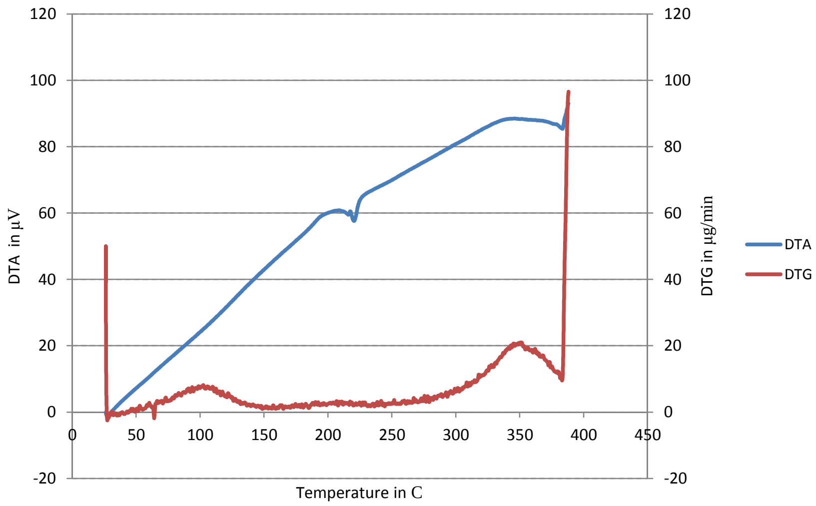

Figure A.1: DTA and DTG of polyamide-6

A conditioned specimen of 6.0 mg was prepared for a double testing cycle, in which the material was heated from room temperature to 300 °C at 10 °C/min. After staying for 5 minutes at this temperature, a cooling process was initiated with a rate of 10 °C/minute. The temperature of the samples cooled at a lower rate than initiated by the program, as can be seen in Figure A.2. Because of this, the second run, initiated after 105 minutes, started with a sample temperature of 62 °C, with a lowest temperature of 60 °C. Due to the starting temperature of 60°C, no second degree transition of the T_g could be observed in the second run. Therefore, a third run was needed with the same sample, which started with a sample temperature of 30 °C. In this case, a T_g of 57 °C could be observed.

In the first run, the influence of water on the endothermic heat was observed. The total heat of the measured peak was either 47.7 or 21.7 J/g, depending on whether the area was measured from the plateau around 40 °C or 70 °C, respectively. Coupling these values to the endothermic heat of water of 2259 J/g resulted in a mass percentage of water of either 2.11% or 0.96 %, respectively. Both values are around the value found during the TGA, earlier. Therefore, further tests are needed. Due to this evaporation in the first run, the sample was assumed to be dry in this second run.

As the film was transparent, i.e. amorphous before the DSC-test started because of a fast cooling process during production, crystallization could be observed in the first heating run with a crystallization peak at 197.67 °C, which is shown in Figure A.2. This crystallization during heating occurs at the same temperature as the crystallization during the cooling cycle. This crystallization is immediately followed by melting when higher temperatures are reached. In the second and third run, no crystallization during heating is found. From the curves during cooling, the relative crystallinity was measured by the area of the exothermic peak. The results of the three runs are given in Table A.1. Using 190 J/g for 100% crystalline PA-6, as used by Tjong and Bao [45], results in the relative crystallinities of the used samples. These measured values for the crystallinity of Polyamide-6 are intermediate values for the crystallinity of the material.

The melting onset temperature found and presented in A.1 can be used to set a temperature

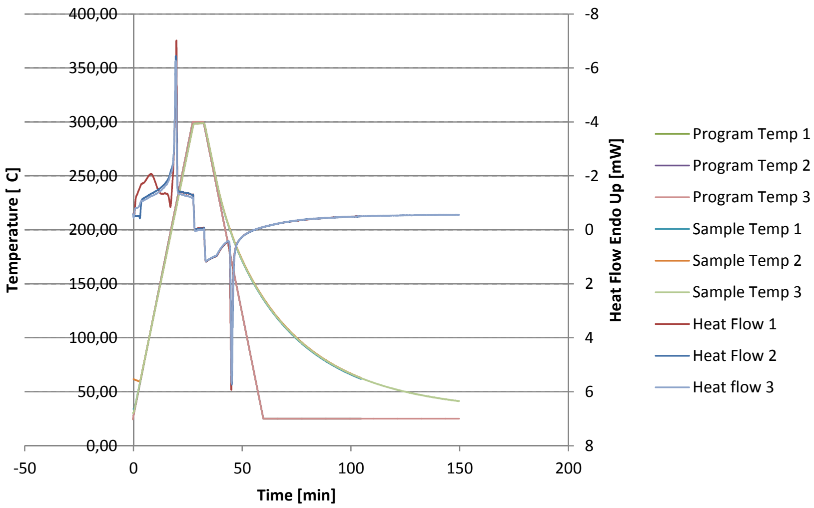

Figure A.2: Temperature and heat curves of three DSC runs against time of PA-6

	Unit	**Run 1**	**Run 2**	**Run3**
Crystallization Heat, Original	J/g	-64.76	-63.28	-63.62
Crystallization Heat, Normalized, 2.11 %	J/g	-66.16	-64.64	-65.00
Crystallization Heat, Normalized, 0.96 %	J/g	-65.39	-63.89	-64.24
Crystallinity Original	%	34.09	33.30	33.49
Crystallinity Normalized, 2.11 %	%	34.82	34.02	34.21
Crystallinity Normalized, 0.96 %	%	34.42	33.66	33.81
Sample melting peak temperature	°C	221.47	218.38	218.22
Sample melting onset temperature	°C	214.6	210.0	209.7
Sample crystallization peak temperature	°C	196.33	196.35	196.06

Table A.1: Retrieved data from the DSC test results

for the JOOS-press in preparing the ultrasonic welding energy director films.

A.3 Dynamical Mechanical Analysis

In order to assess the difference in thermo-mechanical properties of conditioned and dry polyamide 6 specimens, a dynamic mechanical analysis in tensional mode has been performed. The conditioned samples have been stored in ambient conditions and prepared for analysis. Dried samples have been stored in a vacuum oven at 50 °C for at least 48 hours before testing.

A Dynamic Mechanical Analysis in tensional mode has been performed, of which the results are presented in Figure A.4.

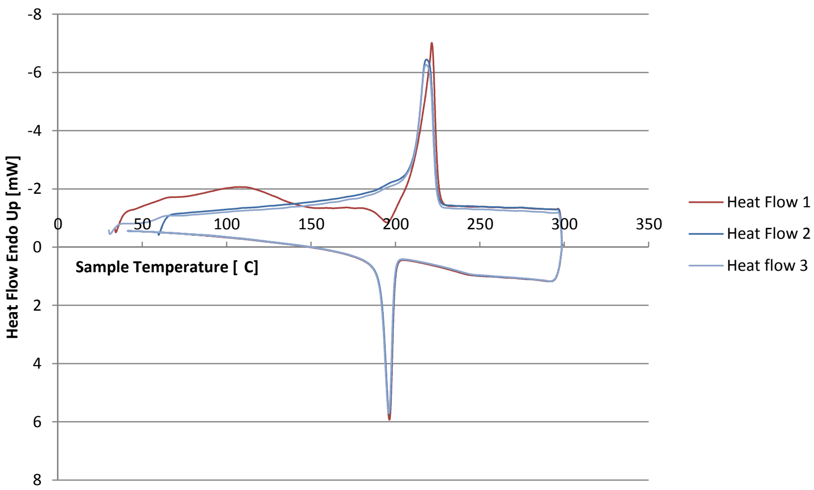

Figure A.3: Heat curves of three DSC runs against sample temperature of PA-6

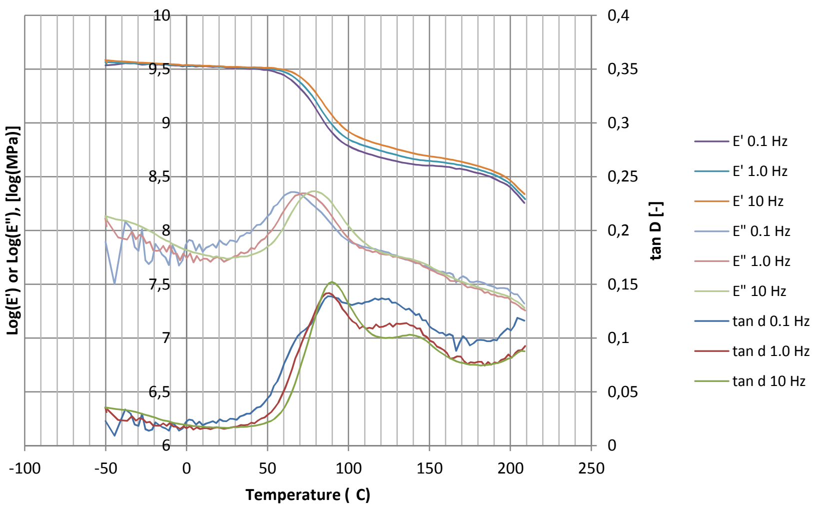

Figure A.4: Storage modulus, loss modulus and tan δ against temperature of used PA-6 material

Appendix B

Welding Force Feedback

During welding, phases in power feedback curves were found to be non-similar for hybrid welds in which the CFR-PA6 adherend acted as a top adherend. Similarities were however found in the force feedback, which have been analyzed further to understand more about the process of welding.

In Figure B.1 is presented how force, power and travel are in general related within the vibration phase. It can be found, that a minimum is found at the moment when onset of sonotrode displacement occurs as a result of flow of thermoplastic out of the welding overlap. Before this, an increase in force is found as room is made for the sonotrode to vibrate. The perceived force declines as the thermoplastic becomes softer with increased force. During the displacement phase, in stages 3 to 5, the force stays overall constant. When the vibration phase is stopped, a sudden drop in applied force is observed, together with a sudden rise in displacement. Both are perceived as a result of the end of vibration, as the sonotrode stops vibrating and approaches in rest the overlap surface.

Next to these changes on a larger scale, a high frequency response is observed throughout welding in the force feedback. This phenomenon is further analyzed by means of a Fourier analysis, in which a fast Fourier transform has been applied. Results are presented in Figure B.2. A dominating peak around 100 Hz can be found for a sampling rate of 500 Hz. This is also found in all other analyzed welds, as found in Appendix C.2. As the welding frequency lies around 20.1 kHz, the peak appears to be a result of aliasing. This can be explained by the equation for an aliasing frequency, in equation B.1. Here, f_a is the aliasing frequency, R the sampling rate of 500 Hz, n a positive integer. This results a frequency $R \cdot n$ of 20 kHz closest to the signal frequency f_s, when an n of 40 is applied.

$$f_a = |R \cdot n - f_s| \tag{B.1}$$

Using the outcome of the fast Fourier transform, the high frequency feedback and lower frequency feedback can be separated and then inverted. Results of such an inversion is presented in Figure B.3. From this, behavior in the low frequency domain and high frequency domain can be analyzed separately.

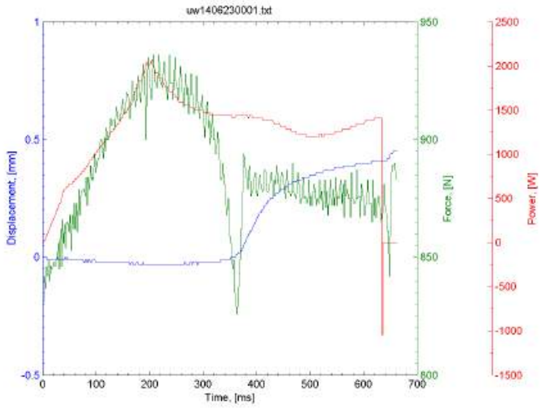

Figure B.1: Displacement, power and force feedback of a welded joint between two composite adherends.

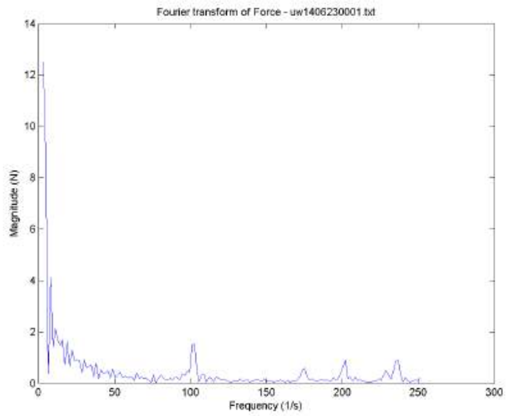

Figure B.2: Amplitude for several frequencies after applying a scaled Fourier transform.

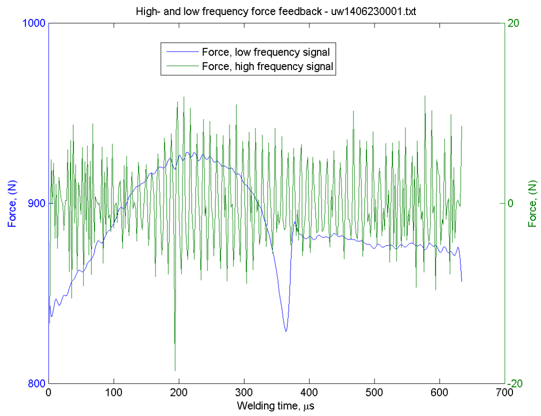

Figure B.3: Force feedback divided in high and low frequency feedback.

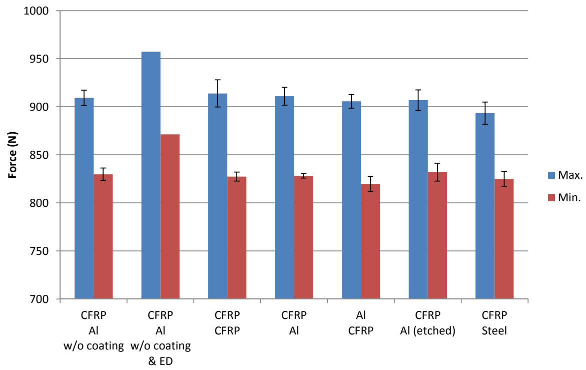

Figure B.4: Maximum force vs. minimum force during welding. The first mentioned substrate was in contact with the sonotrode during welding.

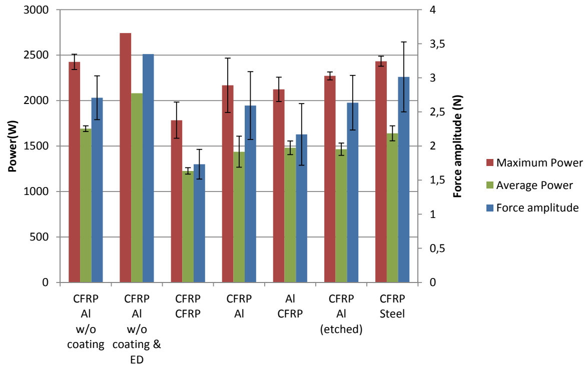

Figure B.5: Comparison of consumed power during welding and the experienced high frequency power feedback at peak amplitude around 102 Hz. The first mentioned substrate was in contact with the sonotrode during welding.

In Figure B.4 the relation between Force maximum value and minimum value is presented. For steel samples, it can be observed that the maximum force value lies comparatively low. Further, the absence of an ED results in an increased maximum and minimum force during welding. Fracture in the energy director is thought to play a role in this lower maximum force, as this appears to occur before the maximum experienced force is reached and the ED is still relatively cold.

In Figure B.5, a comparison is made between the maximum power, the average power and the found amplitude around 102 Hz in the applied fast Fourier transform. It appears that the experienced frequent changing force in the load sensor has a positive correlation with the dissipated power during welding for equal clamping force and amplitude. Further, it can be clearly observed, that a lower equivalent stiffness of the welding overlap correlates with both an increased maximum- and average power and a higher force Fourier peak amplitude around 102 Hz.

Appendix C

Welding Data

For all presented welds, the welding data is separately presented in the following Sections. First, sonotrode displacement, dissipated power and clamping force are presented in Section C.1. This is followed by a Fourier analysis of the force feedback for each weld in Section C.2. In Section C.3 the resulting division of high and low frequency force feedback is presented, as discussed in Appendix B.

C.1 Displacement, Power and Force

In the upcoming figures, the sonotrode displacement, dissipated power and clamping force are presented for each welding series. This is presented:

- for non-hybrid welds in Figure C.1.
- for non-hybrid welds with 66% displacement in Figure C.2.
- for uncoated grit blasted aluminium to CFR-PA6 in Figure C.3;
- for uncoated grit blasted aluminium to CFR-PA6 without using an ED in Figure C.4;
- for grit blasted and coated aluminium to CFR-PA6 in Figure C.5;
- for grit blasted and coated aluminium to CFR-PA6, until 80% displacement in Figure C.6;
- for grit blasted, etched and coated aluminium to CFR-PA6 in Figure C.7;
- for grit blasted, etched and coated aluminium to CFR-PA6 with optimized displacement in Figure C.8;
- for grit blasted and coated aluminium to CFR-PA6, with aluminium as top adherend in Figure C.9;
- for grit blasted and coated steel to CFR-PA6 in Figure C.10.

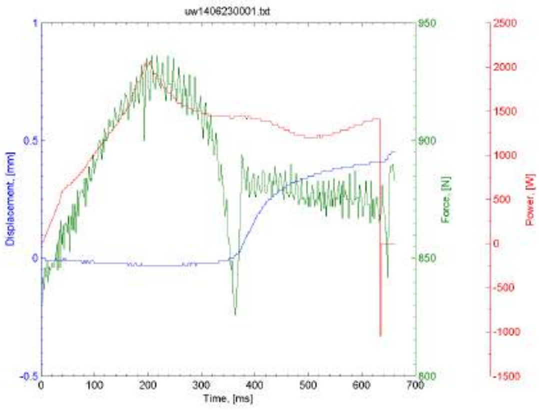

(a)

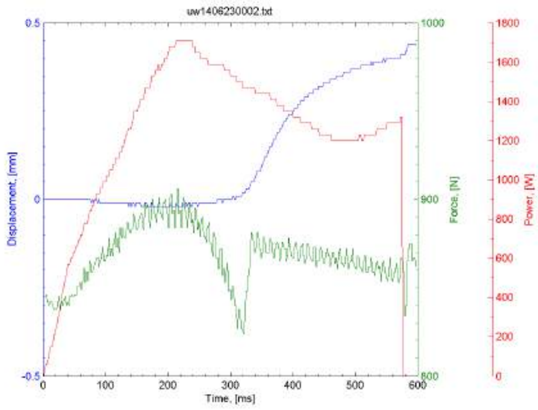

(b)

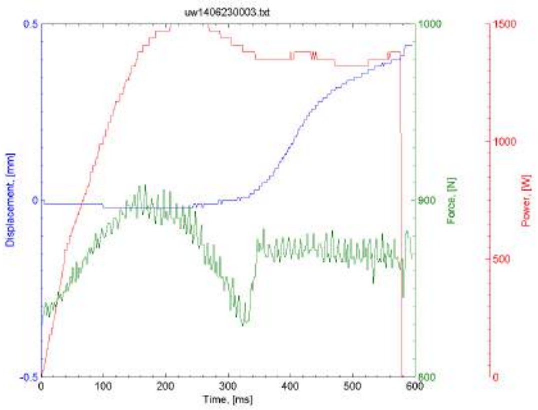

(c)

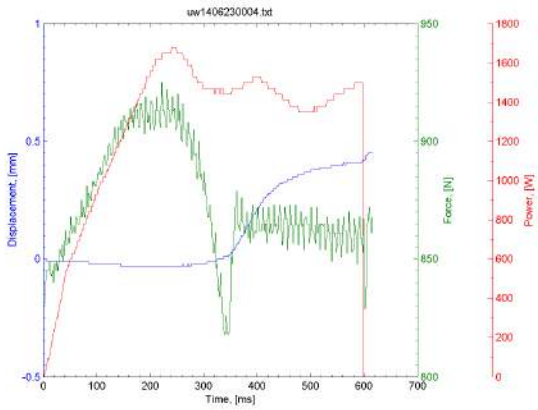

(d)

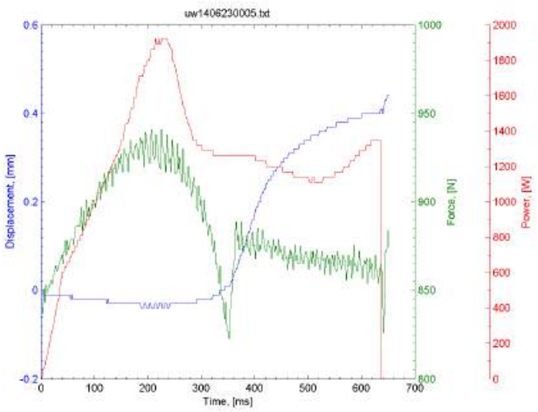

(e)

Figure C.1: Displacement, force and power data for composite to composite weld number 1 to 5.

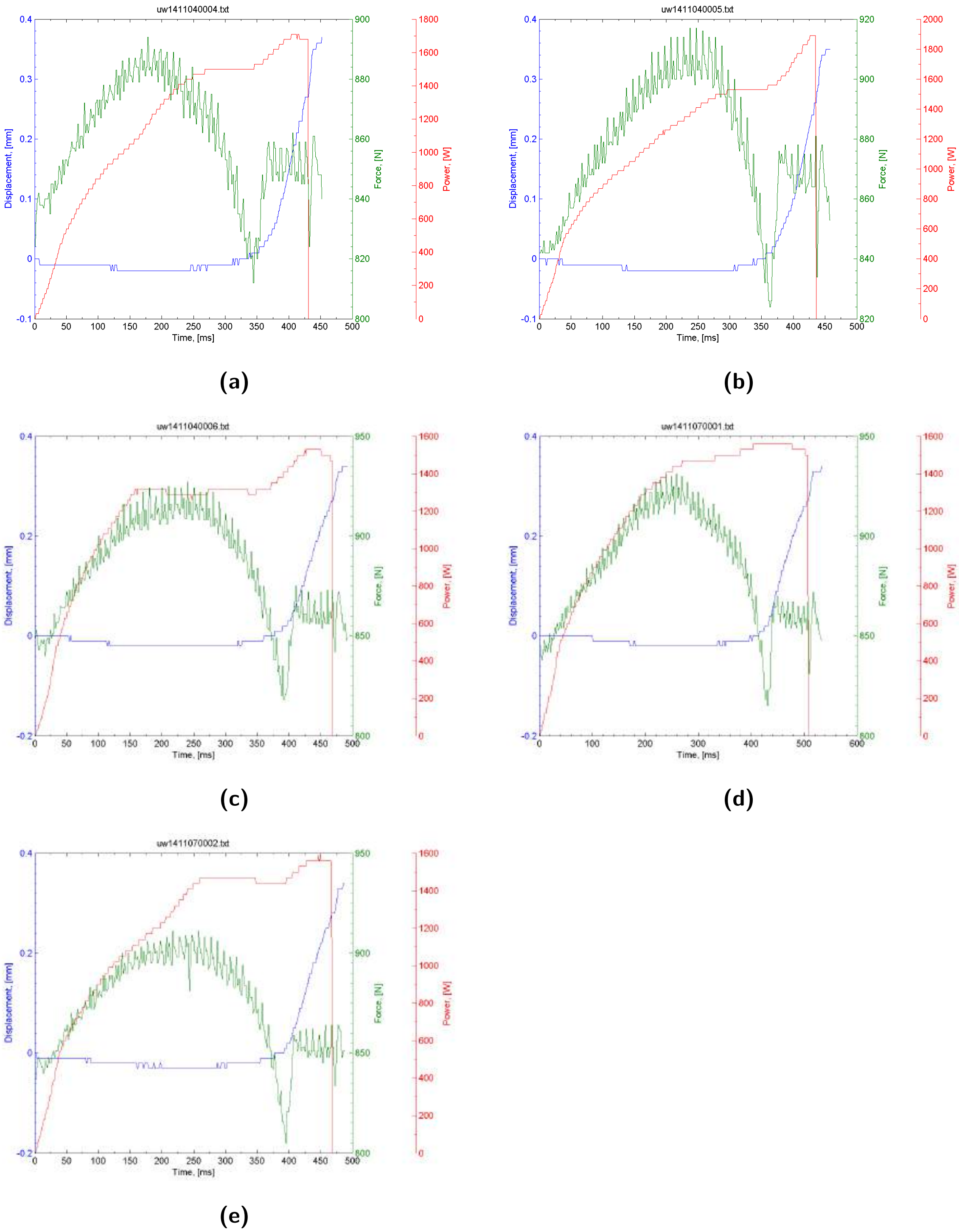

Figure C.2: Displacement, force and power data for composite to composite weld with 66 % displacement, number 1 to 3, 6 & 7.

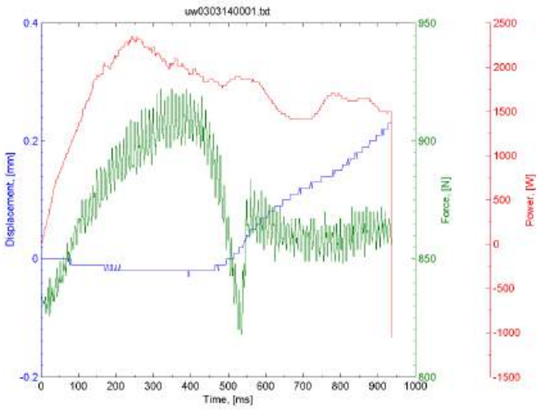

(a)

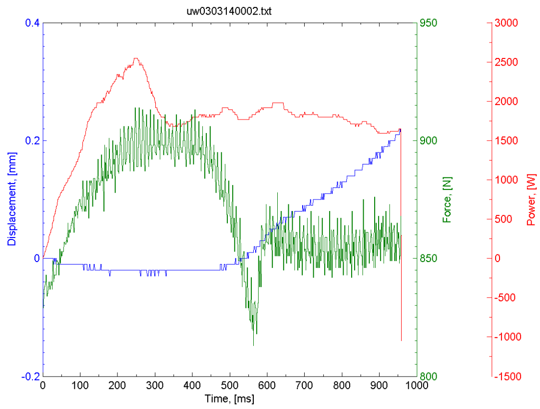

(b)

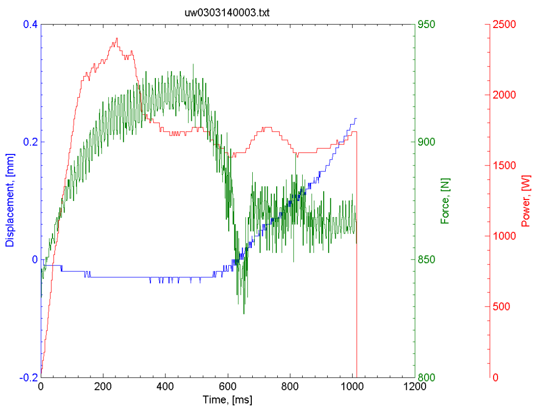

(c)

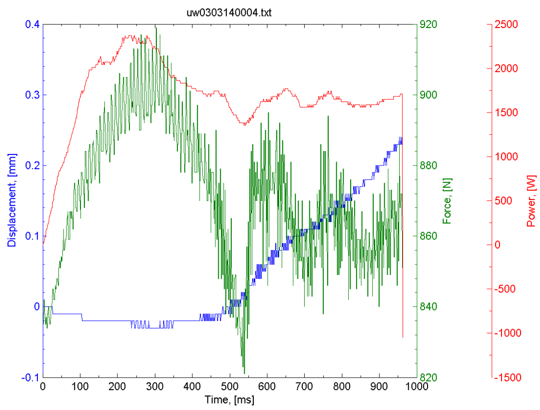

(d)

Figure C.3: Displacement, force and power data for welds between grit blasted non-coated aluminium and composite, weld number 1 to 4.

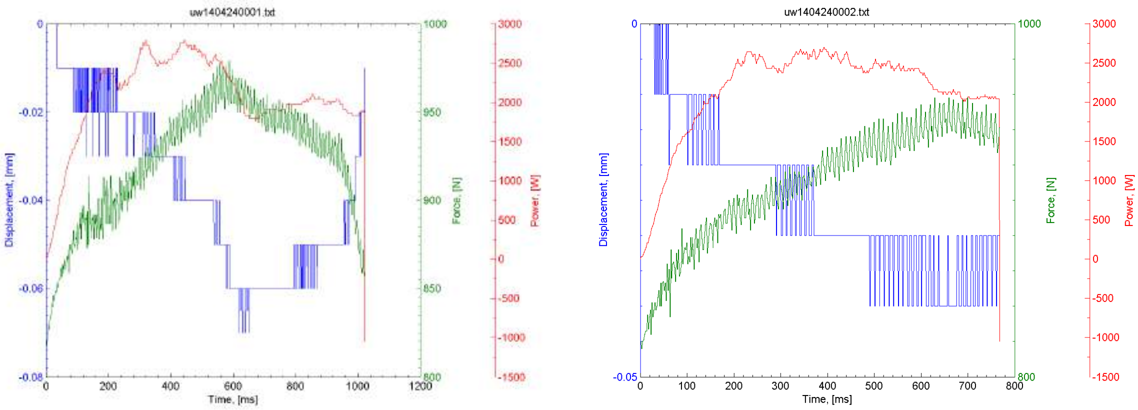

(a) **(b)**

Figure C.4: Displacement, force and power data for welds between grit blasted non-coated aluminium and composite without using an energy directing thermoplastic.

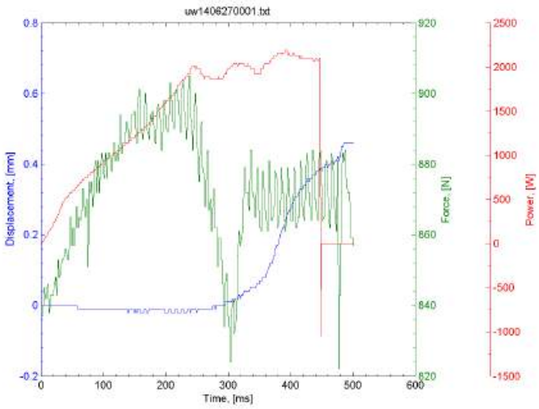

(a)

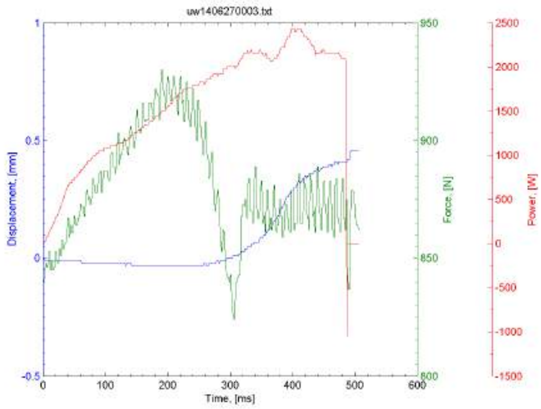

(b)

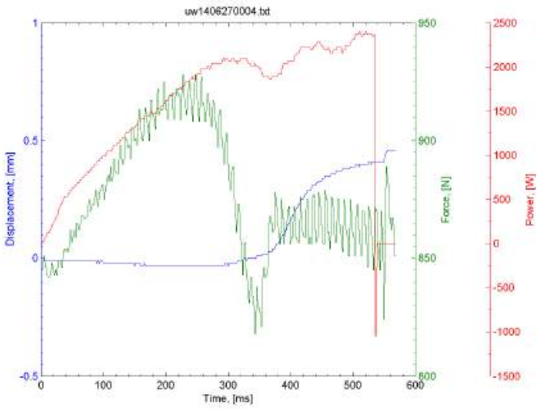

(c)

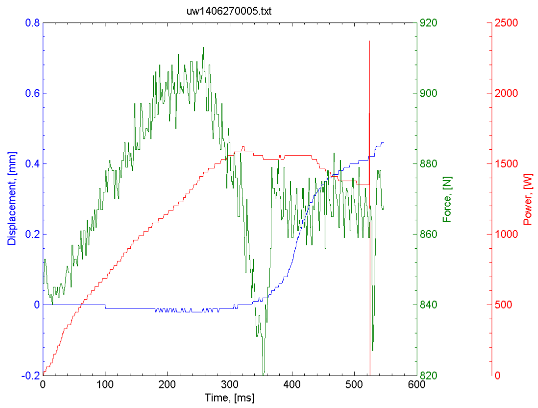

(d)

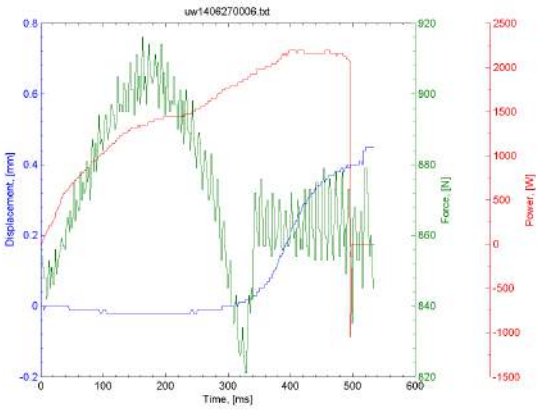

(e)

Figure C.5: Displacement, force and power data for composite to grit blasted and coated aluminium (bottom) weld number 1 and 3 to 6.

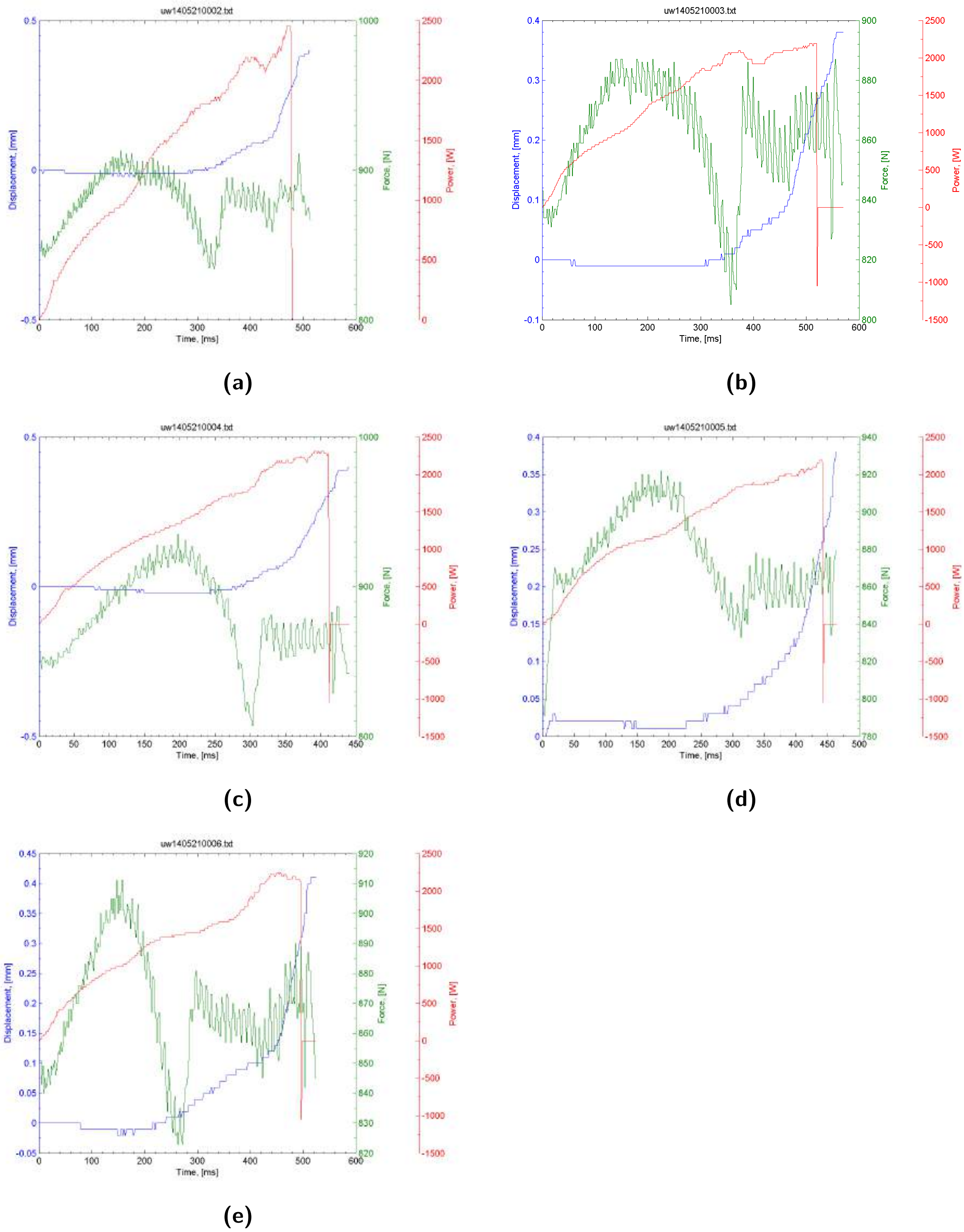

Figure C.6: Displacement, force and power data for composite to grit blasted and coated aluminium (bottom) weld until 80 % displacement, number 2 to 6.

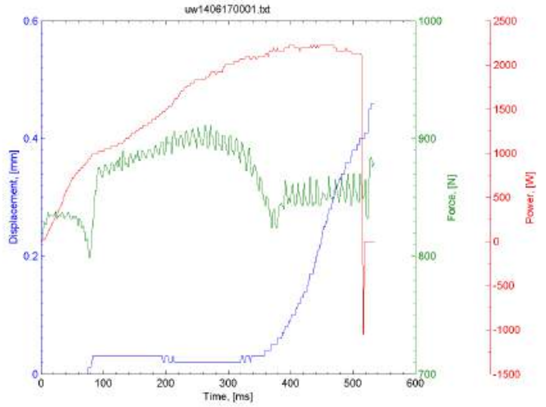

(a)

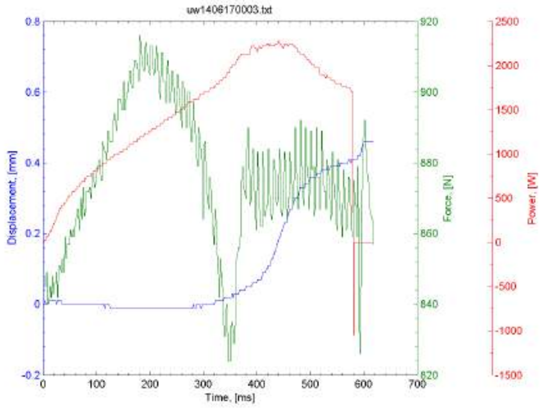

(b)

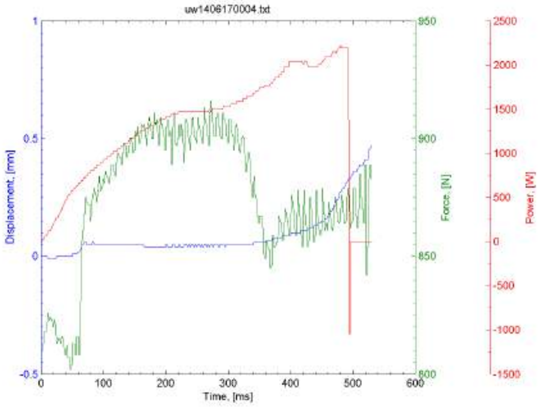

(c)

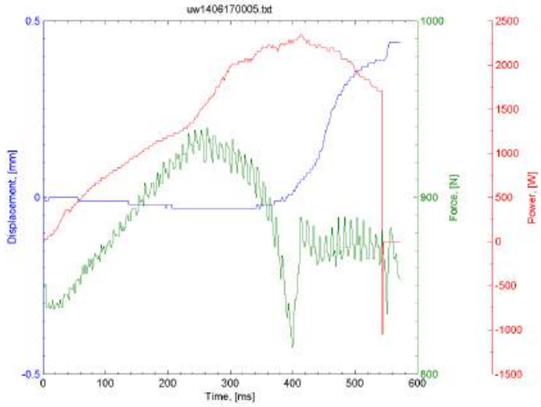

(d)

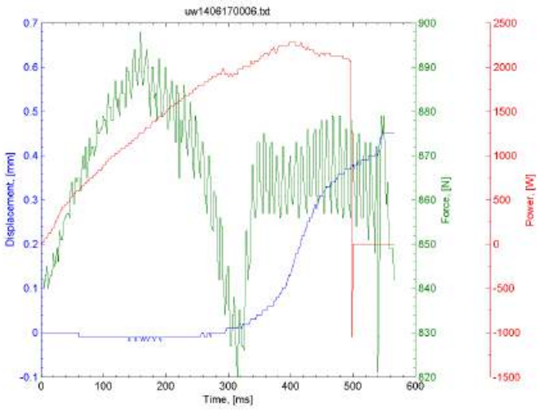

(e)

Figure C.7: Displacement, force and power data for composite to grit blasted, etched and coated aluminium (bottom) weld number 1 and 3 to 6.

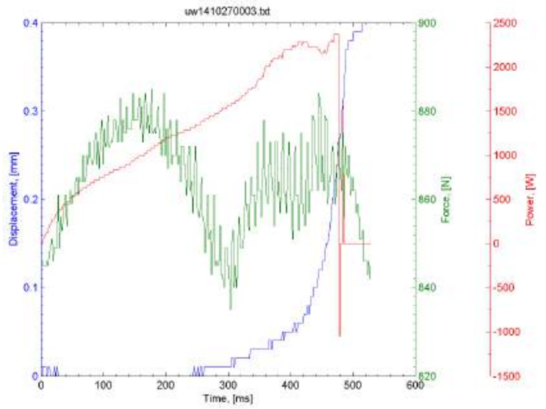

(a)

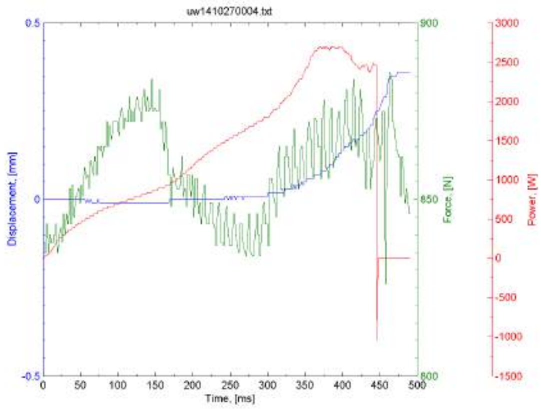

(b)

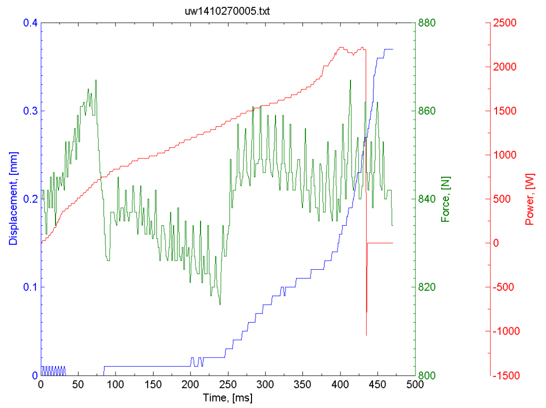

(c)

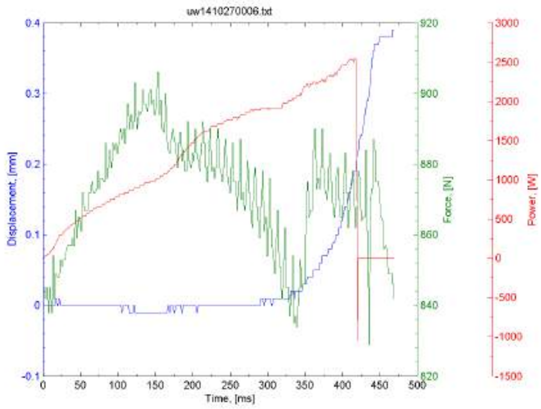

(d)

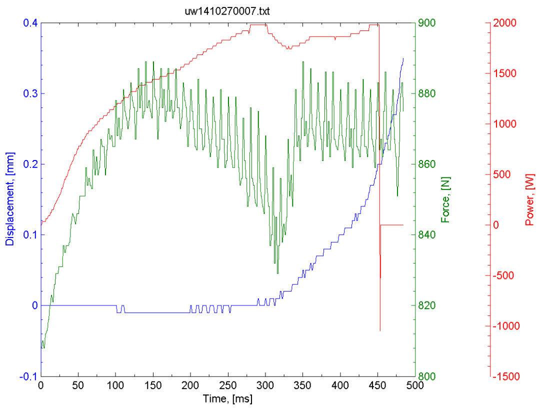

(e)

Figure C.8: Displacement, force and power data for composite to grit blasted, etched and coated aluminium (bottom) welded until 66% displacement, weld number 1 to 5.

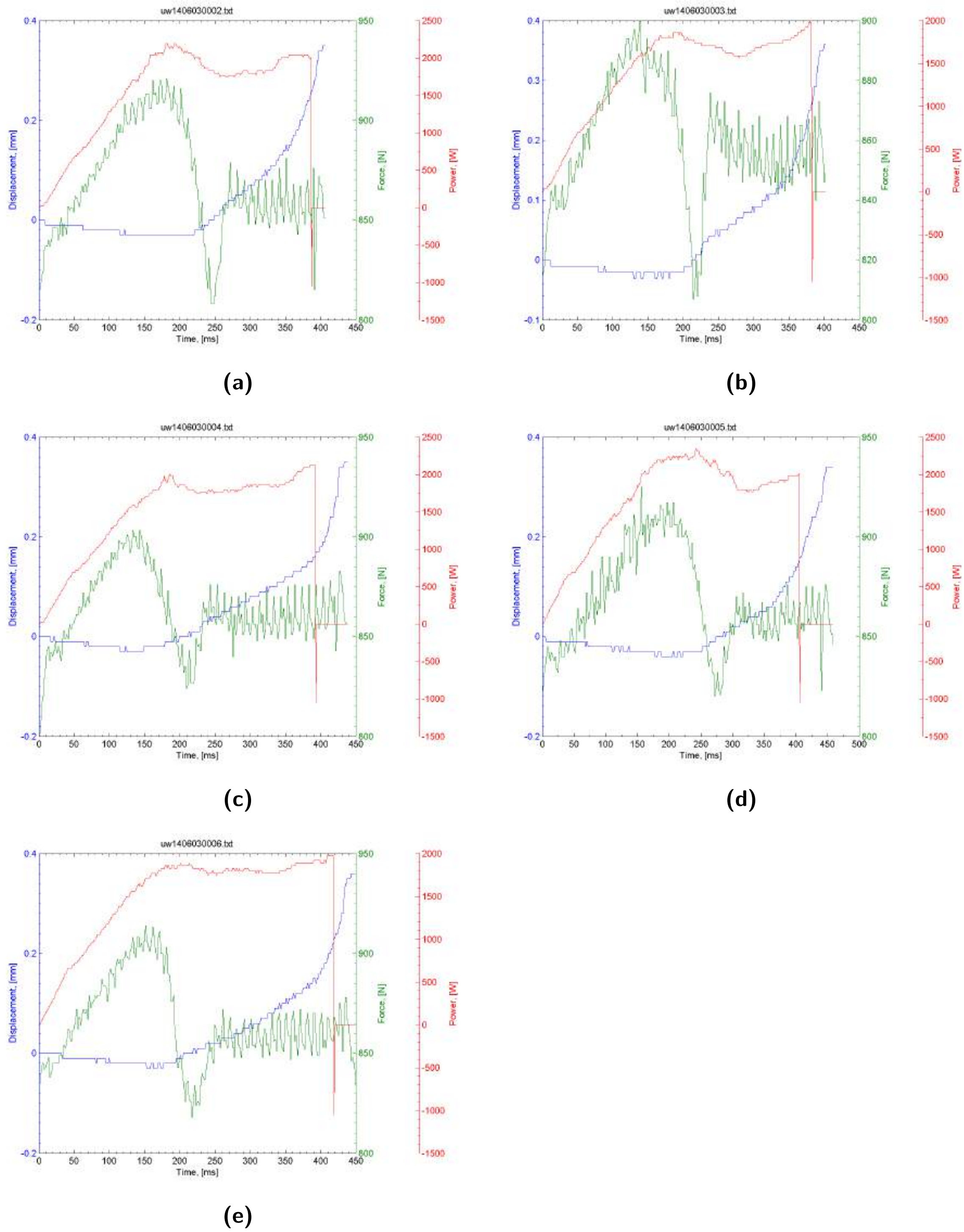

Figure C.9: Displacement, force and power data for grit blasted and coated aluminium (top) to composite weld number 2 to 6.

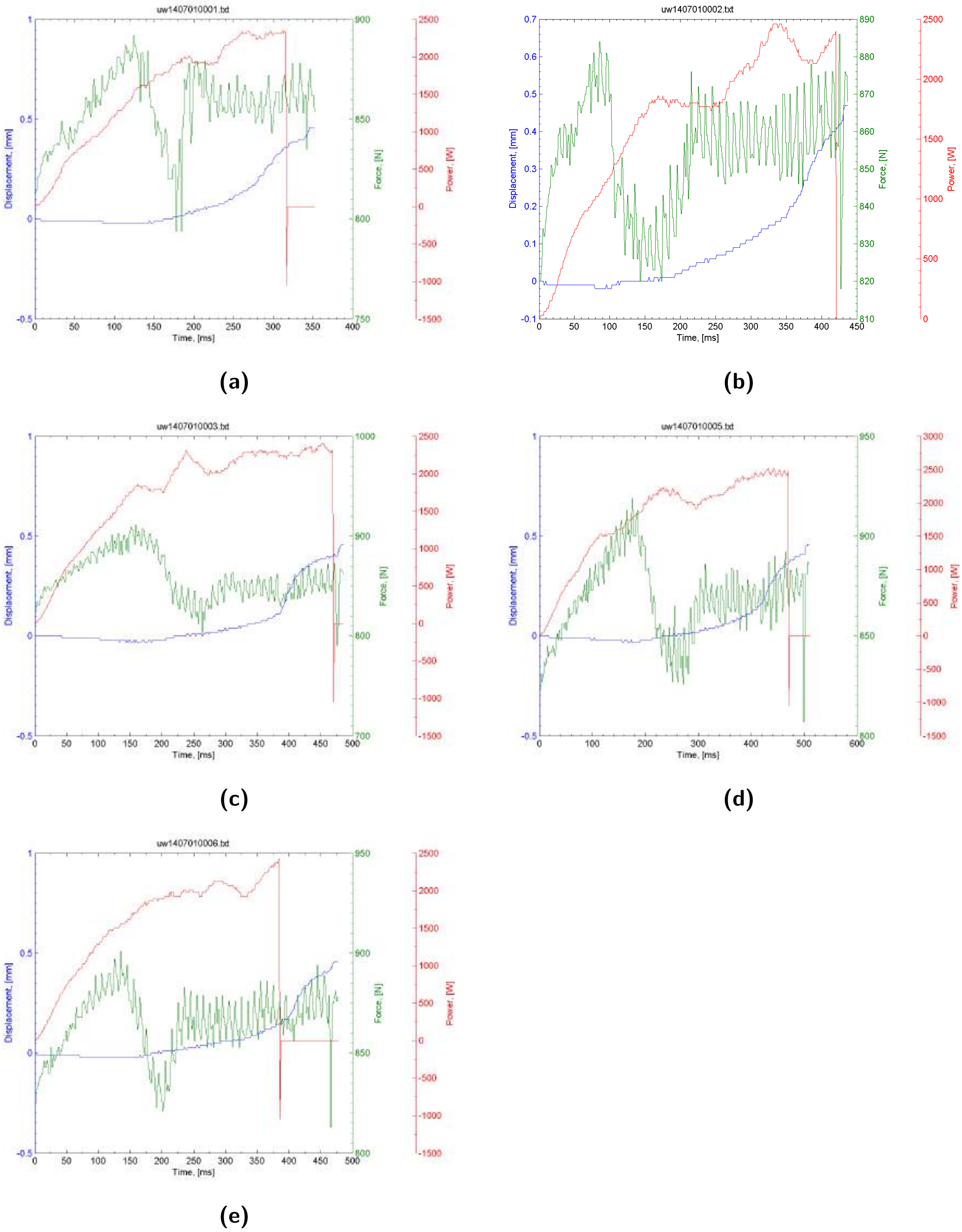

Figure C.10: Displacement, force and power data for composite to grit blasted and coated steel (bottom) weld number 1 to 3 and 5 & 6.

C.2 Fourier Transform of Force Data

In the upcoming figures, the Fourier transforms of individual welds are presented for each welding series. This is presented:

- for non-hybrid welds in Figure C.11;
- for non-hybrid welds with 66% displacement in Figure C.12.
- for uncoated grit blasted aluminium to CFR-PA6 in Figure C.13;
- for uncoated grit blasted aluminium to CFR-PA6 without using an ED in Figure C.14;
- for grit blasted and coated aluminium to CFR-PA6 in Figure C.15;
- for grit blasted and coated aluminium to CFR-PA6, until 80% displacement in Figure C.16;
- for grit blasted, etched and coated aluminium to CFR-PA6 in Figure C.17;
- for grit blasted, etched and coated aluminium to CFR-PA6 with optimized displacement in Figure C.18;
- for grit blasted and coated aluminium to CFR-PA6, with aluminium as top adherend in Figure C.19;
- for grit blasted and coated steel to CFR-PA6 in Figure C.20.

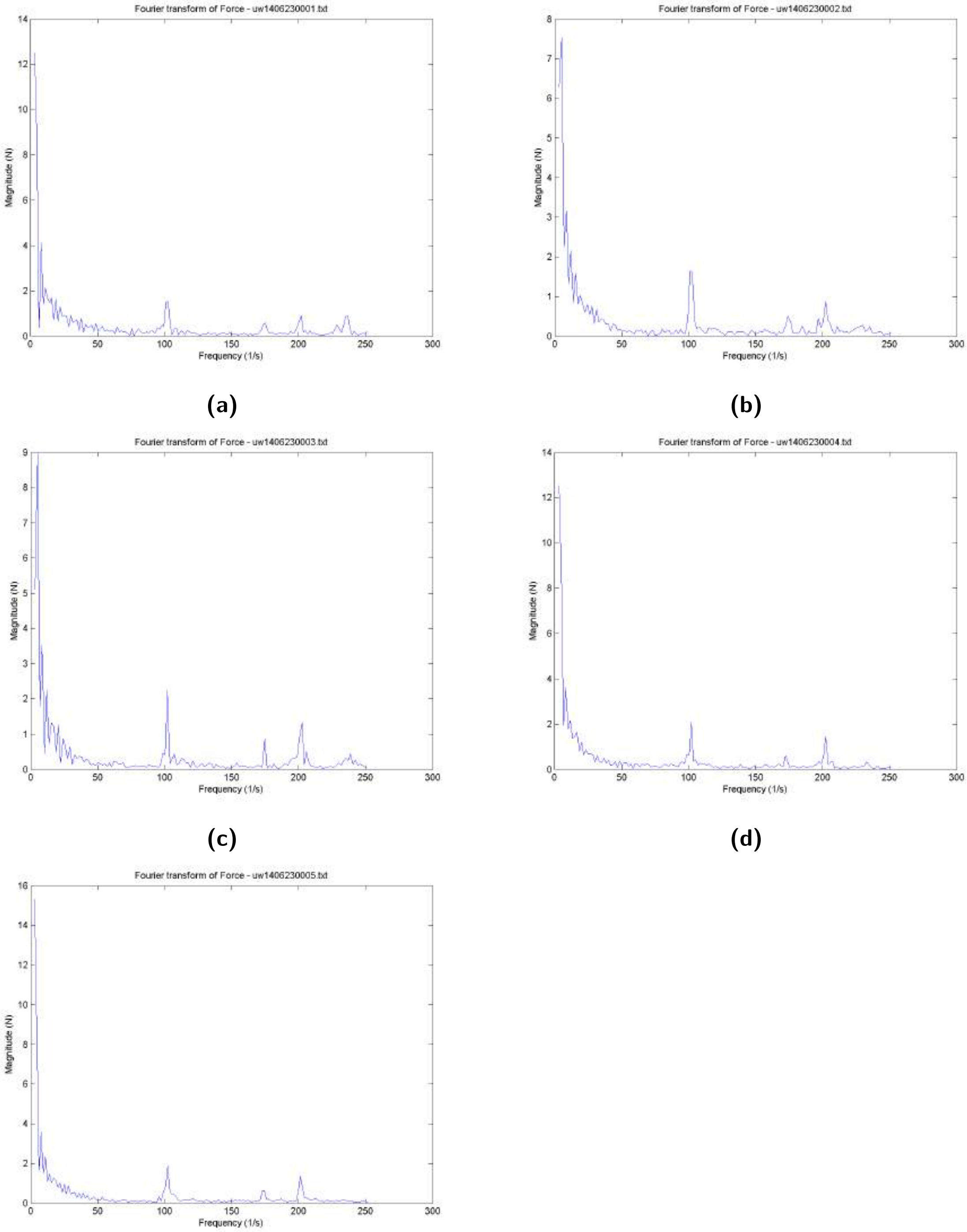

(a) **(b)** **(c)** **(d)** **(e)**

Figure C.11: Absolute magnitude of Fourier transform of Force data for composite to composite weld number 1 to 5.

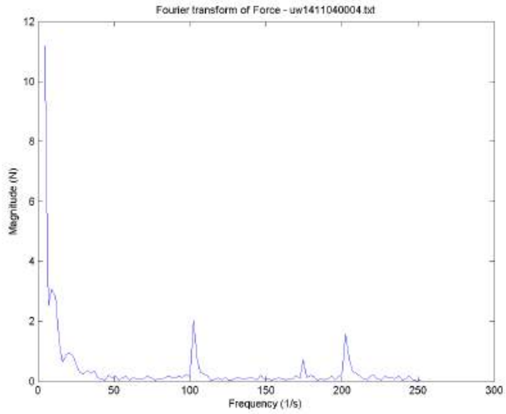

(a)

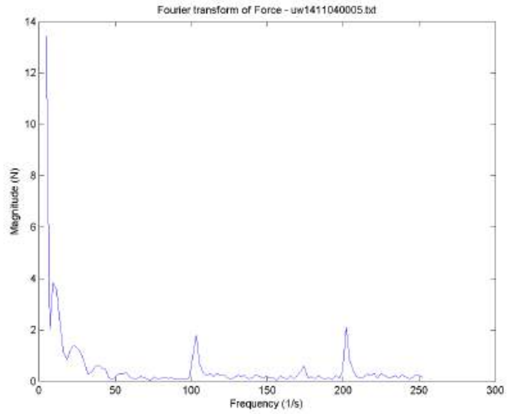

(b)

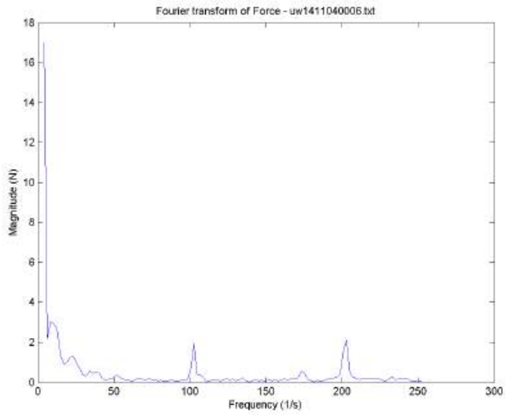

(c)

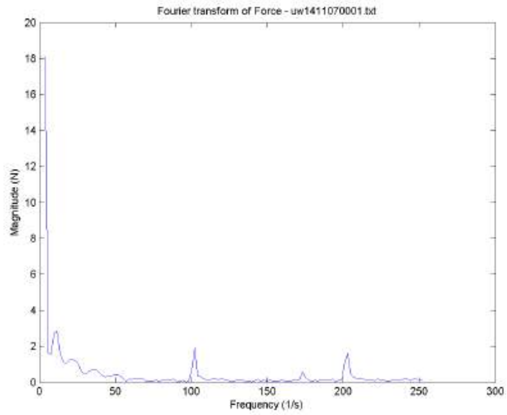

(d)

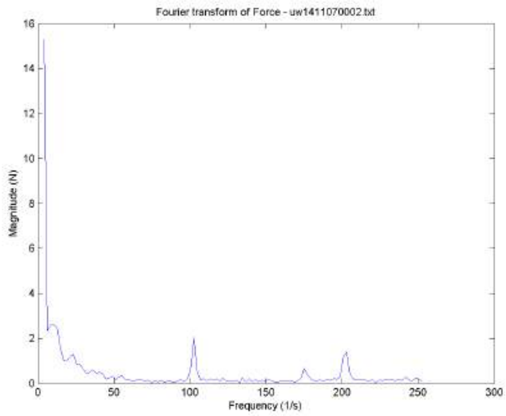

(e)

Figure C.12: Absolute magnitude of Fourier transform of Force data for composite to composite weld with 66 % displacement, number 1 to 3, 6 & 7.

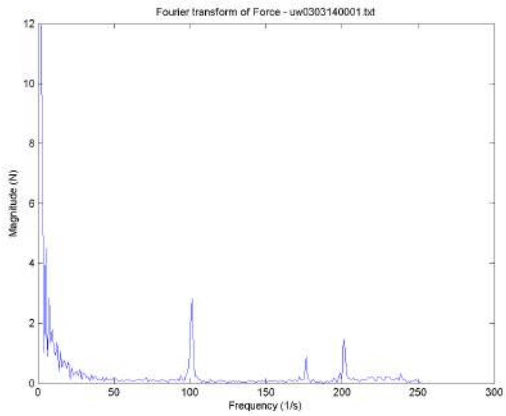

(a)

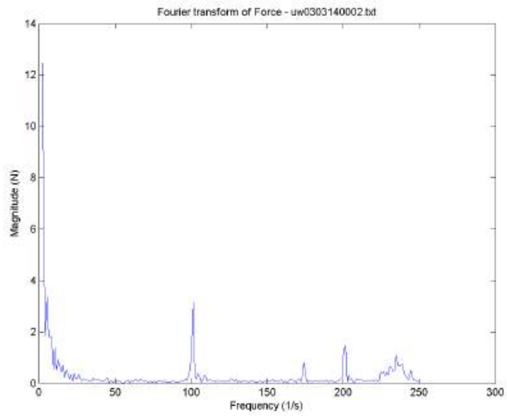

(b)

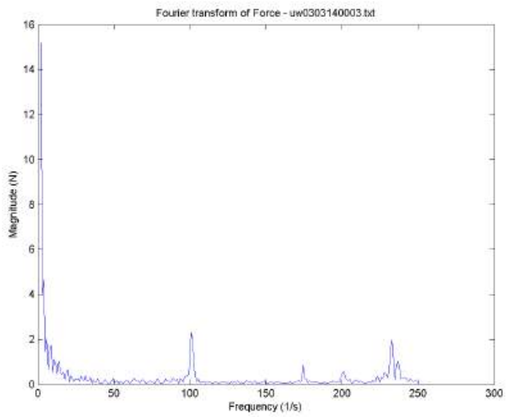

(c)

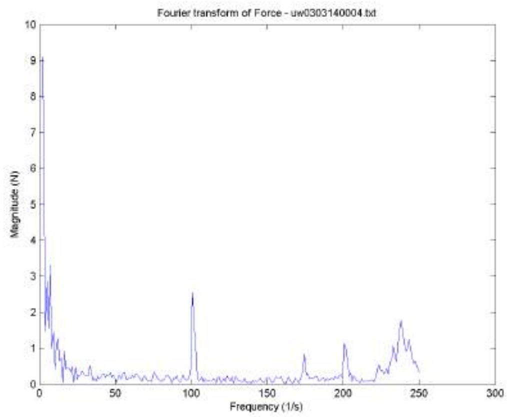

(d)

Figure C.13: Absolute magnitude of Fourier transform of force data for welds between grit blasted non-coated aluminium and composite, weld number 1 to 4.

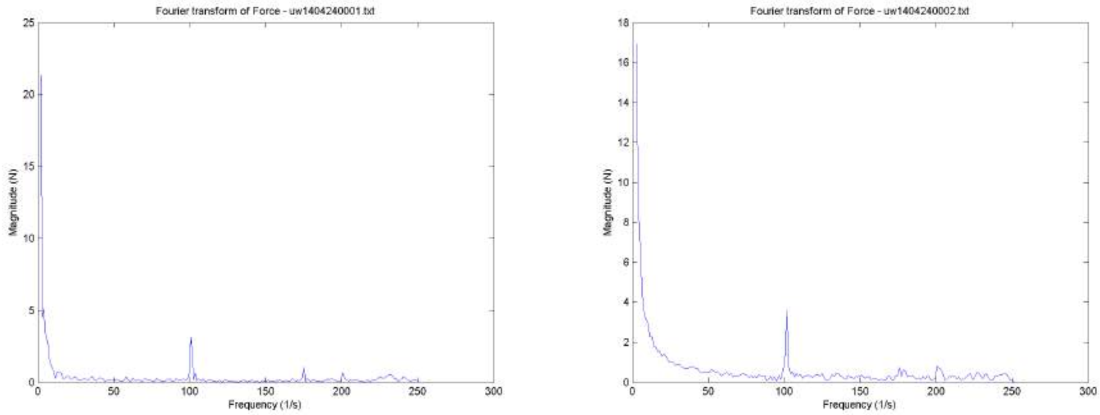

(a) **(b)**

Figure C.14: Absolute magnitude of Fourier transform of force data for welds between grit blasted non-coated aluminium and composite without using an energy directing thermoplastic.

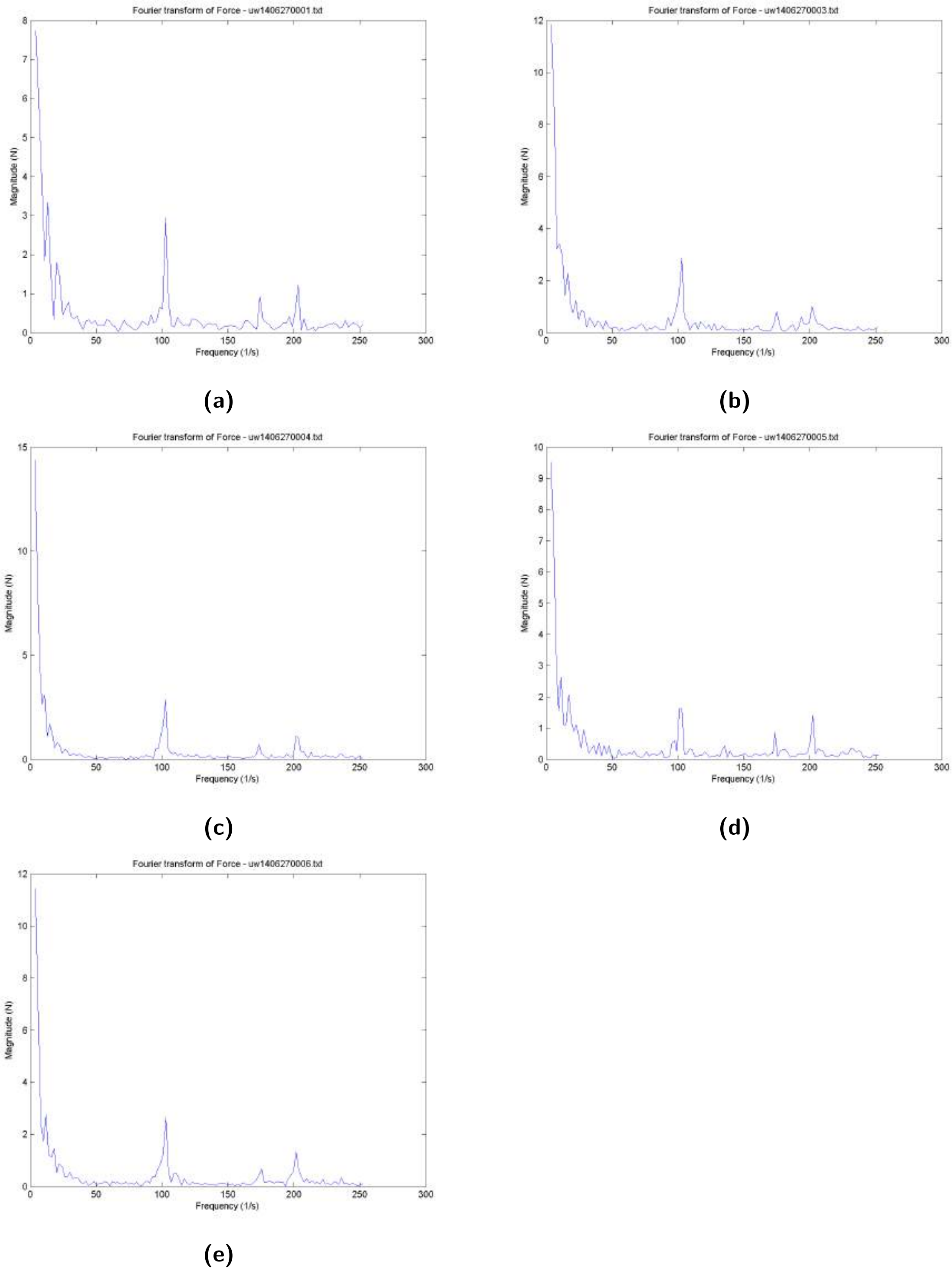

Figure C.15: Absolute magnitude of Fourier transform of force data for composite to grit blasted and coated aluminium (bottom) weld number 1 and 3 to 6.

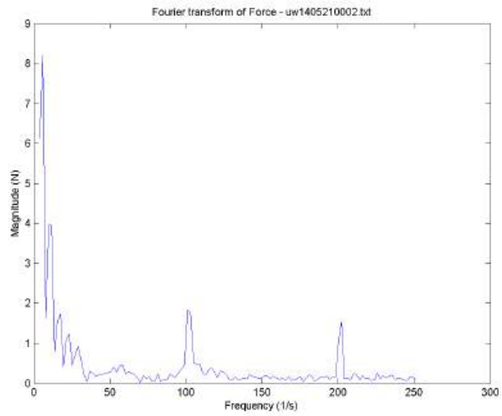

(a)

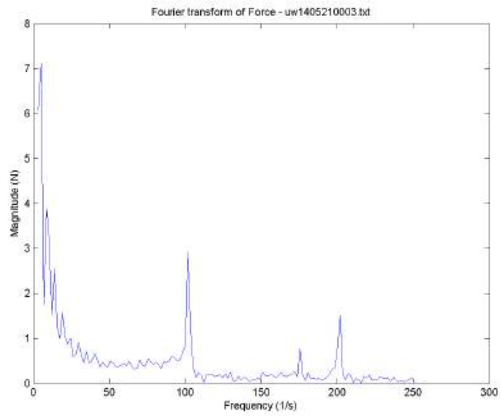

(b)

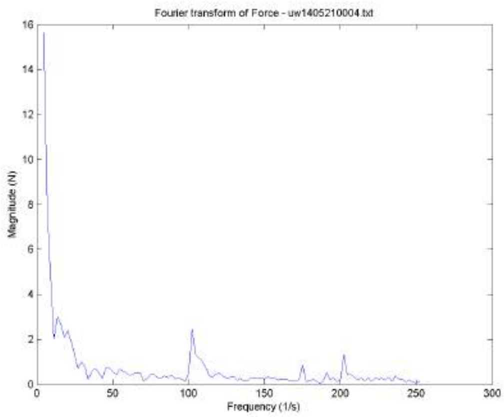

(c)

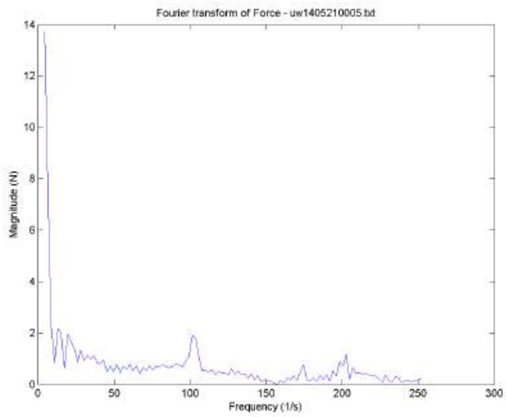

(d)

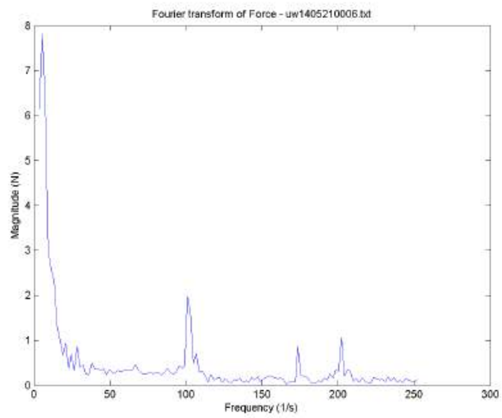

(e)

Figure C.16: Absolute magnitude of Fourier transform of force data for composite to grit blasted and coated aluminium (bottom) weld until 80% displacement, number 2 to 6.

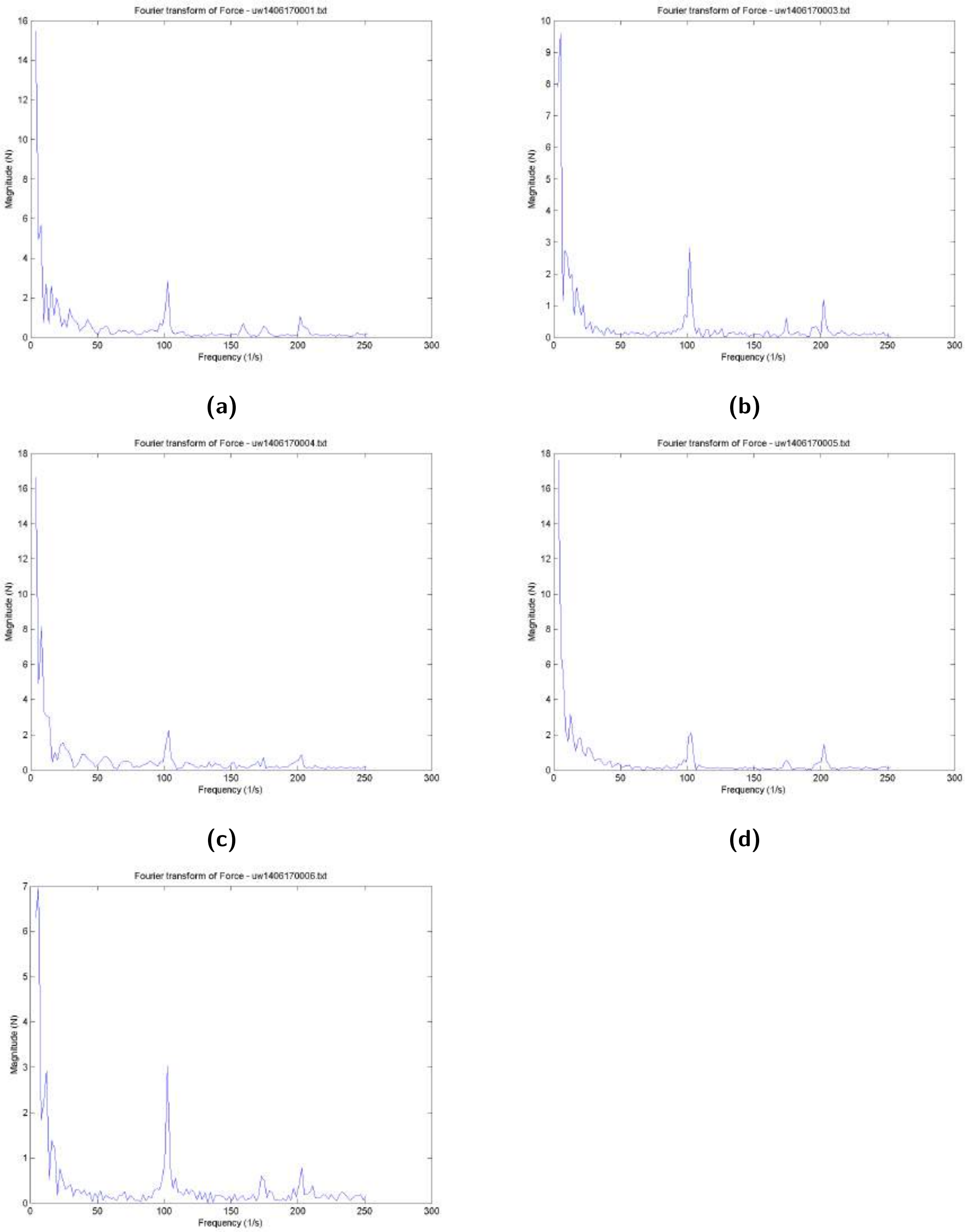

(a) (b) (c) (d) (e)

Figure C.17: Absolute magnitude of Fourier transform of force data for composite to grit blasted, etched and coated aluminium (bottom) weld number 1 and 3 to 6.

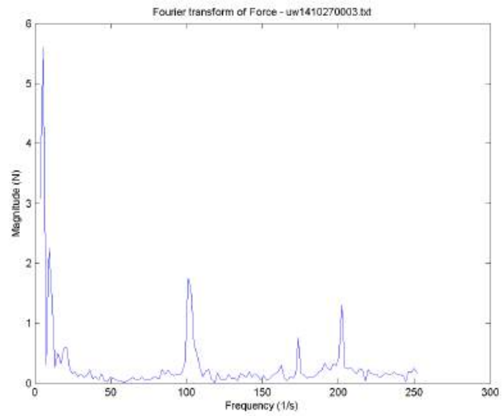

(a)

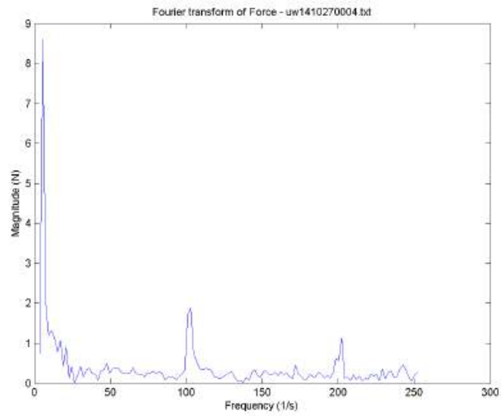

(b)

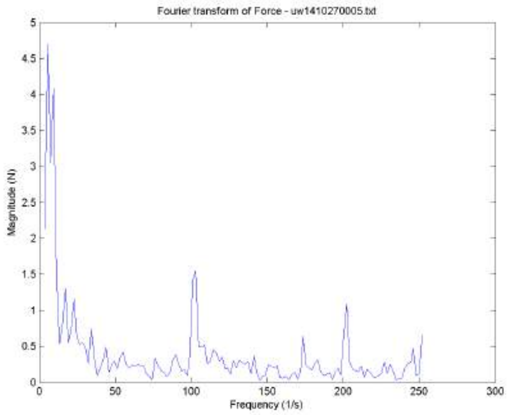

(c)

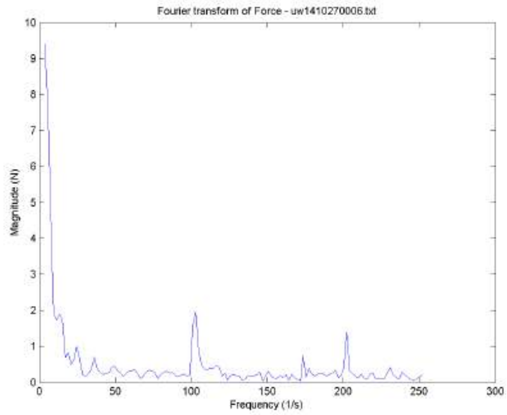

(d)

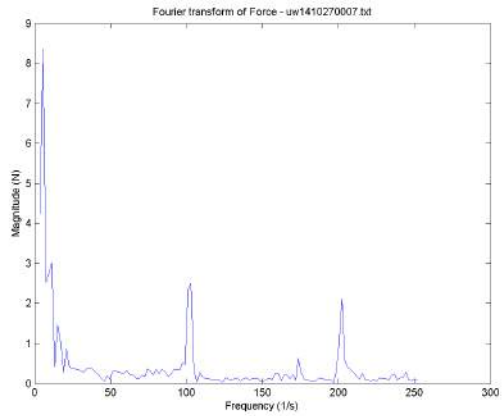

(e)

Figure C.18: Absolute magnitude of Fourier transform of force data for composite to grit blasted, etched and coated aluminium (bottom) welded until 66% displacement, weld number 1 to 5.

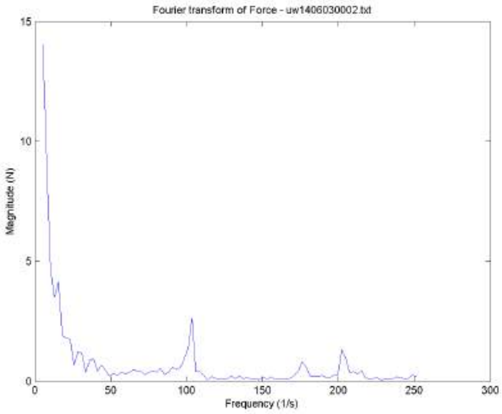

(a)

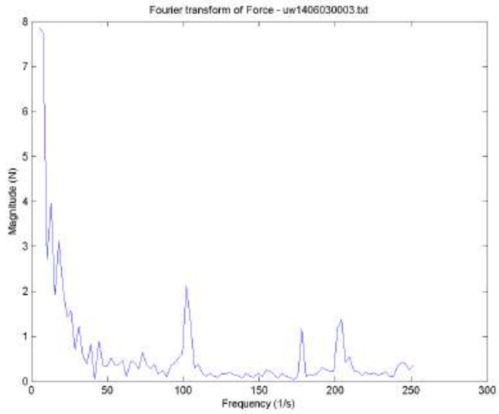

(b)

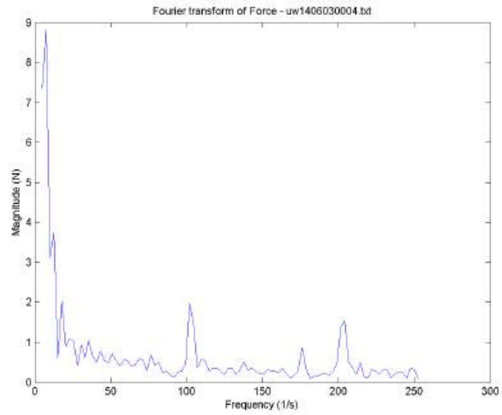

(c)

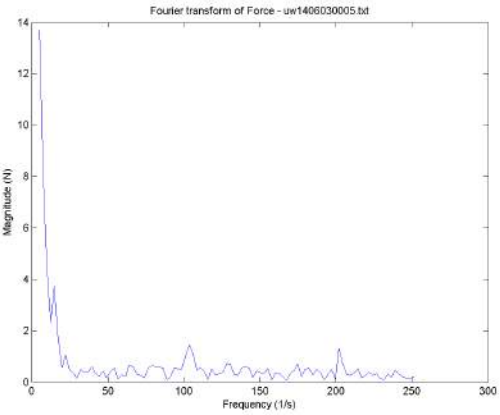

(d)

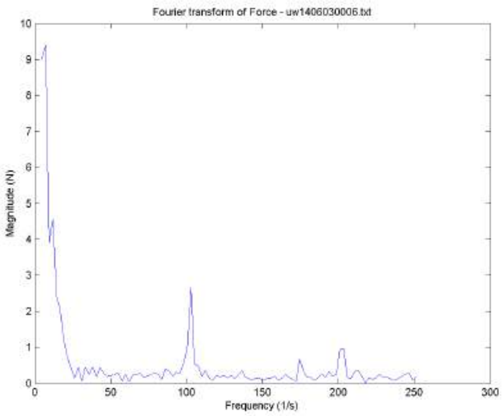

(e)

Figure C.19: Absolute magnitude of Fourier transform of force data for grit blasted and coated aluminium (top) to composite weld number 2 to 6.

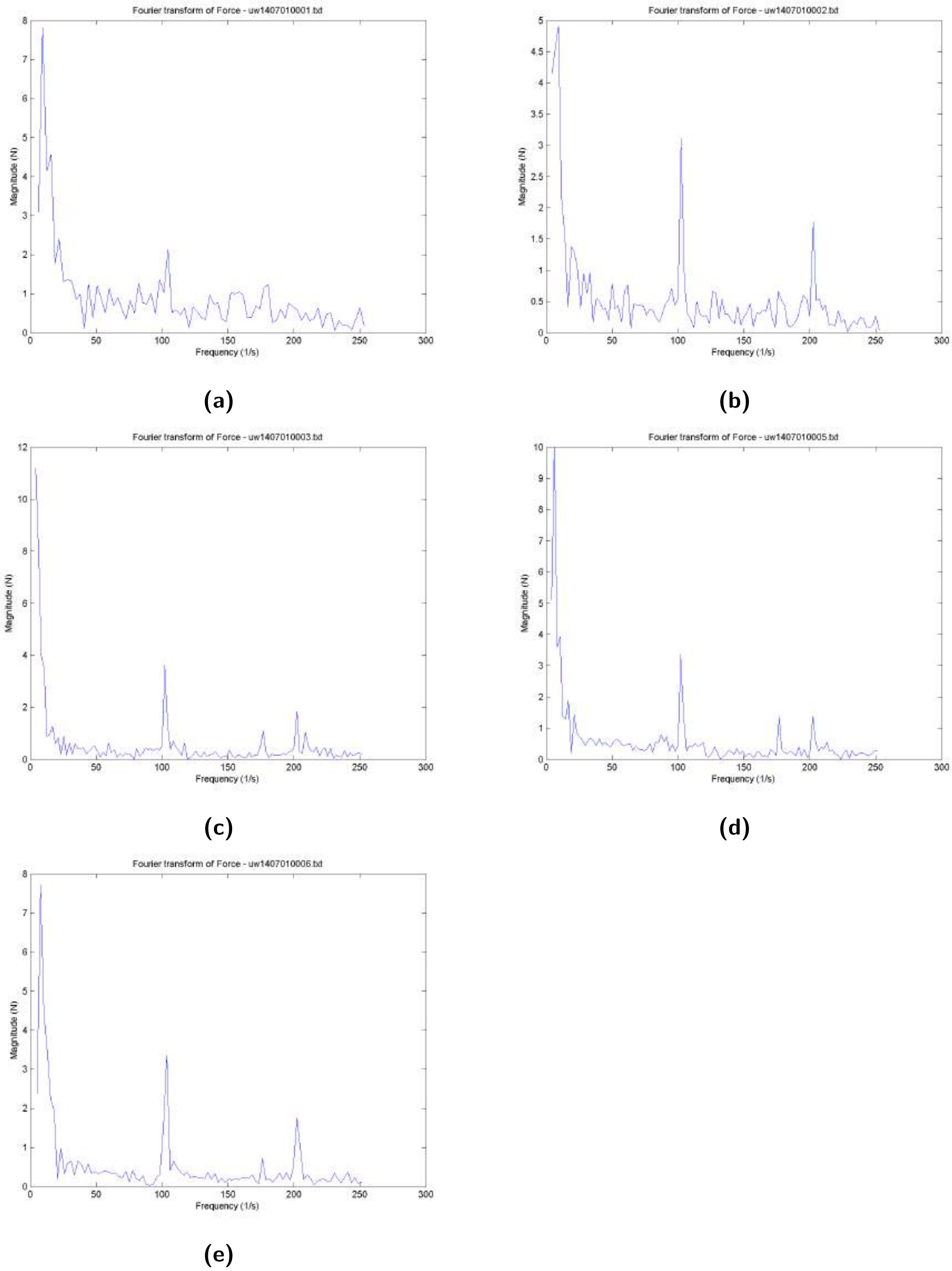

Figure C.20: Absolute magnitude of Fourier transform of force data for composite to grit blasted and coated steel (bottom) weld number 1 to 3 and 5 & 6.

C.3 Division of Force Data in High and Low Frequency

In the upcoming figures, the divided high- and low frequency force feedback of individual welds are presented for each welding series. This is presented:

- for non-hybrid welds in Figure C.21;
- for non-hybrid welds with 66% displacement in Figure C.22.
- for uncoated grit blasted aluminium to CFR-PA6 in Figure C.23;
- for uncoated grit blasted aluminium to CFR-PA6 without using an ED in Figure C.24;
- for grit blasted and coated aluminium to CFR-PA6 in Figure C.25;
- for grit blasted and coated aluminium to CFR-PA6, until 80% displacement in Figure C.26;
- for grit blasted, etched and coated aluminium to CFR-PA6 in Figure C.27;
- for grit blasted, etched and coated aluminium to CFR-PA6 with optimized displacement in Figure C.28;
- for grit blasted and coated aluminium to CFR-PA6, with aluminium as top adherend in Figure C.29;
- for grit blasted and coated steel to CFR-PA6 in Figure C.30.

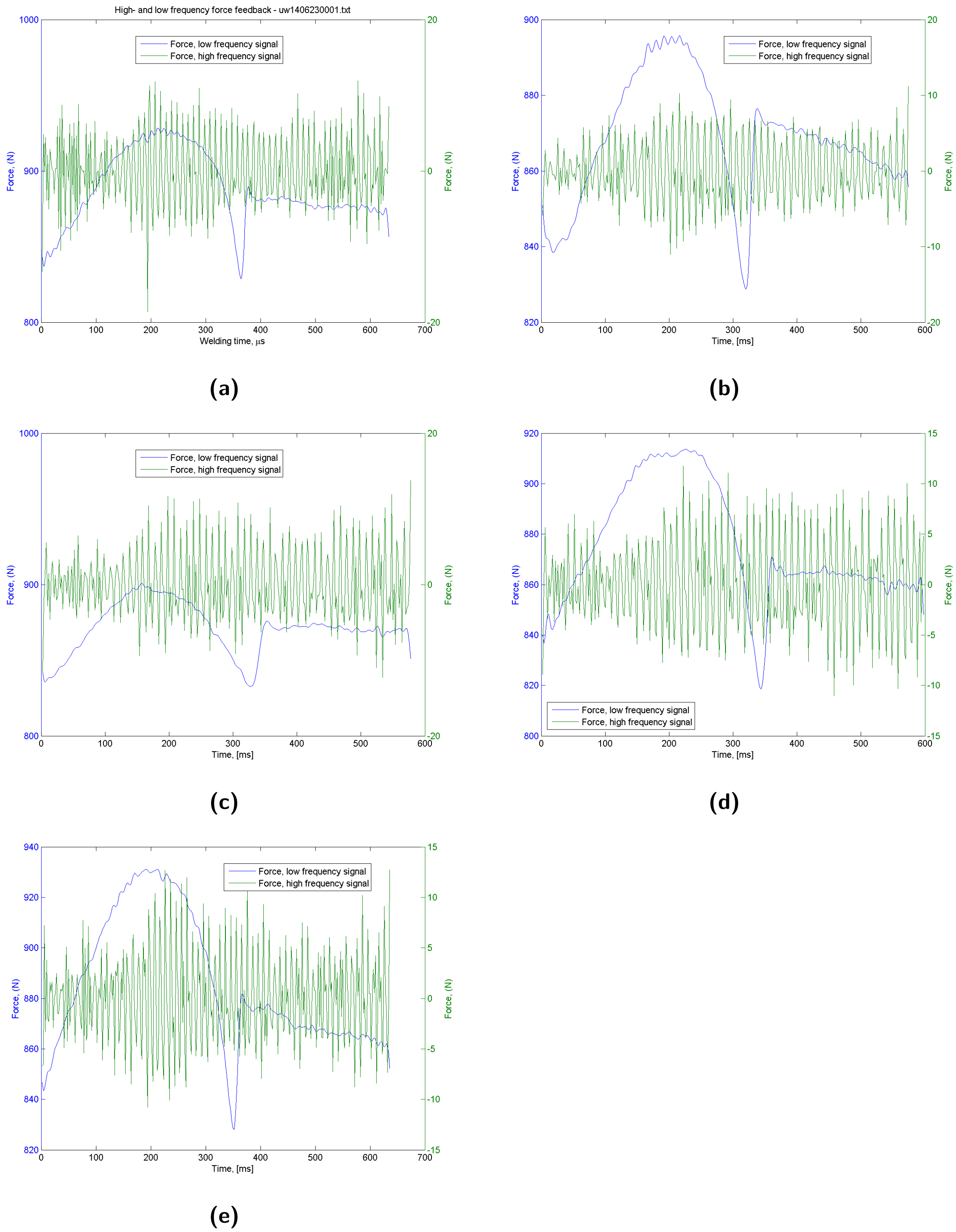

Figure C.21: Divided high- and low frequency response of force data for composite to composite weld number 1 to 5.

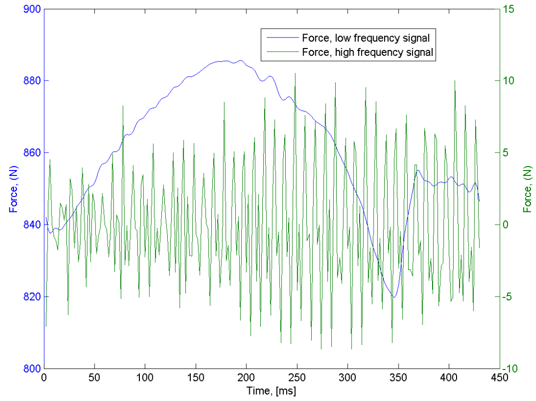

(a)

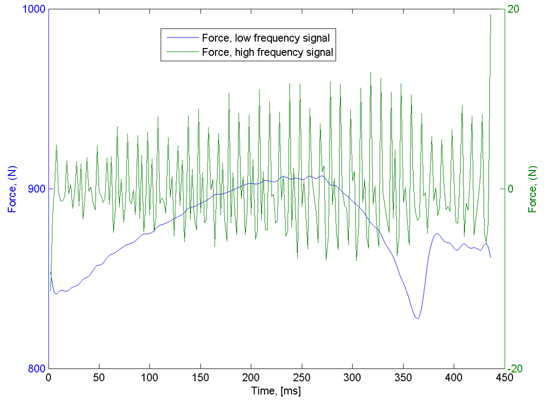

(b)

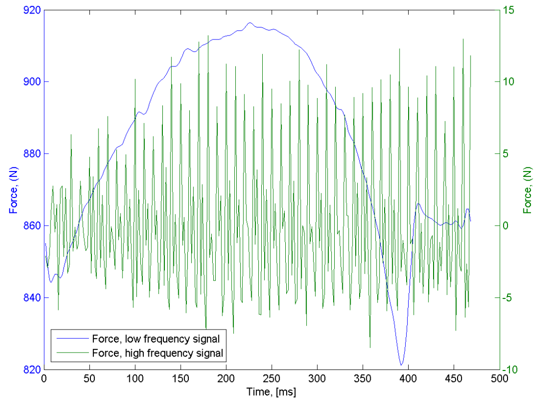

(c)

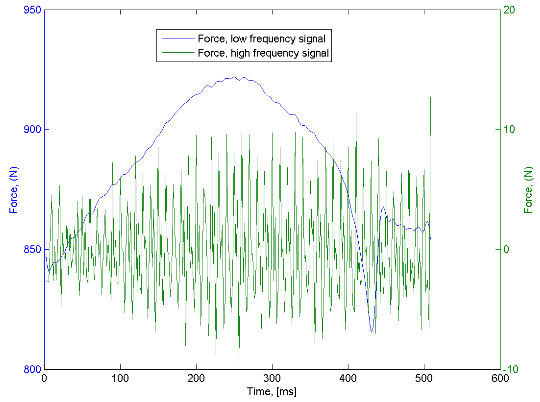

(d)

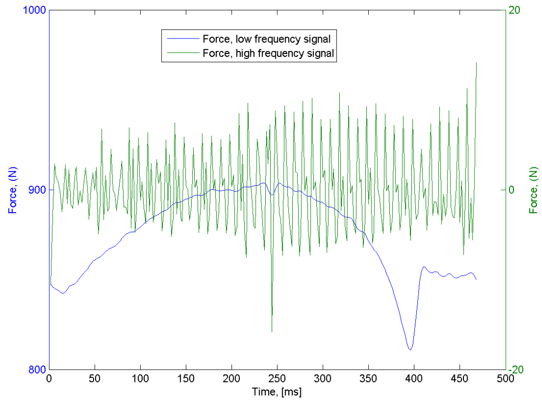

(e)

Figure C.22: Divided high- and low frequency response of force data for composite to composite weld with 66 % displacement, number 1 to 3, 6 & 7.

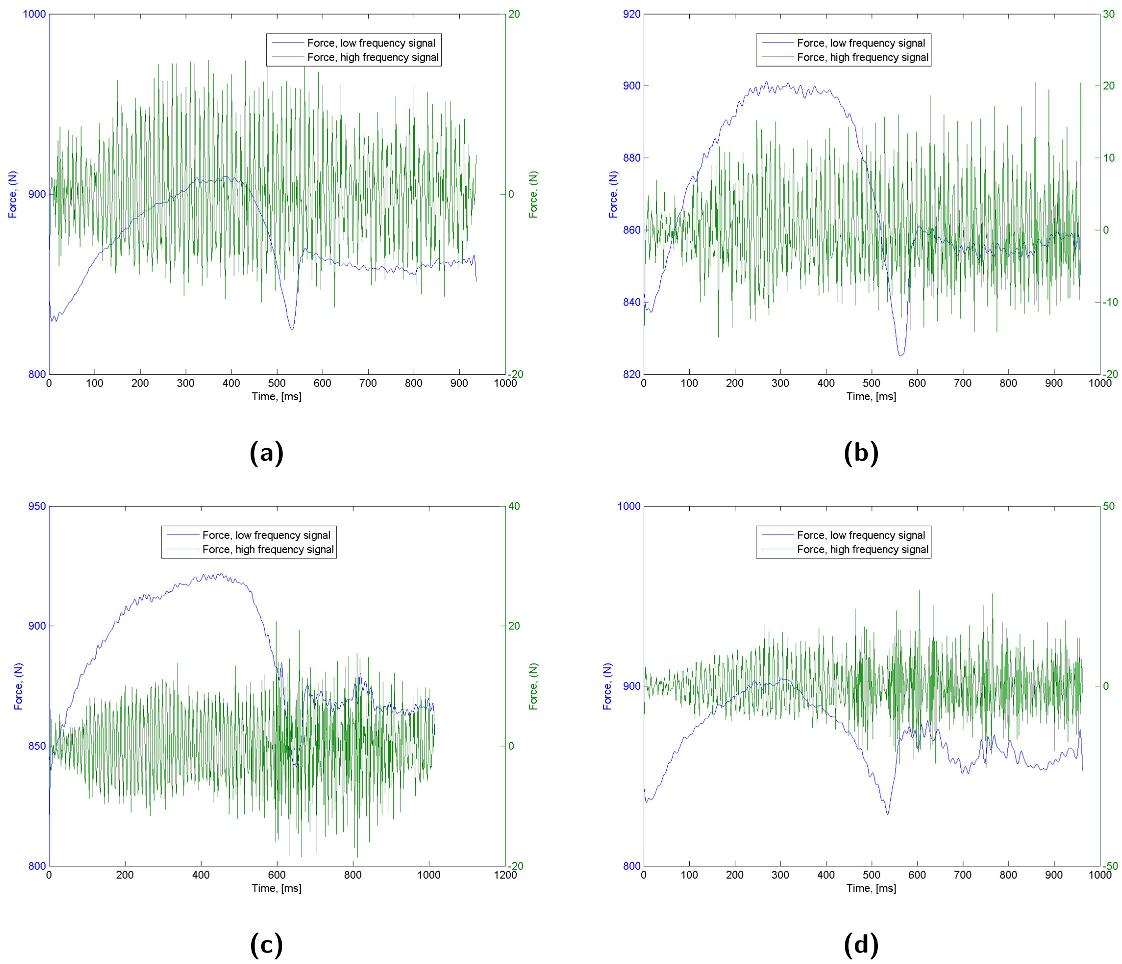

Figure C.23: Divided high- and low frequency response of force data for welds between grit blasted non-coated aluminium and composite, weld number 1 to 4.

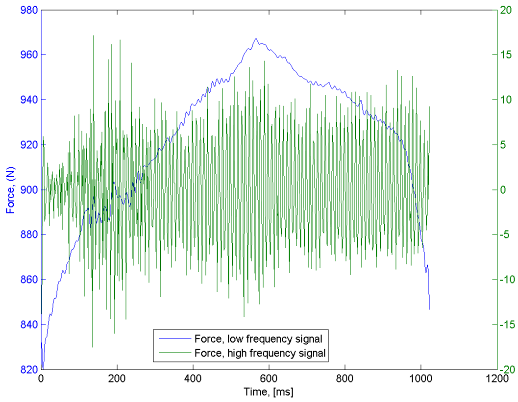

(a)

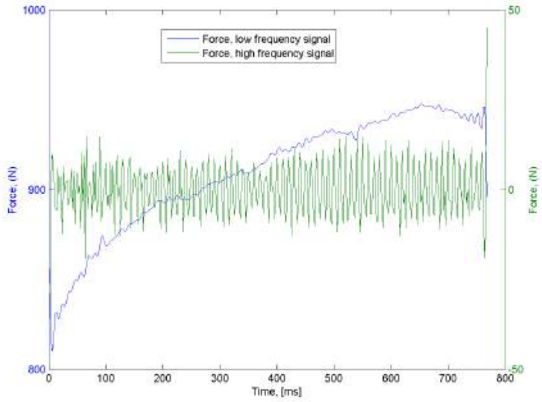

(b)

Figure C.24: Divided high- and low frequency response of force data for welds between grit blasted non-coated aluminium and composite without using an energy directing thermoplastic.

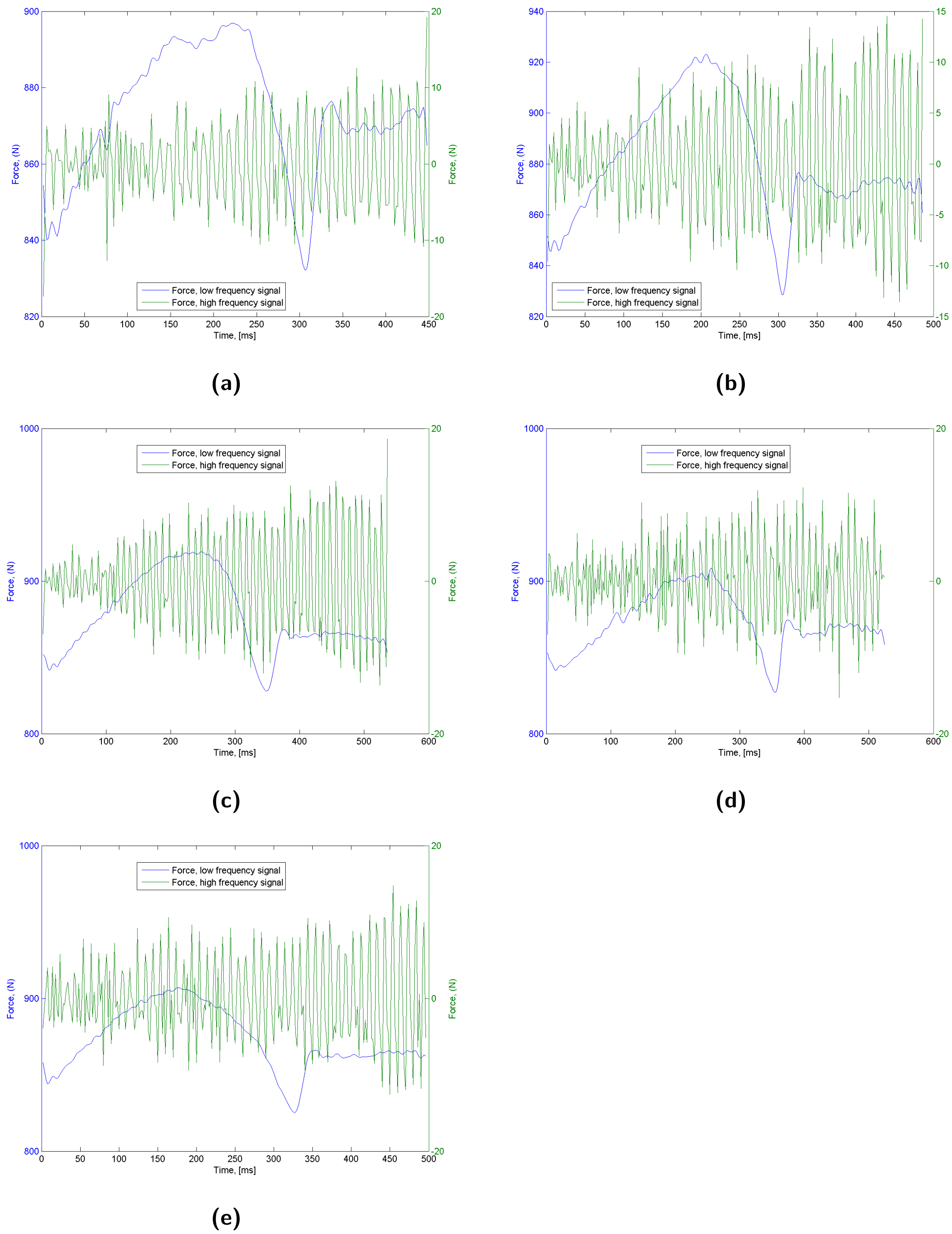

Figure C.25: Divided high- and low frequency response of force data for composite to grit blasted and coated aluminium (bottom) weld number 1 and 3 to 6.

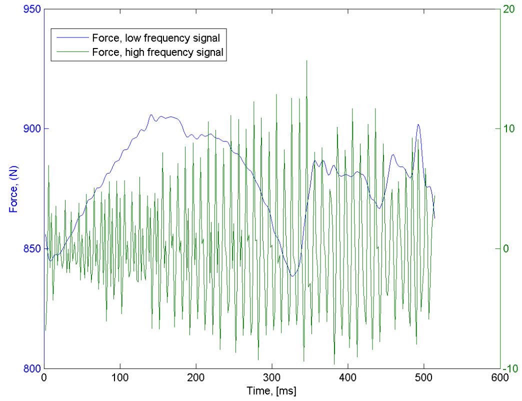

(a)

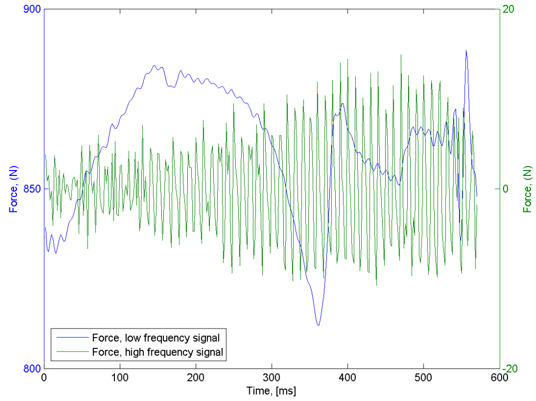

(b)

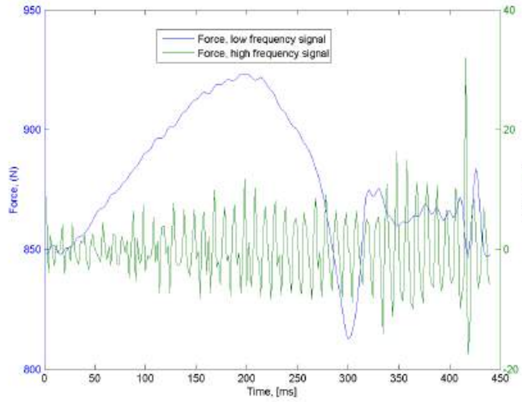

(c)

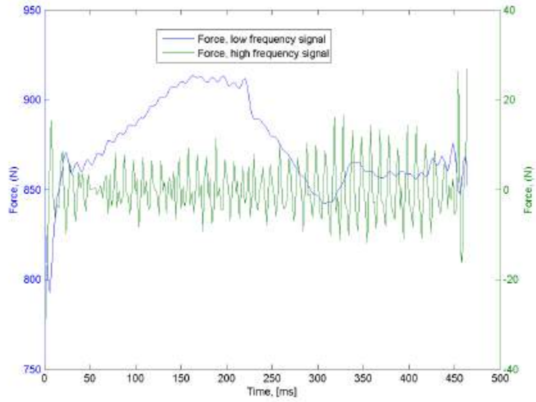

(d)

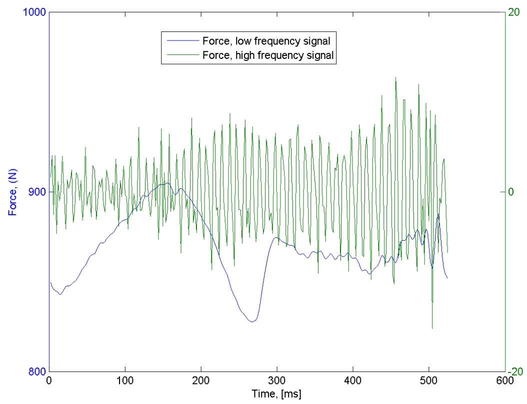

(e)

Figure C.26: Divided high- and low frequency response of force data for composite to grit blasted and coated aluminium (bottom) weld until 80% displacement, number 2 to 6.

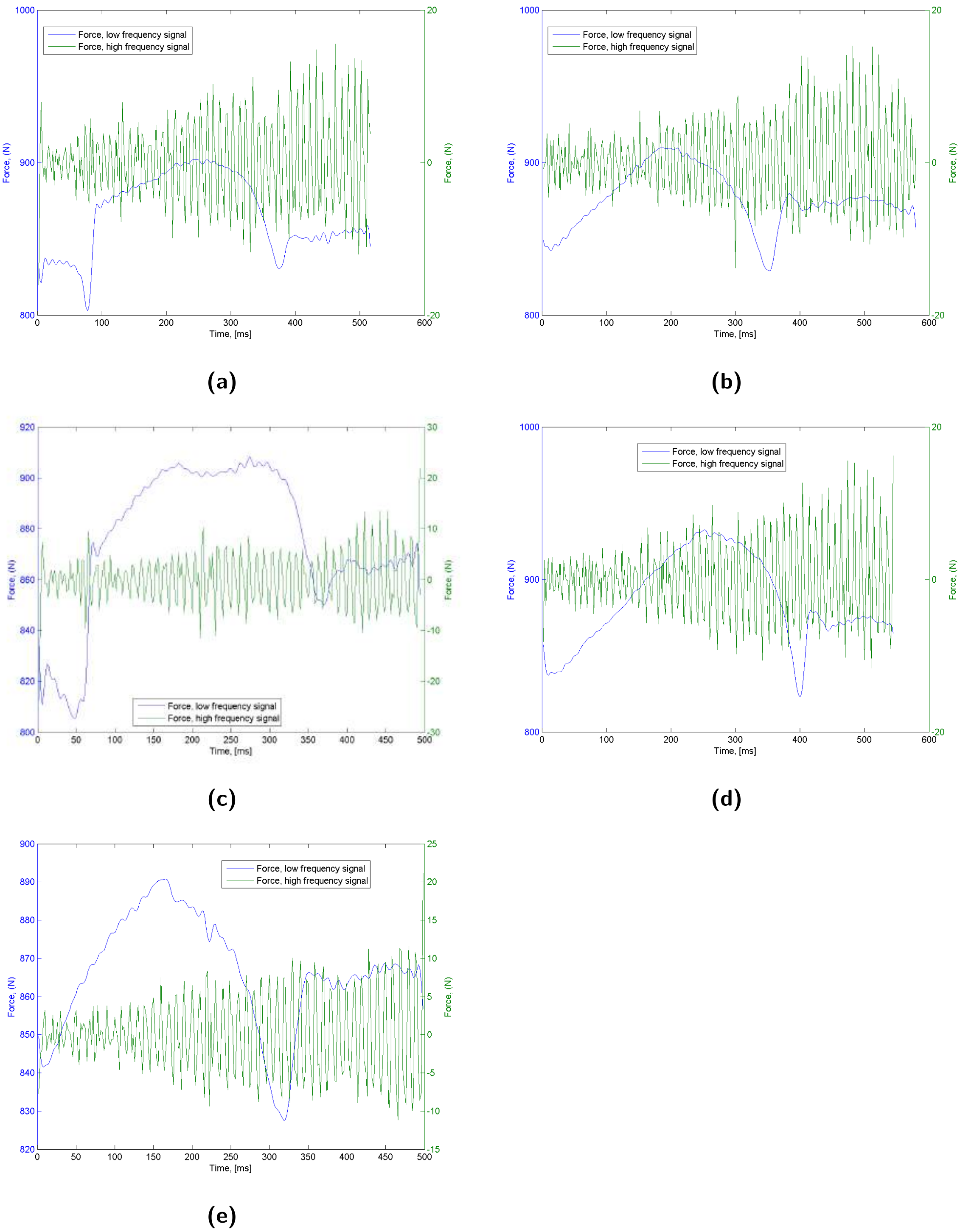

Figure C.27: Divided high- and low frequency response of force data for composite to grit blasted, etched and coated aluminium (bottom) weld number 1 and 3 to 6.

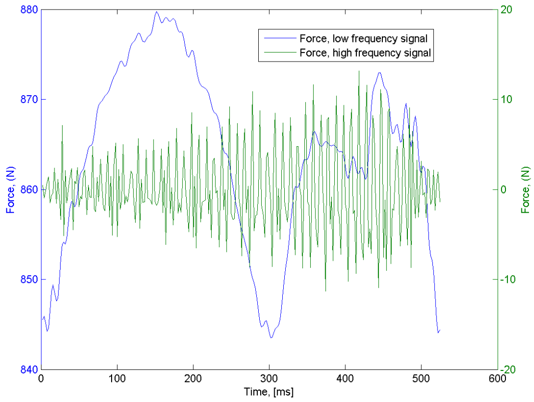

(a)

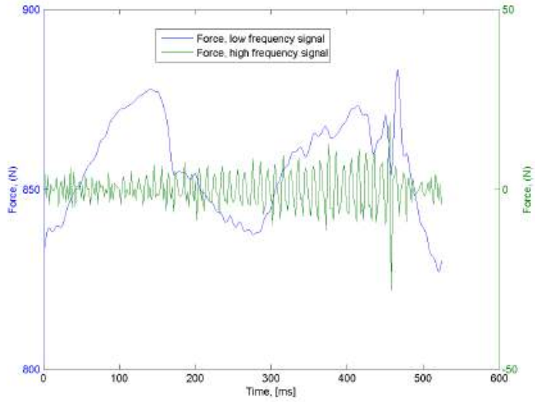

(b)

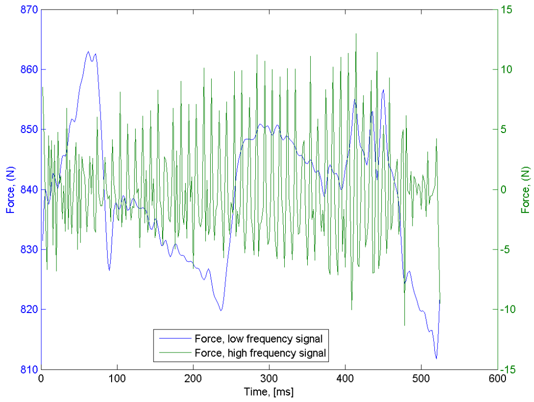

(c)

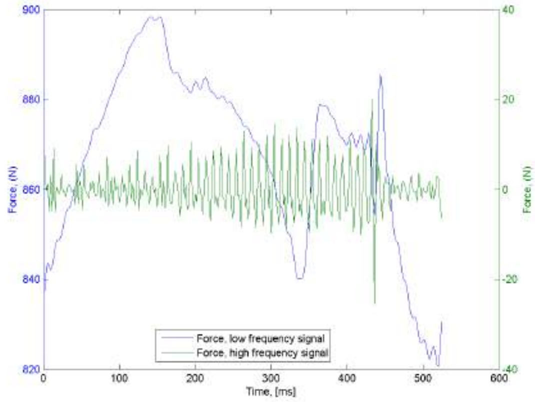

(d)

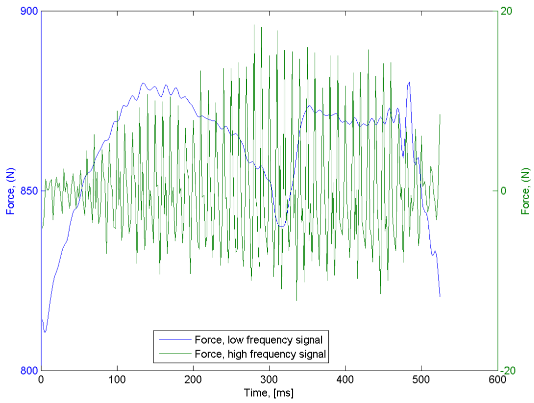

(e)

Figure C.28: Divided high- and low frequency response of force data for composite to grit blasted, etched and coated aluminium (bottom) welded until 66% displacement, weld number 1 to 5.

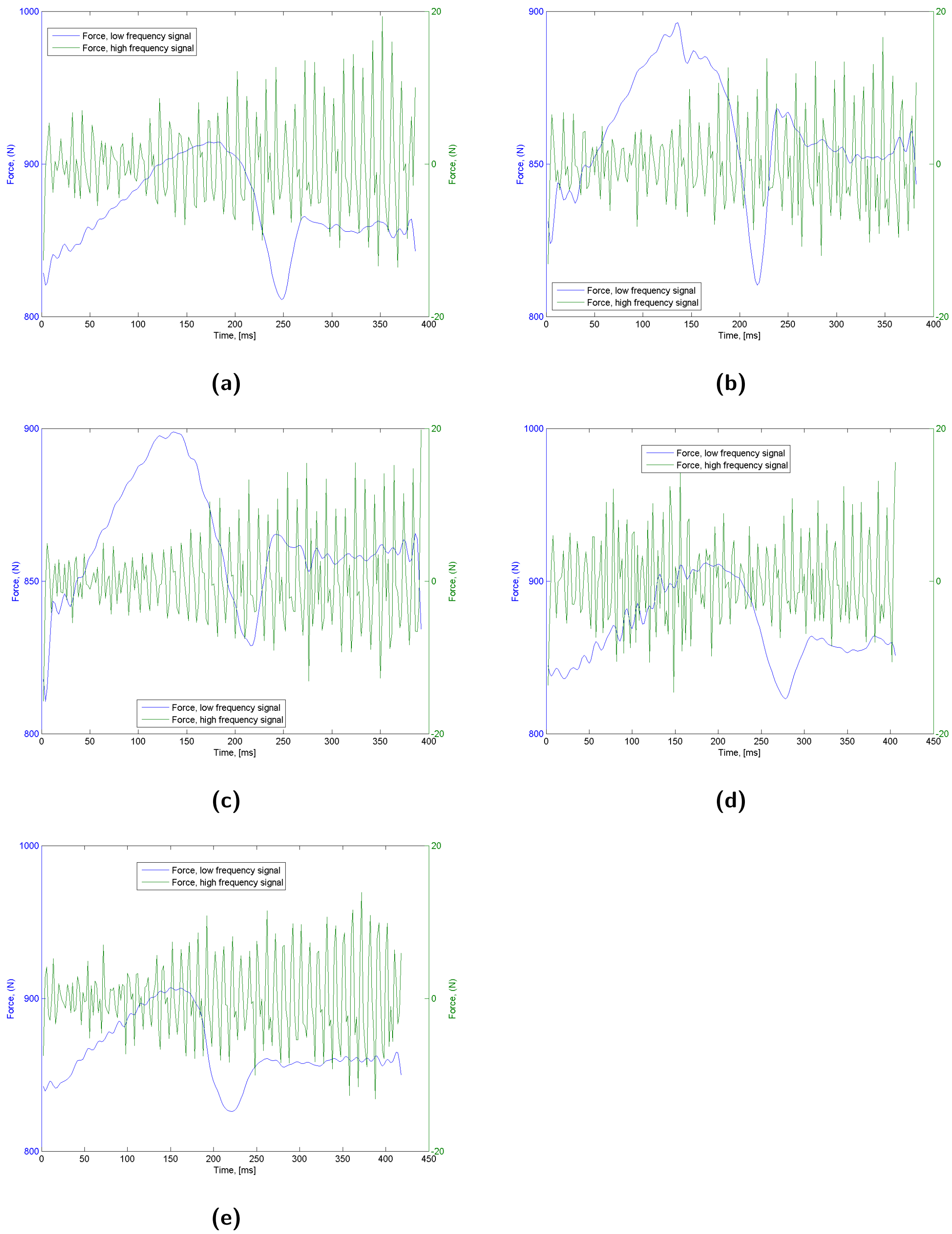

Figure C.29: Divided high- and low frequency response of force data for grit blasted and coated aluminium (top) to composite weld number 2 to 6.

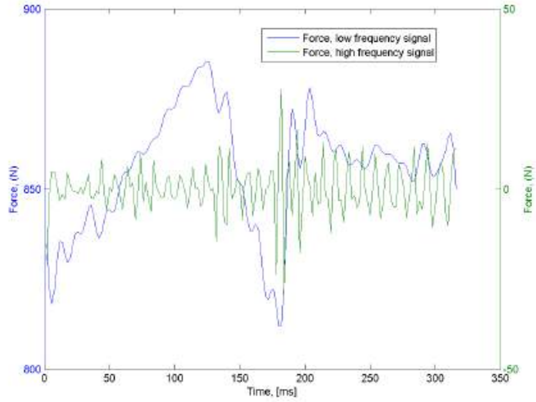

(a)

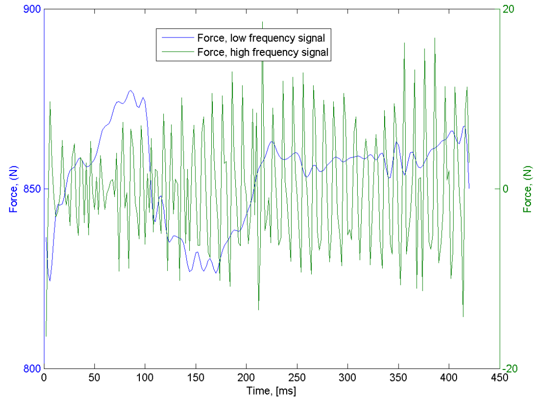

(b)

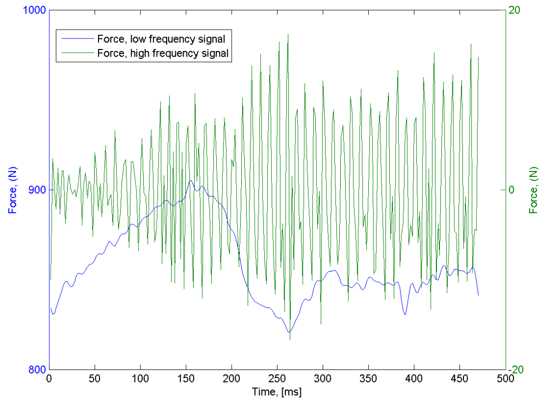

(c)

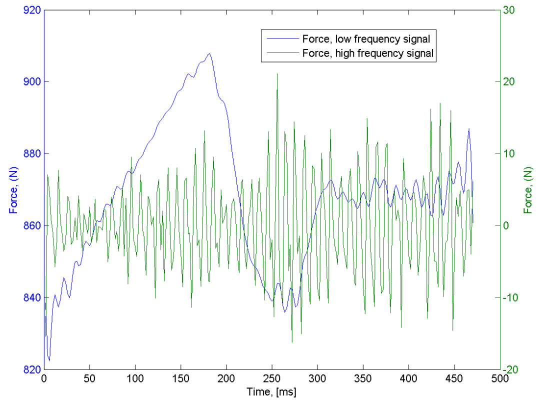

(d)

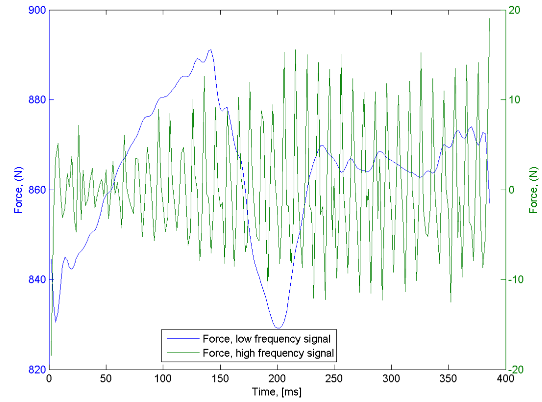

(e)

Figure C.30: Divided high- and low frequency response of force data for composite to grit blasted and coated steel (bottom) weld number 1 to 3 and 5 & 6.

Appendix D

Fracture Surfaces

In this Appendix, the resulting fracture surfaces after single lap shear testing of the discussed series in Chapter 5 are presented. The substrate surfaces after welding for the discussed welding series in Chapter 3 which did not result in a successful joint are presented in Section D.2.

D.1 Substrate Surfaces after Unsuccessful Welding

In this Section, in Figures D.1 and D.2, the unsuccessful welded substrates are presented between CFR-PA6 and grit blasted aluminium, with and without ED, respectively.

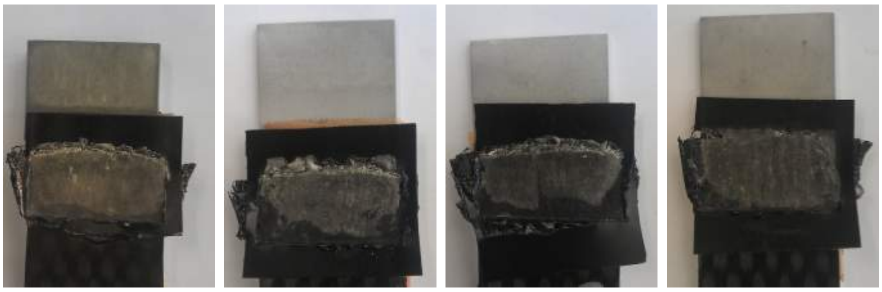

(a) (b) (c) (d)

Figure D.1: Fracture surfaces of ultrasonic welded joints between CFR-PA6 and non-coated grit blasted aluminium (bottom).

(a) (b) (c) (d)

Figure D.2: Fracture surfaces of ultrasonic welded joints between CFR-PA6 and non-coated grit blasted aluminium (bottom).

D.2 Fracture Surfaces of Successful Welded Joints after Single Lap Shear Testing

In this Section, the fracture surfaces of single lap shear tested joints are presented. This is presented:

- for non-hybrid welded joints in Figure D.3.
- for non-hybrid welded joints with 66 % displacement in Figure D.4.
- for grit blasted and coated aluminium to CFR-PA6 in Figure D.5;
- for grit blasted and coated aluminium to CFR-PA6 at 80% displacement in Figure D.6;
- for grit blasted, etched and coated aluminium to CFR-PA6 in Figure D.7;
- for grit blasted, etched and coated aluminium to CFR-PA6 with 66 % displacement in Figure D.8;
- for grit blasted and coated aluminium to CFR-PA6, with aluminium as top adherend in Figure D.9;
- for grit blasted and coated steel to CFR-PA6 in Figure D.10.
- for a series of adhesively bonded reference joints of grit blasted, etched and coated aluminium to CFR-PA6 in Figure D.11.

(a) (b) (c) (d) (e)

Figure D.3: Fracture surfaces of ultrasonic welded joints between two CFR-PA6 substrates. Average SLSS: 37.6 MPa, c.o.v.: 3.1%

(a) (b) (c) (d) (e)

Figure D.4: Fracture surfaces of ultrasonic welded joints between two CFR-PA6 substrates, welded until 66 % displacement of the thickness of the used ED. Average SLSS: 33.2 MPa, c.o.v.: 9.5%

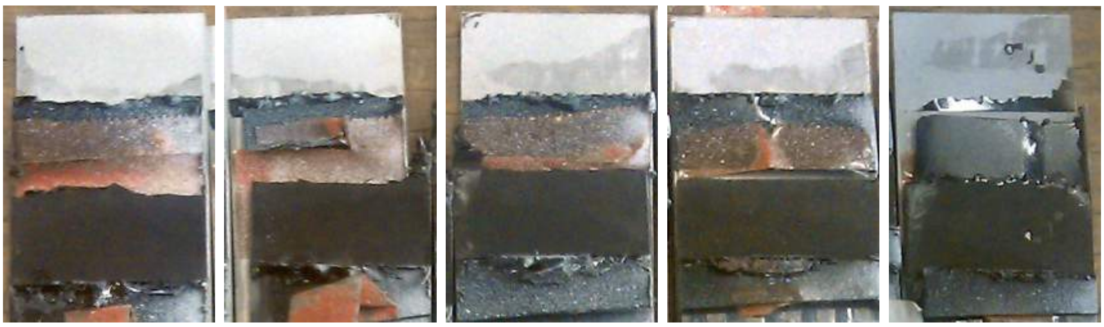

(a) (b) (c) (d) (e)

Figure D.5: Fracture surfaces of ultrasonic welded joints between CFR-PA6 and grit blasted aluminium (bottom). Average SLSS: 10.3 MPa, c.o.v.: 13.8%

(a) (b) (c) (d) (e)

Figure D.6: Fracture surfaces of ultrasonic welded joints between CFR-PA6 and grit blasted aluminium (bottom) welded until 80 % displacement. Average SLSS: 12.1 MPa, c.o.v.: 7.5%

(a) (b) (c) (d) (e)

Figure D.7: Fracture surfaces of ultrasonic welded joints between CFR-PA6 and grit blasted and etched aluminium (bottom). Average SLSS: 16.5 MPa, c.o.v.: 2.2%

(a) (b) (c) (d) (e)

Figure D.8: Fracture surfaces of ultrasonic welded joints between CFR-PA6 and grit blasted and etched aluminium (bottom) with a welding displacement of 66 %. Average SLSS: 15.1 MPa, c.o.v.: 7.5%

(a) (b) (c) (d) (e)

Figure D.9: Fracture surfaces of ultrasonic welded joints between CFR-PA6 and grit blasted aluminium (top). Average SLSS: 11.2 MPa, c.o.v.: 10.0%

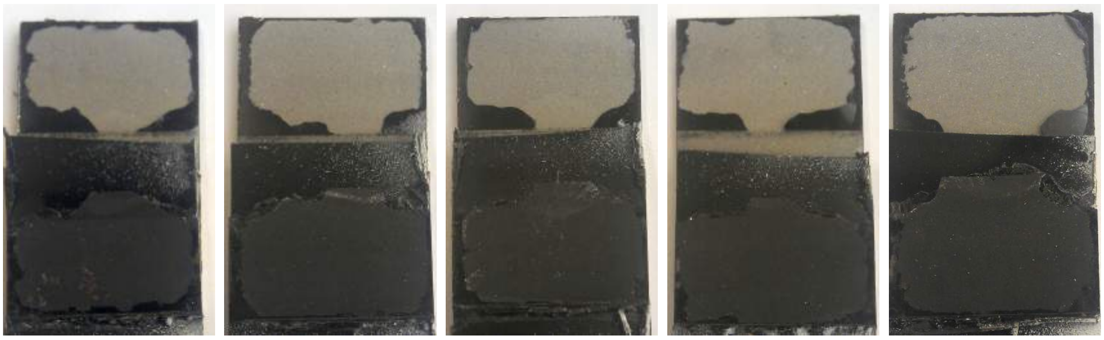

(a) (b) (c) (d) (e)

Figure D.10: Fracture surfaces of ultrasonic welded joints between CFR-PA6 and grit blasted steel (bottom). Average SLSS: 8.5 MPa, c.o.v.: 7.7%

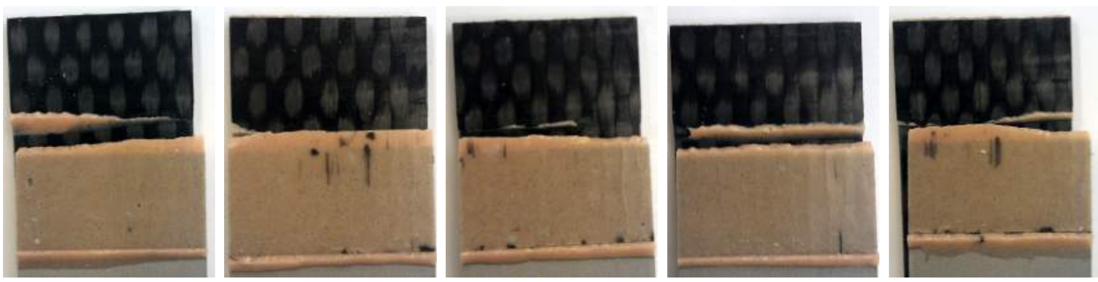

(a) (b) (c) (d) (e)

Figure D.11: Fracture surfaces of adhesively bonded CFR-PA6 to grit blasted and nitric acid etched reference samples. Average SLSS: 20.5 MPa, c.o.v.: 11.9%